Joule Heating Flow Control Methods for High-Speed Flows

A. Russell,* H. Zare-Behtash, and K. Kontis

School of Engineering, University of Glasgow, Scotland G12 8QQ, UK

(Dated: January 20, 2016)

Abstract

Joule heating is the generation of heat by the passage of current through a conductor. This is a review of a group of flow control methods that employ Joule heating to do so and can collectively be called energy deposition flow control methods. The energy deposition flow control methods discussed are surface plasma actuators, laser energy deposition and microwave generated plasma. These type of actuation methods are of particular interest for applications to high-speed flows. Conventional, mechanical actuation methods can be problematic in supersonic/hypersonic use as they require large forces to move and do not have fast enough response times depending on the application. Energy depositing actuators overcome these two problems as they have no moving parts and the response times can be in nanoseconds. This promising application to high-speed flows is one of the main driving factors behind the research in energy deposition flow control technologies. This review brings together the fundamental physics behind the operation of such methods. Both the fundamental characteristics of the flow control methods as well as the experience of their applications in high-speed flows is covered. A brief discussion of potential areas that require further study for each type of actuator/technique is also provided. Finally, a discussion of the possible future applications of energy deposition flow control methods is presented.

*a.russell.2@research.gla.ac.uk

I. INTRODUCTION

One of the current issues with the development of high-speed transport aircraft is fuel efficiency, which has a direct impact on cost and endurance of the current supersonic/hypersonic propulsion systems. An important phenomenon that impacts upon the performance of these propulsion systems are shock wave-boundary layer interactions (SBLI). These interactions can cause boundary layer separation and adverse pressure gradients, both of which lead to an overall decrease in efficiency of the system.[1] There have been many different techniques devised in the past to either control SBLI or to alleviate its adverse effect on the flow. Most methods focus on the mitigation of the negative effects of SBLI's. Two examples are bleed air systems[2] and vortex generators (a family of devices such as micro ramps[3] and vanes[4]). However, both of these devices have notable setbacks. The bleed air system is a large system that increases the weight and, depending on the design, can also influence the drag of the propulsion systems. Vortex generators generally are passive devices; they therefore do not require any power input or infrastructure for their operation. However this means that they are always in "operation". As they are designed for a specific flight condition, at any other operating regime the device does not operate optimally and could in theory be detrimental to the propulsion systems performance.

A relatively new family of flow control devices for SBLI's are those that use the principles of Electrohydrodynamics (EHD) and Joule heating for flow control. This review examines dielectric barrier discharge surface actuators, pulsed plasma synthetic jet actuators, laser induced plasma discharge actuation and microwave generated plasma discharge actuation. These devices have a number of benefits: they are forms of active flow control implying they can be switched on or off, can have an impact from distance (such as laser and microwave devices), and are reasonably small in size.

The review begins with a brief explanation of active flow control. The fundamental operation, previously research applications and possible future applications are then discussed for each category of flow control device. The review discusses studies of high speed flow as a whole, with no specific focus on either laminar or turbulent studies. The final section is a brief discussion of the possible application of energy deposition methods for flow control to a high speed flow control problem, high speed engine intakes.

II. ACTIVE FLOW CONTROL

Research in active flow control began in earnest in 1904, as a result of the discovery of the boundary layer by Prandtl.[5] A comprehensive definition of flow control is given by Flatt (1961):[6] "boundary layer control includes any mechanism or process through which the boundary layer of a fluid flow is caused to behave differently than it normally would were the flow developing naturally along a smooth straight surface." For active flow control a couple of additions are made to the above definition. An active flow control technique should at least be able to be switched on and off whilst also having the ability to tune the magnitude of different parameters related to the flow control technique.[7] There are numerous techniques/actuators that fit this description e.g. suction, oscillating surfaces, magnetohydrodynamic control, steady jets etc. However this paper will focus on a selection of EHD and Joule heating flow control methods. What these methods all have in common is that the medium for control is the ionisation of atoms/molecules in the flow and this ionisation in turn affects the flow characteristics.

A. Nanosecond Pulse Dielectric Barrier Discharge (DBD) Plasmas

The application of electrical phenomena to control airflow started almost 50 years ago with the first scientific paper on the subject published in 1968 by Yung et al.[8] Work on plasmas as a viable tool for airflow control however did not start to grow until the 1990's. The first published paper using a surface dielectric barrier discharge (DBD) device was in 1998 by Roth.[9] The dielectric barrier discharge effect itself was first proposed in 1857 by Ersnt Werner von Siemens as a means to produce ozone.[10] The basic geometry of a simple DBD is shown in Figure 1. This type of device will only work with an AC voltage supply as the dielectric prevents DC voltage operation. DBD plasma actuators control flows either through the generation of an ionic wind (AC-DBD's) or through the generation of pressure waves (ns-DBD's) that interact with the baseline flow.

The basic principle for the plasma generation is that the applied voltage ionises molecules in the air at the positive electrode and these then travel between the electrode and the surface of the dielectric barrier between the air and the grounded electrode. This occurs for one half of the AC voltage cycle, for the other half the electrons move from the surface of the

dielectric towards the electrode. As the electrons build up on the dielectric surface the local field strength decreases until it reaches a point at which no more discharges may occur until the polarity of the AC voltage changes at the next half cycle. Although the streamer, the channel through which the ionised particles travel between the electrode and the dielectric, has collapsed at this point and no more electrons/ions are travelling across it, there is still enough energy left behind for it to be considered separate from the rest of the volume of air. This is known as the microdischarge remnant. This phenomenon allows another streamer to form at the same location when the polarity of the supply changes as this area will require less energy to ionise than its surroundings. This is therefore the reason that single streamers (figure 2 shows these streamer) are visible in plasmas. A uniform plasma would be apparent if the streamers formed in different locations. Each time a streamer is formed, the electric field strength at the surface of the dieleletric decreases which effectively terminates the microdischarge quickly, within a few nanoseconds. This termination means that the streamers do not overheat and allow the DBD to operate non-thermally.[11] The way in which the generated plasma helps to control the flow is by the electric wind. This term describes the movement of gas due to ions and electrons being repulsed from a high voltage electrode which was first fully described by Faraday in 1838.[12] This is created by ions and electrons colliding with the neutral particles in the region and imparting momentum onto them.

Moreau[12] presents an in-depth look at the use of surface plasma actuators for low speed as part of his overall review on plasma actuators as a whole. There are a number of different plasma based devices such as DBD's, surface corona discharges, pulsed plasma synthetic jets etc. that have proven capable of flow control at low speeds ($U_\infty < 30$m/s). However, as the aerospace industry deals with much higher freestream velocities, research is required for these actuators to become more capable and suited for application in the aerospace industry.

1. High-Speed Operation of ns-DBD's

The challenge of using DBDs for high speed flows is that their performance is limited by the ion charge density in the region of the actuator. The strength of the EHD effects that generate the electric wind have been quantified by Macheret et al.[13] by relating electrostatic

force and fluid momentum given in equation 1,

$$Z_{EHD} = \frac{en_{+}\Delta\varphi}{\rho U_{\infty}^{2}} \tag{1}$$

where e is the electron charge, n_+ is the density of positive ions, $\Delta\varphi$ is the voltage drop in charge region, ρ is density and U_∞ is flow speed. It is suggested that equation 1 leads to a value of close to unity for appreciable flow control. Therefore using this equation, and based on the assumption that the EHD interaction parameter (Z_{EHD}) is equal to unity, Macheret et al.[13] determined that a DBD actuator using an AC voltage supply could operate effectively at a maximum flow speed of 72m/s. Therefore this type of actuator would appear to have no effective use at supersonic or hypersonic speeds. However the flow velocities in the boundary layer of a supersonic or hypersonic flow are significantly smaller than the freestream velocities. Therefore it has been considered that AC-DBD's could have a useful effect on the boundary layer. A study by Pal et al.[14] examined the use of AC-DBD's on a Mach 1.6 wall jet. The results presented no statistically significant effect on the flow with the inclusion of AC-DBD plasma actuators. However this was merely a preliminary study and more research should be done to examine this in more depth. This review however will focus on the ns-DBD rather than AC-DBD plasma actuators as they show more promise as an effective method of active flow control in supersonic and hypersonic flows.

In recent years there have been a number of studies published that have examined high voltage pulses of just nanoseconds(ns) in duration both experimentally and numerically. Some of the first work published in the area was from Likhanskii et al.[15] who suggested that the actuator function could be improved by using a pulsed voltage supply with very high reptition rates (MHz) in order to give a period for the pulses of a few nanoseconds. This postulation was based on the physical phenomenon by which DBDs function (described above). It was suggested that the period for which the positive ions moved towards the dielectric was maximised by ensuring very fast replenishing of the electrons on the dielectric surface. The optimal wave form was postulated to be one of nanosecond high voltage pulses to generate the plasma combined with a DC bias to "push" the gas.

One of the first published papers regarding experimental data on ns-DBD's was by Opaits et al.[16] who carried out experiments using different waveforms based on the principles outlined in an earlier paper by Likhanskii et al.[15] They found that it was possible to efficiently generate plasma using nanosecond high voltage pulses. However the earlier suggestion of

using a DC biased signal superimposed on the ns pulses was found to be ineffective at forcing the flow as charge built up on the dielectric. Instead, a sinusoidal AC voltage with high voltage nanosecond pulses was used. The advantage of using separate signals to control the plasma generation and the gas forcing is that they can be altered independently of one another unlike the simple sinusoidal AC supply DBD actuators.

The basic operating principle of ns-DBD actuators was however not understood until further work was carried out. Roupassov et al.[17] showed that the method of flow control by which AC DBD actuators functioned was not how ns-DBD actuators functioned. It was shown, through an experimental campaign, that near-zero values of induced gas velocity were generated by the ns-DBD actuator. In the same paper it was shown that the rapid heating of the plasma discharge region generated a pressure wave. The paper by Popov.[18] provides a two step explanation for the rapid heating of the gas observed when operating a ns-DBD. First, nitrogen in the air is excited to one of the higher discrete energy levels available (Bohr[19] explains these discrete energy levels). Secondly, these excited nitrogen molecules undergo oxygen quenching which generates heat (along with an allotrope of oxygen, atomic oxygen). The shock waves generated by this phenomenon (and the secondary vortices) serve as an effective method of momentum transfer into the boundary layer. This has been proven to be useful for separation control up to M=0.85 among other things (discussed in-depth later).[17]

Further work was carried out by Takashima et al.[20] in order to gain a greater understanding of the phenomenon responsible for the shock wave created by the ns-DBD. It was discovered that each plasma discharge filament generated a compression wavelet. Figure 3 illustrates this as each individual compression wave can be observed along with the single shock wave generated by their superposition. It was also demonstrated that a filamentary plasma was capable of producing compression waves of higher amplitude and speeds than a diffuse plasma could.

2. Characterisation of ns-DBD's

Benard et al.[21] present an in-depth study of the impact of various electrical characteristics on the performance of a ns-DBD actuator. They showed that for a single voltage pulse there are actually two discharges: the first is due to the ionisation of the air by the positive

electrode, and the second occurs due to the discharge caused by charge build up on the dielectric surface. The main area focused on in this study was the effects of either positive or negative voltage pulses. The first conclusion made was that positive pulse deposits more energy in the surrounding gas than the negative pulses. Secondly, it was shown through imaging of the plasma that positive pulses generated a streamer based plasma while negative pulses generated a more diffuse plasma . It was also found that voltages of positive polarity produced a stronger pressure wave than those of negative polarity. Positive polarity pulses were also found to be more efficient when the energy per pulse was greater than 0.2mJ/cm. These conclusions were arrived at based on shock intensity which was calculated based on a normalised image intensity and tracking of the shock front. This conclusion appears to be inconsistent with that of Dawson et al.[22] as they determined that negative voltage pulses deposited more energy into the gas in all cases. There could be a number of factors important in this conclusion however such as the limited range of energy per pulse considered in the study of Benard et al.[21] in comparison to that of Dawson et al.,[22] different actuator geometries and different power supply used. The study by Takashima et al.[23] also provides some insight into the effect of pulse polarity on the discharge. They showed that although for both pulse polarities increasing frequency leads to a more filamentary discharge (see figure 4) the effect was more pronounced for negative pulse polarities. As another conclusion made in the paper was that filamentary discharges lead to the production of stronger pressure waves, this suggests that voltage pulses of negative polarity are more useful for flow control applications due to the increased pressure wave strength.

Benard et al.[21] also investigated the effect of pulse width on the electrical characteristics of the discharge and on the pressure wave formation. From this investigation it was discovered that pulse width has no impact on the energy deposited in the rising period of the pulse. However it did result in a decrease in deposited energy on the falling period, up to 40% depending on the pulse width used. It was shown that, as there are two current peaks for one pulse and the polarity of the current does not alter the topology of the pressure wave, each pulse generates two pressure waves. For smaller pulse widths both discharges are within the local acoustic time scale and thus both contribute to the same compression wave.[24] However, if the pulse width is made larger then multiple compression waves are visible as is shown in figure 5. This observation is important as it shows the possibility of using the actuator for control methods at different frequencies simultaneously.

Aba'a Ndong et al.[25] focus on characterisation of the geometric parameters of the ns-DBD actuator. The main parameters monitored to gauge performance were current and the energy per pulse per unit actuator length. The first variable investigated was the length of the actuator. It was found that increasing the length resulted in a decreasing current and thus a decrease in energy per pulse. The dielectric thickness was also varied from 120μm to 360μm. It was shown that, similarly to actuator length, increasing dielectric thickness led to a decrease in current and thus energy per pulse. The electrode spacing i.e. distance between the positive and ground electrode, was also investigated. This variable presented some interesting results where increasing the gap from 0 to 1 mm resulted in an increase in current amplitude which then decreased when the gap was increased to 2mm and 3mm. Figure 6 illustrates this trend. When the electrode gap is $\geqslant$ 1mm two current peaks are visible, i.e. the current waveform is composed of two components. There is the capacitive current which is a results of the change of voltage, and there is the discharge current which occurs when the surrounding air is ionised as a result of the applied electric field.[25] The reason for the increase in electrode gap separating the two components is that the increase in electrode gap reduces the electric field for the same applied voltage. Therefore the discharge current is delayed as a result of the slower ignition of the discharge due to the reduced electric field strength. It was also shown that between 6kV and 10kV the electrode gap of 1mm was the most effective. Further work is necessary particularly to examine the effect of the electrode gap as the trend shown appears to be rather unusual.

Zhao et al.[26] recently studied the shock generated by ns-DBD actuators both experimentally and computationally. They assume that the plasma region is "jump-heated", i.e. the heating process occurs too rapidly for the gas outside of the plasma layer to respond. Then assuming a constant volume for the plasma region during heating (appropriate as heating occurs on a much smaller time scale than the acoustic time scale), the blast wave generated is analogous to the bursting of a shock tube diaphragm. Therefore, from a Rankine-Huginot equation and the shock tube equation the temperature, pressure etc. of the plasma region can be calculated if the shock speed is known. The values calculated are then used as initial conditions for the 2D compressible Navier-Stokes equations solver used. Equations 2-4 are the three equations used by Zhao et al.[26] to calculate these initial conditions (subscript 1, 2

and s refer to ambient, post-heating and post shock properties):

$$u_s = a_1\left(\frac{\gamma_1 - 1}{2\gamma_1} + \frac{\gamma_1 + 1}{2\gamma_1}\frac{P_s}{P_1}\right)^{1/2} \tag{2}$$

$$\frac{P_2}{P_1} = \frac{P_s}{P_1}\left[1 - \frac{(\gamma_2 - 1)(a_1/a_2)(P_s/P_1 - 1)}{\sqrt{2\gamma_1}\sqrt{2\gamma_1 + (\gamma_1 + 1)(P_s/P_1 - 1)}}\right]^{-2\gamma_2/(\gamma_2 - 1)} \tag{3}$$

$$\left(\frac{\gamma_2}{\gamma_2 - 1}\right)\frac{P_2}{\rho_2} - \left(\frac{\gamma_1}{\gamma_1 - 1}\right)\frac{P_1}{\rho_1} - \frac{1}{2}(P_2 - P_1)\left(\frac{1}{\rho_1} + \frac{1}{\rho_2}\right) = q_h \tag{4}$$

where u_s is the shock speed, a is the speed of sound, P is pressure and γ is the specific heat ratio. Equation 2 allows the calculation of post-shock pressure ratio if the shock speed is known. From this pressure ratio the post-heating state pressure, P_2, can be calculated from equation 3. Finally, using this pressure, the heat addition as a result of the ns-DBD, q_h can be calculated from equation 4. Using both the experimental and computational data it was shown that the strength and speed of the generated shock could be controlled by altering the supply voltage. Increasing the supply voltage lead to an increase in shock strength and speed.

A study by Dawson et al.[24] confirms much of the conclusions made in the previous two studies by Zhao[26] and Aba'a Ndong.[25] The study confirms the effects of dielectric thickness and actuator length on energy per pulse and thus on pressure wave strength shown by Aba'a Ndong et al.[25] Dawson et al.[24] also confirm the conclusion from Zhao et al.[26] that increasing voltage increases the pressure wave strength. The qualitative nature of using image intensity to determine pressure wave strength is noted by the author. However measurements for all voltages studied were recorded in an identical manner, so quantitative results based on the relative results is believed to be valid. An area discussed by Dawson et al.,[24] that is not examined in the previous studies, is the influence of the actuator operating frequency. It was found that as the frequency was increased the gross power, the integration of absolute values of current and voltage, and power increased. This effect is attributed to a thermal transient in the system with a time constant large enough that all of the data captured are within it. This residual effect of heating is evident in figure 7. This plot shows the difference in gross energy per pulse obtained for the same range of frequencies depending on whether the results recorded go from low to high or from high to low frequencies. The effect of the

residual heating is evident by the increase in energy if the recording is taken at the end of a series of results compared to being taken at the beginning.

Further work is required to study the characteristics of ns-DBD's and to study the optimal design of such actuators. Little work has been published on determining the efficiency of ns-DBD's. There is scarce knowledge regarding how effectively ns-DBD's transform supplied electrical energy into heat energy in the flow, the source of the pressure waves. Therefore studies are needed that focus on the energy efficiency of the actuators, rather than their effectiveness for flow control.

3. Applications of ns-DBD

There have been a number of studies on the application of ns-DBD for flow control. Roupassov et al.,[17] Wu et al.[27] and Chen et al.[28] have all examined the use of ns-DBD actuators to control subsonic flow separation, using both experimental and computational methods. Figure 8 taken from Roupassov et al.[17] shows the improved aerofoil performance through the application of a ns-DBD plasma actuator. When the actuators are in operation it is clear that the lift force is increased (with an optimal frequency range of approximately 1-2kHz). This is due to the flow remaining attached, without the actuators the flow is separated. The slight increase in drag force is due to the turbulization of the boundary layer.[17] Wu et al.[27] and Chen et al.[28] both noted a similar performance improvement in their respective work.

Nishihara et al.[29] demonstrated that ns-DBD actuators can be used to alter the location of a shock generated by a wedge. Figure 9 illustrates the impact that the compression wave generated by the plasma has on the original baseline shock generated by the wedge. Their work showed an increase in shock angle. However with a different actuator location it may also be possible to decrease the shock angle which may be useful in some applications as shock angle is proportional to shock strength for a fixed incoming Mach number. Therefore the shock strength, for a given incoming Mach number, could be controlled by changing the angle of the shock wave. It was also noted that the generated shock wave excites oscillations in the flow. If the frequency of the excited oscillations can be matched to the instabilities in the flow this could be used to control the flow.

A further application that has been studied is the ability of ns-DBD's to increase the

shock stand-off distance for blunt bodies. This has benefits in improving the drag characteristics and reducing heat transfer. Nishihara et al.[30] demonstrated that this was possible by applying a surface ns-DBD plasma actuator to a cylinder in a Mach 5 flow (a schematic of the ns-DBD used for this experiment is shown in figure 10). They achieved an increased stand-off distance of the bow shock by up to 25%. A study carried out later by Bisek et al.[31] presented a comparison between experimental and numerical results for a configuration similar to Nishihara et al.[30] Both 2D and 3D simulations were carried out using an aerothermodynamic Navier-Stokes code. A phenomenological model of dissipative heating was used for the ns-DBD, meaning that the numerical model of the actuator was based on empirical observations and assumptions. An example of which is the assumption that all energy was deposited in the translational/rotational mode (based on previous work on rapid gas heating by Popov et al.[18]). The heating model was included in the Navier-Stokes equations through a source term, S, as seen in equation 5:[31]

$$\frac{\partial E}{\partial t} + \Delta \cdot ((E+p)\mathbf{u} - \boldsymbol{\tau} \cdot \mathbf{u} + \mathbf{q} + \sum (\mathbf{J}_{sp} h_{sp})) = S \tag{5}$$

where E is the total energy per volume, $\boldsymbol{u}$ is the mass averaged velocity, $\boldsymbol{\tau}$ are the viscous stresses, $\boldsymbol{q}$ is the total heat flux, $\boldsymbol{J}_{sp}$ is the species diffusion flux and h_{sp} is the species enthalpy. The value of S was determined from various observations made regarding the plasma generation such as: the cylindrical shape of the generated plasma and the concentration of the plasma in the cylindrical region. These observations led to a hyper-Gaussian distribution function being used to generate a near uniform energy deposition rate within the cylindrical discharge volume see equation 6:[31]

$$S = \frac{Q}{Kabc} exp\left(- \left|\frac{\hat{r}}{a}\right|^{\xi} - \left|\frac{\hat{\theta}}{b}\right|^{\eta} - \left|\frac{\hat{z}}{c}\right|^{\zeta} \right) \tag{6}$$

where Q is the total energy deposited, ξ, η, ζ are deposition density parameters, K is a constant based on the values of ξ, η, ζ, the cylindrical coordinate system used is defined by $\hat{r}, \hat{\theta}, \hat{z}$ and a, b, c define the deposition volume. The first, 2D, computations had large discrepancies when compared with the experimental data. Thus a 3D numerical model was created and solved in an attempt to determine the source of the discrepancy. It was found that due to the thick boundary layer and small tunnel test section, the inviscid, core supersonic flow area shrunk and thus the velocity slowed. This led to an increase in static

pressure after the shock wave. This effect was clearly not apparent in the 2D model and was only realised in the 3D computations.

Im et al.[32] investigated the possibility of controlling the turbulent boundary layer in a model of an inlet duct at Mach 4.7. Using a low power input, one of the benefits of ns-DBD's compared to other energy deposition based flow control methods, they demonstrated that it was possible to control the boundary layer thickness and regularity. As stated by Curran,[33] the boundary layer characteristics play an important role in the efficiency and unstart characteristics of a ramjet/scramjet. Therefore the work by Im et al.[32] demonstrates that there is a distinct possibility of using ns-DBD's to aid in the efficient and safe operation of future ramjets/scramjets.

4. Future Work on ns-DBD's

There has clearly been great interest in ns-DBD's in recent years due to their application to high-speed aerodynamics in areas such as SBLI control and drag reduction. Although the research carried out has been wide ranging, there are some aspects which have not been studied and can provide significant insight. The first is the use of 2D actuator designs instead of the standard linear 1D actuator. There has been significant research in this area for standard AC-DBD actuators at low speeds.[34–41] These studies have shown that 2D actuators create an out-of-plane velocity component that does not exist with 1D linear actuators. This out-of-plane velocity enhances mixing in the region which could prove useful for a number of applications e.g. plasma assisted combustion. However as ns-DBD's function in a different manner to standard AC-DBD's the benefits of using 2D actuators is unclear and thus requires further study.

Another area of novel research that applies both to AC-DBD's and ns-DBD's is the use of multiple encapsulated ground electrodes.[42–46] These actuators involve the use of multiple ground electrodes "buried" at various depths in the dielectric, see figure 11. The benefits of these DBD designs for standard AC-DBD's is that studies have shown an increase in the achieved induced flow. However, ns-DBD's do not generate an induced flow but instead control the flow by pressure waves. Thus it is unclear if these multi encapsulated electrode designs could be a beneficial design for their operation. It may be possible, for example, that using multiple electrodes could produce a front of multiple, discrete pressure waves which

could be used to control bow shocks.

A further area of research that has been conducted for AC-DBD's is the development of multi-barrier plasma actuators (MPBA).[47,48] These are DBD plasma actuators formed of multiple layers of dielectric and electrodes. It was shown that, for the same surface area between the edge of the exposed electrode and the furthest edge of the bottom electrode, an MPBA would have a higher thrust to power consumption ratio than that of a standard, one dielectric barrier, two electrode DBD design. Although, as mentioned above ns-DBD plasma actuators operate in a fundamentally different way to AC-DBD's, it would be interesting to examine the effect of this actuator configuration on its performance. For application to both AC-DBD's and ns-DBD's further work is necessary to better understand the limitations of this technique with regards to how many layers could be used. The later study by Durscher et al.[48] provides an initial look into this which suggests the initial MBPA design with just one additional electrode was most effective. However further research should be carried out to determine categorically the best design for an actuator using this concept.

Finally, an area where very little work has been carried out is on the impact of external factors on the performance of ns-DBD actuators. Most studies have been conducted at ambient conditions. It has been shown in the work carried out for AC-DBD actuators that factors such as atmospheric pressure,[49,50] surface temperature[49,51] and shock wave interaction[52] influence the actuator performance. There is little to no current research available on the impact these types of parameters have on the performance of ns-DBD actuators.

B. Localized Arc Filament Plasma Actuators

Localised arc filament plasma actuators (LAFPA's) are a recently developed category of surface plasma actuators. These actuators operate by either manipulating instabilities in the flow through pressure disturbances or through the generation of streamwise vorticity caused by localised Joule heating. They were originally developed at Ohio State University by Samimy et al.[53] These actuator control the flow using the same concept as the other surface plasma actuator technologies, rapid heating of the fluid due to the pulsed electrical discharges i.e Joule heating. This rapid heating results in the formation of pressure waves that impact the flow field. This pressure wave results from the thermal heating of the initial air breakdown. The resistance across the air gap between the electrodes (see below) is much

greater at this point than after breakdown and therefore, from Joules first law, the heat released will be much greater as it is proportional to the resistance. The actuator design itself is simply a pair of electrodes separated by an air gap, often tungsten to minimise erosion caused by high temperatures, that protrude from the surface into the flow. These electrodes are connected to a high voltage and high frequency power supply. In initial studies by Samimy et al.[53] it was determined that without shielding from the flow, the plasma would be stretched and blown off during each discharge. To prevent this phenomenon a simple groove was cut 1mm deep to house the actuators (see figure 12). From plots of the measured voltage before and after the addition of the ring groove it was seen that the groove prevented the plasma from being blown off when the AC voltage is at a minimum.

In the first papers available on LAFPA's, the actuators performance was characterised for a number of variables. Samimy et al.[53] showed that although the plasma behaviour itself is similar at high input frequencies, there is a reduction in peak voltage and current. This was thought to be because of the reduction in time between voltage peaks resulting in less plasma decay between peaks. This in turn results in a smaller breakdown voltage required. It was also found that the relationship between the forcing frequency (frequency at which actuators produce plasma discharge) and supply frequency was dependant on the magnitude of the supply frequency. At the original supply frequency of 10kHz, breakdown occurred at both the positive and negative peaks of the supply frequency resulting in a forcing frequency twice that of the supply. However at the higher frequency examined, 20kHz, plasma only formed at the negative peaks resulting in a forcing frequency equal to that of the supply. The authors do not provide any explanation for why this may be the case at higher frequencies. Parallels could be drawn however with the previously discussed NS-DBD actuators however. As discussed previously Takashima et al.[23] showed that, for NS-DBD actuators, higher frequency exaggerated the filamentary nature of the discharge more so for negative than positive polarity pulses. Although these technologies have different operating principles it seems these two studies show trends somewhat similar in nature. Samimy et al.[53] also compared the power consumption at different frequencies with and without the groove to house the actuator electrodes. As expected, at lower frequencies, the ring groove results in a significant reduction in power consumption. However at higher frequencies, above 30kHz, the power consumption for both cases converge to that of the no-flow case as there is not enough time between AC current peaks for the plasma to be

"blown off" of the electrodes.

A later study by Utkin et al.[54] provided more insight into the effect of the supply voltage on the actuator performance. Part of the study involved the examination of the effect of frequency and pulse duration have on performance. Temperature measurements of the plasma were carried out by measuring emission spectra of partially rotationally resolved nitrogen. This is a valid measure of actuator performance as it is known that the primary medium for flow control by these actuator originates from rapid heating of the flow. The first conclusion made was that a higher value for supply frequency resulted in greater temperatures. This conclusion is based on two results, the first is the emission spectrum shown in figure 13. A much higher intensity peak is visible at the wavelength corresponding to Tungsten, 400.8nm, at 20kHz than at 5kHz supply frequency. This indicates a greater level of electrode erosion at the higher frequency which is a result of higher temperatures. Another set of results that indicates the same conclusion is figure 14 which shows the effect of pulse duration on plasma temperature for a supply signal of both 5kHz and 20kHz. The general trend can be observed that the temperature at 20kHz is significantly greater than at 5kHz. This trend is likely due to the reduced time for cooling between discharges at higher frequencies. Utkin et al.[54] also concluded that based on figure 14, the temperature sharply rises as pulse duration is increased from 4 to 20μs, so convective cooling by the flow is insignificant at these durations. However the stagnation of temperature from around 20 to 100 μs indicates that it is a factor for greater pulse durations. However, it is worth noting that the frequency was not kept constant for all pulse durations which may have had an impact on the results.

The dashed line in figure 14 demonstrates the results of a simple, unsteady, quasi-one-dimensional arc filament model. The arc filament is modelled as a uniform square wave heat source (similar in description to the power signal dissipated by the actuator) confined to a cylindrical region. The model assumes that, for short pulse durations the effect of the flow on the filament can be ignored due to it being "shielded" by the ring groove. The model is used to estimate the pressure and temperature rise produced by the filament. The arc filament model is included in the compressible, unsteady Navier-Stokes energy equation. The final term of equation 7 is the term that accounts for the arc filament:

$$\rho c_v \frac{\partial T}{\partial t} + \rho c_v u \frac{\partial T}{\partial r} = \frac{1}{r}\frac{\partial}{\partial r}\left(r\lambda\frac{\partial T}{\partial r}\right) + 2\mu\left[\left(\frac{\partial u}{\partial r}\right)^2 + \left(\frac{u}{r}\right)^2\right] - P\frac{\partial u}{\partial r} + \frac{UI}{\pi r_0^2 L} \tag{7}$$

where ρ , u, T and P are density, radial velocity, temperature and pressure respectively. r is the radial coordinate, c_v is the specific heat of air at constant pressure, μ is the viscosity of air and λ is the thermal conductivity of air. U is the arc voltage, I is the arc current, r_0 is the filament radius and L is the arc length. The dashed line in figure 14 shows a comparison of the results obtained from experiment and those obtained from the model. Although each specific result does not necessarily correlate well with the model, the general trend of the model at low pulse durations follows the expected trend from the experimental data.

Figures 15a and 15b show the radial pressure profiles for various times after the initial sparking of the arc filament at two different conditions. Figure 15a shows the pressure profile with the actuator active the entire time while 15b shows the profile when the actuator is turned off after 5μs. It is observed that the pressure wave at 10μs is identical in both cases, illustrating that the discharge being terminated before this time did not have a negative effect. The reason for this is that the wave at 10μs is weakly supersonic (observe the steep gradient of wave) and so is not "aware" of any changes to the flow field behind it. To further investigate this effect more lengths of discharge need to be investigated to determine the optimal pulse duration.

The study by Hahn et al.[55] provides some insight into the impact of the groove that was added in the previous work to stabilise the plasma filament. In this study a new nozzle was designed similar to that of the previous work[53] except that the LAFPA's were located at the downstream face of the nozzle and the ring groove was removed. The performance of both nozzles was examined through application to the control of a high speed jet (discussed in more detail later). The LAFPA's effect on jet mixing was the objective of the investigation. This was monitored in a number of ways: centreline Mach number, jet width, centreline turbulent kinetic energy (TKE) and also overall sound pressure level. The findings will be discussed in detail later. The effect of pulse width on actuator performance was studied in depth. The authors performed a comprehensive study of pulse width effect on the level of actuator control at a single frequency (a potential problem with the previous study was the use of multiple frequencies). They used the jet centreline Mach number as a measure of actuator control (the significance of this variable is explained in the next section). Figure 16 provides a plot illustrating the effect of pulse width on jet centreline Mach number. It demonstrates how lower pulse widths result in a lower centreline Mach number i.e. increased mixing in the jet which, in this case, was the aim. From this result the author suggests that

this implies the initial arc formation process is the key to the LAFPA control method. This is because it is at this point, when the resistance to the electrical signal is largest, that the most energy is dissipated into the flow. The author does however point out that these results alone are not enough to confirm this hypothesis.

1. Applications of LAFPA's

Using LAFPA's for flow control has been investigated in depth for two fluid flow phenomena in particular: high-speed jets and SBLI's.

The first investigation of LAFPA's for high-speed jet control was in by Samimy et al.[53] It was suggested that the actuators could exert control over the flow in one of two ways: streamwise vorticity generation or forcing the jet at an instability frequency. Streamwise vorticity generation was previously identified as a means for controlling the mixing[56] and noise characteristics[57] of high speed jets. However, these methods involved the use of tabs on the surface of the nozzle. These introduce blockages which reduce thrust and also do not provide optimal performance at off-design conditions. Forcing the jet at a frequency related to one of the jet's instabilities has been carried out at high subsonic speeds[58] however, due to the requirements for high amplitude and high frequency excitation, this control method has not been successfully applied to supersonic jet control. The study by Samimy et al.[53] was the first carried on the subject and such the analysis of its application is fairly limited. The authors did manage to show, qualitatively, that the LAFPA's did increase mixing.

A later study by Samimy et al.[59] provides more in-depth analysis of the control of high-speed jets using LAFPA's. In this study the source of the jet is a Mach 1.3 converging-diverging nozzle with an exit diameter of 2.54cm. The power supply connected to the actuators was designed in such a way that it was capable of supplying the large spike in voltage necessary for initial breakdown at the beginning of each pulse but would also maintain a steady current of approximately 0.25A after breakdown. The actuator setup was capable of operating at a variety of azimuthal modes however this study limited itself to the modes m = 0,1 and ±1. The modes can be described in simple terms with reference to figure 17. For m = 0, all actuators are operated at the same time. For m = 1, actuators operate with a phase delay of $m(\frac{360}{8})^\circ$ between neighbouring actuators. Finally for m = ±1, actuators 1,2, and 8 operate at the same time and actuators 4-6 operate at the same time

but 180° out of phase with 1, 2 and 8. Actuators 3 and 7 are node points in this azimuthal mode which mean they always have a magnitude of zero i.e. the actuators are turned off. Equation 8 provides a mathematical formula for the amplitude of each actuator, A_a, which is dependant on the mode the system is being operated in:

$$A_a = A_o g(2\pi f_F t - m\phi_a) \tag{8}$$

where $A_o$is the amplitude, f_F is the forcing frequency, t is the time, m is the azimuthal model and ϕ_a is the azimuthal location of the actuator, a. $g(t)$ is a step function based on the duty cycle where $g(t) = 1$ if $0 < 2\pi f_F - m\phi_a < 2\pi\delta$ and $g(t) = 0$ if $2\pi\delta < 2\pi f_F - m\phi_a < 2\pi$. The first variable examined was the effect of forcing frequency on the jet mixing characteristics. Figure 18 presents instantaneous images taken of the laser light scattered by the jet at 5 different forcing frequencies. The images only shows the mixing layer as the scattering of the laser sheet is done by the condensation of particles from the warm ambient air entrained into the cold, dry jet. It is clear that the most significant impact is visible when the frequency is set at 5kHz which corresponds to a Strouhal number of 0.33. Another set of results presented was of the effects of forcing mode on the mixing characteristics. Figure 19 shows the phase-averaged image for each different forcing mode, m = 0,1 and ±1, based on 30 phase-locked images. As expected the asymmetric mode, m=0, has symmetrically aligned (vertically/radially) structures in the jet while the helical, m=1, and flapping, m=±1, modes have vertically staggered structures. PIV quantitatively confirmed these results by measuring the jet centreline Mach number and the jet centreline Turbulent kinetic energy. Therefore it was shown that forcing the jet at the preferred-mode Strouhal number with the flapping azimuthal mode was the most effective at enhancing mixing.

Hahn et al.[55], also examined the influence of LAFPA's on high speed jets. As discussed previously, part of this work was investigating the impact of the ring groove on the operation of LAFPA's and also the effect of supply voltage pulse width. However they also present some interesting results of the effects of LAFPA's operation on jet mixing characteristics and the impact on far field noise levels. Their findings agreed with those of Samimy et al.[59] They also corroborated that the flapping mode is more effective at enhancing mixing than the asymmetric mode. It was also shown that using higher forcing frequencies resulted in a

delayed decay of the centreline Mach number in comparison to the baseline case. This in turn leads to a reduction in far field noise levels. Figure 20 presents a more in-depth representation of the impact that Strouhal number has on noise levels. The figure shows the average acoustic energy dependency on Strouhal number. Average acoustic energy is an average of the overall sound pressure level that was measured by an array of microphones. The results collected for two different modes are shown and it demonstrates that the difference to the noise levels for the modes shown is minimal, although m = 3 is marginally more effective for noise reduction. The main point to take from figure 20 is the noticeable reduction in noise achieved when forcing with higher Strouhal numbers. From the presented data it seems that the reduction appears to stagnate as it approaches a Strouhal number of 3. However more data is necessary for any conclusions to be made on the limitations of the maximum noise reduction. Other studies by Samimy et al.[60,61] also confirm the findings related to noise mitigation. These studies[60,61] indicated however that the azimuthal mode m = 3 is significantly more effective for noise mitigation than m = 0. Hahn et al.[55] made the same conclusion however the differences seen when using each of the different modes were less significant.

Another topic for the application of LAFPA's is the control of SBLI's. This topic was first considered by Caraballo et al.[62] The interest of the study was in the manipulation of SBLI's. It was initially suggested that the mechanism for control was two-fold. The first was the generation of streamwise vorticity in a similar manner to that of micro ramps[63] or tabs.[64] The second is the manipulation of the unsteadiness apparent in SBLI using the broad frequency range capability of LAFPA's. Dupont et al.[65] showed that the upstream leg of a lambda shock wave oscillates at a Strouhal number of 0.03 while the downstream leg oscillates at a Strouhal number of 0.5. These frequencies are easily achievable by LAFPA's. There were two factors examined that had an impact on the effectiveness of the control method: actuator location relative to the SBLI and frequency of the actuator operation. A number of locations were considered but only the results of the two most interesting were presented. They were directly upstream and slightly downstream of the SBLI. Figures 21a (upstream locaion) and 21b (downstream location) demonstrate the effect that the location of the actuators have on performance. It is clear that the upstream location has a more significant impact than the downstream location. Figure 22 illustrates the increase in boundary layer velocity seen when the actuators are operated at a Strouhal number of 0.03 compared to

the baseline case and the actuators being forced at a Strouhal number of 0.5. The authors concluded that it was the unsteadiness of the upstream leg of the λ-shock that was controlled by the LAFPA's. This is based on the greater impact the actuators had operating at the oscillation frequency of the upstream leg, St = 0.03, than that of the downstream leg, St =0.5. However this requires further investigation as the actuators were not operated at the higher frequencies in the downstream position, which is closer to the downstream leg of the SBLI. The other conclusion was that the upstream position of the actuators was much more effective at altering the flow conditions. The first conclusion would appear to reinforce this as the manipulation of the unsteadiness of the SBLI will be effective closer to the shock impingement. Also, previous work on LAFPA's[59] has shown that they are ineffective when located in a separated region. This would suggest, as the results suggest, that the downstream location would be an ineffective choice for actuator location.

A more recent study by Webb et al.[66] expands on the previous work by Caraballo et al.[62] on the use of LAFPA's for SBLI control. The interesting outcome of this work is that there are noticeable disagreements in the conclusions drawn from the two studies. Webb et al.[66] found that the impact on the SBLI region was simply to shift it upstream. This is a somewhat different conclusion to Caraballo et al.[62] who suggested that actuation by LAFPA's increased the boundary layer velocity. Webb et al.[66] and Caraballo et al.[62] also disagree on the mechanism of control itself. Caraballo et al.[62] suggested that the excitation of the SBLI unsteadiness was the main mechanism however Webb et al.[66] suggested that simply the heating of the boundary layer is the control mechanism. Compelling evidence presented in the study supports the conclusion of Webb et al.[66] Firstly, there was no significant "peak-effectiveness"[66] frequency observed within the range $f_F \leqslant 1.5$. This suggests that forcing the SBLI at its natural frequencies was not a factor in the control. Secondly, the actuator location upstream of the SBLI had little significant impact on its performance. When attempting to excite an instability or natural frequency, the region of excitation is an important factor in its effectiveness. Therefore it was suggested that heating the boundary layer was the mechanism for control as it has been shown in previous work by Jaunet et al.[67] that heating the boundary layer upstream of a shock wave will result in its upstream movement. Therefore based on these two studies it is clear than LAFPA's can have a noticeable effect on SBLI's. However more research is necessary to better understand the mechanism of the control they exert on the flow.

The final application discussed here is for supersonic cavity flows due to the proposed usage of cavities for supersonic combustion and isolator unstart delay/prevention in scramjets. Previous studies using different types of flow control[68–70] have shown this can produce promising results. There has been some interest in the application of LAFPA's to augment the shear layer resonance of supersonic cavity flows. Webb et al.[71,72] investigated this application. The objective of these studies was to augment the shock-trapping capabilities[73] of cavities within a supersonic isolator. In order for the system to be robust it must be able to both enhance the resonance characteristics of a weakly resonating cavity whilst also being able to suppress the resonance characteristics of a strongly resonating cavity. This is done by attempting to excite/suppress the natural shear layer (Rossiter) resonance characteristics of the cavity. Webb et al.[71,72] showed in both cases that this was possible and could be effective. However more work is necessary to improve the understanding of how this mechanism works.

2. Future Work on LAFPA's

From the aforementioned discussion, there are clearly many useful applications for LAFPA's, however there is still a great deal of scope for future research and improvements.

More investigations are necessary to better understand the performance characteristics of LAFPA's for high-speed flow control applications. Studies need to be undertaken on the impact of increasing/decreasing the energy that is deposited into the flow. As it has been suggested in the body of the work discussed, the majority of the energy deposited into the flow is a result of the initial spark, very short nanosecond pulses should be examined to better understand the impact of pulse durations.

For application to SBLI's and supersonic cavity flows, further study is required to gain a better understanding of the fundamental effects on the flow. Particularly for the application to cavity flows, flow visualisations such as Schlieren photography and PIV would help to provide a better understanding of the impact the actuators have on the flow.

C. Pulsed Plasma Synthetic Jets

Pulsed plasma synthetic jets (PPSJ) are another type of joule heating flow control device that were originally developed by Cybyk et al.[74] in 2004. The devices control the flow either by the generation of a "hot spot" in the flow or through the re-energising of the boundary layer. These devices come under the classification of being a "synthetic jet actuator".[75] They can be considered as a further evolution of synthetic jet actuators because they involve no moving parts such as pistons or oscillating diaphragms common to previous designs.

A schematic of a simple PPSJ layout is given in figure 23. The basic principle is to use high voltage electricity (typical values range from 2kV to 5kV) between two electrodes to generate a high temperature plasma in a small cavity. The expansion of the gas inside the cavity due to the heating causes a plasma jet to exit at high speed into the flow (depending on the design, initial jet speeds of approximately 450m/s have been reported[76]). The exit of the jet from the cavity leads to a pressure reduction inside which consequently draws air into the cavity, refilling it ready for the next pulse.

PPSJ's function using the same physical principle as the ns-DBD i.e. Joule heating. The two electrodes (see figure 23) are supplied with a high voltage which electrothermally heats the gas (see section on nanopulse DBD plasma actuators for more details). This heating of the plasma increases the pressure of the gas and forces it out of the orifice located at the top of the cavity.

There are a number of different design parameters that have been studied relating to the performance of PPSJ type actuators. One variable is the geometry of the actuator. Wang et al.[77] investigated the possibility of adding a third "trigger" electrode to the standard actuator (see figure 24 for location of trigger electrode). The reasoning for the inclusions of a trigger electrode is that it allows an increase in the electrode gap without increasing the discharge voltage. It does so by providing a trigger spark between it and the anode in order to pre-ionise the air. This is important as based on Paschen's law (see equation 9),[78] the breakdown voltage is related to the electrode gap:

$$V_B = \frac{apd}{ln(pd) + b} \tag{9}$$

where V_B is the breakdown voltage, a and b are constants dependant on the gas composition and d is the gap distance in meters. The larger electrode gaps are necessary in order to use

larger cavities which in turn are necessary to increase the momentum of the jet created.[77] However, a previous study by Popkin et al.[79] suggested a more efficient manner of introducing a trigger spark. This involved the use of just two electrodes and utilising the anode as the trigger electrode. This was found to improve the efficiency of the actuator drastically e.g. a jet of the same velocity as the actuator using the third "trigger" electrode design was generated using only approximately half of the stored power (based on the capacitance used).[79] Figure 24 provides a visual representation of the reason behind this increase in efficiency. It is clear that the trigger spark, labelled on the figure, pre-ionises a larger area in the pseudo-trigger design than the external trigger design. This in turn allows the electrodes to be even further apart than for the external trigger design which, as already explained, is beneficial to the effectiveness of the actuator. Another benefit of increasing the gap between electrodes is that the spark generated is in contact with more of the air inside the cavity. As there is more contact between the spark and the air inside the cavity thermal conduction increases. The improvement to the conduction characteristics will cause an increase in fluid temperature compared to the original design. This in turn increases fluid pressure leading to an increase in jet velocity. Therefore the overall efficiency of the actuator is improved as the jet velocity achieved is larger for the same input power.[79] Emerick et al.[76] confirmed the findings of Popkin et al.[79] by showing that there was a noticeable improvement to the jet and blast wave velocity when using a pseudo-trigger, figure 25 illustrates this behaviour. The data plotted for the blast wave (triangle markers) shows that although both configurations have the same initial blast wave speed, the blast wave speed for the external trigger falls to approximately 50m/s slower than that of the series trigger. For the jet itself, the initial speed is actually greater when using an external trigger however, approximately 14μs after the initial discharge the jet speed drops below that of the series trigger and remains below it for the remainder of the discharge. Hence figure 25 illustrates that the series trigger results in increased jet and blast wave velocity for the same electrical input.

Sary et al.[80] performed a numerical parametric study examining the various operational and geometric variables in order to further optimise the actuator. The model includes a number of assumptions, such as inviscid flow, which may limit its accuracy. However, the results were compared with experimental data from a number of other studies[79,81,82] and they were found to be comparable. This indicates that although the model has limitations due to the assumptions made, it can still provide insight into the major flow features. From

this study it was shown that the temperature increase creates a somewhat limiting factor on operating frequency. This is due to a less efficient refill caused by the increased temperatures at higher frequencies. However it was noted that the model used a constant breakdown voltage, in reality this would decrease as the air in the cavity increased in temperature. Narayanaswamy et al.[83] also observed that there is a limit on the frequency used due to the actuator beginning to miss pulses at higher values. The geometric features examined by Sary et al.[80] were the neck radius i.e. radius of the jet exit orifice, and the shape of the neck, namely the angle of the neck from the horizontal (see figure 26). This study was carried out using a numerical model split into two submodels. The first model is coupled to the resistance-inductance-capacitance (RLC) series circuit equations that model electrical supply from an external generator.[80] Equation 10 shows one possible form of the series RLC equation:

$$v(t) = RI(t) + L\frac{dI}{dt} + \frac{1}{C}\int_{-\infty}^{t} I(t)\,\mathrm{d}t \tag{10}$$

where $v(t)$ is the voltage, R is the resistance, I is the current, L is the inductance and C is the capacitance This sub model models the energy deposition through electrical arcing while ignoring the cavity. This model gives information on the energy distribution from the spark which can be used as a source term for the fluids model. The second submodel is a fluids model using 2D euler equations (see equation 11[80]). From the source term (heating due to high voltage spark), effects on the actuators mass flow rate, momentum and jet characteristics can be calculated.

$$\frac{\partial}{\partial t}(r\mathbf{U}) + \frac{\partial}{\partial r}[(r\mathbf{F}(\mathbf{U})] + \frac{\partial}{\partial z}[(r\mathbf{G}(\mathbf{U})] = \mathbf{S} \tag{11}$$

$$\mathbf{U} = \begin{bmatrix} \rho \\ \rho v_r \\ \rho v_z \\ \rho E \end{bmatrix} \mathbf{F}(\mathbf{U}) = \begin{bmatrix} \rho v_r \\ \rho v_r^2 + p \\ \rho v_r v_z \\ v_r(\rho E + p) \end{bmatrix} \mathbf{G}(\mathbf{U}) = \begin{bmatrix} \rho v_z \\ \rho v_r v_z \\ \rho v_z^2 + p \\ v_z(\rho E + p) \end{bmatrix}$$
$$\mathbf{S} = \begin{bmatrix} 0 \\ p \\ 0 \\ r\sigma E_e^2 - rU_{rad} + rS_{diff} \end{bmatrix} \tag{12}$$

where r and z refer to the cylindrical coordinate system, the $r\sigma E_e^2$ term represents the Joule heating source and U_{rad} represents the radiative energy losses. Assumptions are made to simplify the model such as ignoring viscosity in the actuator among other things. Larger neck sizes were found to improve refill efficiency however the jet velocity was decreased, proposed to be a result of less intense pressure gradients at the neck. A study of 3 different neck shapes was carried out,[80] see figure 26 for illustration of geometries, to investigate the effect on actuator performance. With a converging neck the refill of the cavity was found to be more efficient. However the mean temperature was found to rise due to a change in the flow dynamics inside the cavity caused by the change in shape. This study by Sary et al.[80] provides interesting insight into the design of the actuator however the conclusions made should be taken with caution as the model is somewhat limited by its assumptions and thus experimental data is needed to validate.

The effect on the actuator performance from the energy dissipation rate was studied by Belinger et al.[84] They considered an inductive power supply (IPS) and a capacitive power supply (CPS). The capacitive source caused a fast energy discharge while the inductive supply created a slower energy discharge. As the discharge is slower for the IPS the gas is expelled during the discharge such that later in the discharge the ceramic material of the cavity is heated more. This is not the case with the CPS based source as this resembles more a spark discharge with a very high energy dissipation rate. The main point of note regarding the energy dissipation rate is that the faster the rate of dissipation a more powerful jet is created, thus the CPS source produces a more powerful jet. The efficiency of the actuator could be increased more if a power supply of nanopulse in duration was used as this would increase the dissipation rate even more leading to a more powerful jet. Belinger et al.[85] carried out further work solely on a CPS based actuator in order to further investigate its properties. They found that the discharge was very conductive and so the current increased rapidly. Due to the current being in phase with the discharge voltage, the discharge could be modelled using a constant resistance. The constant resistance is calculated from equation 13.[85] This simple model could be used to explain some details of the discharge however it is not applicable to the beginning and extinction of the discharge. This is because at these

points the resistance of the discharge changes due to the changes in conductivity.

$$R_{Discharge} = \frac{2L_{wire}}{\tau} - R_{wire}$$
$$\tau = \frac{T}{lnV_1/V_2} \tag{13}$$

where $R_{Discharge}$ is the resistance of the discharge itself, L_{wire} and R_{wire} are the inductance and resistance of the wire respectively, τ is a damping coefficient and T is the period between the two voltage peaks V_1 and V_2. Emerick et al.[76] showed that the jet velocity created by the PPSJ increases with lowering atmospheric pressure. This indicates that the PPSJ may prove more effective at higher altitudes where the ambient pressure is lower. However the lower density air may counteract this increase, it was not shown by Emerick et al.[76] whether or not this was the case and so further research of this is necessary.

1. Applications of PPSJ's

Narayanaswamy et al.[86] attempted to use an array of PPSJ's for SBLI control at Mach 3. It was shown that the position of a separation shock upstream of a ramp could be controlled using an array of PPSJ actuators. At the jets pulse, the shock wave moved upstream followed by a slower downstream "relaxation" period. It was observed that the movement of the shock was locked to the pulse frequency. Therefore if a PPSJ could be designed to pulse even faster (nanosecond pulses) there could be assumed to be a quasi-steady control of the shock location. The mechanism by which the pulsed jets control the shock location is thought to be due to the jets effect on the separation bubble itself. The upstream motion is explained by the "hotspot" theory.[87] This is because the high temperature jet results in an increase in the local speed of sound (see equation 14) which in turn results in a decrease in Mach number:

$$a = \sqrt{\gamma RT} \tag{14}$$

where a is the speed of sound, γ is the specific heat ratio and R is the ideal gas constant. From compressible gas dynamics equation 15 is known to be correct:

$$\frac{\rho_2}{\rho_1} = \frac{(\gamma+1)M_1^2}{(\gamma-1)M_1^2+2} \tag{15}$$

where M is Mach number. From equation 15 it is clear that with decreasing Mach number the density ratio across the shock wave decreases. It has also been shown in the past by a

number of studies[88–90] that shock stand-off distance, Δ, is proportional to the inverse density ratio across the shock:

$$\Delta \propto \frac{\rho_1}{\rho_2} \tag{16}$$

Therefore, with decreasing Mach number, density ratio across the shock decreases and, as stand-off distance is proportional to the inverse of the density ratio, shock stand-off distance will increase. This movement upstream of the separation shock also causes the separation bubble to "grow" upstream as is observed in figure 27. It was proposed that the slower downstream motion of the separation shock is due to the longer time-scale by which the separation bubble moves back downstream after the pulsed plasma jet. The importance of the actuator location was also shown in their study with the actuator placed upstream of the separation bubble there was a significant change to the separated flow dynamics. However the actuator placed in the separation bubble had little effect on the separated flow dynamics.[86]

Anderson et al.[91] presented a computational study of plasma synthetic jets. An analytical solution for a single pulse plasma synthetic jet actuator was considered. Using two-dimensional CFD they proved the accuracy of the one dimensional analysis. This could therefore be used as a tool in design in the future. They went further with the study and examined the effectiveness of a pulsed plasma synthetic jets as a replacement for mechanical flaps on aircraft. Using an "effectiveness" parameter, η, that was defined as the ratio of pitch rates of the two actuators (see Eq (17) where $\frac{d\theta}{dt}|_{PJ}$ is the pitch rate of the PPSJ and $\frac{d\theta}{dt}|_{aero\ surface}$ is the pitch rate of the mechanical actuator) they compared the performance of the two actuators.

$$\eta = \frac{\frac{d\theta}{dt}|_{PJ}}{\frac{d\theta}{dt}|_{aero\ surface}} \tag{17}$$

After further manipulation of Eq (17) they achieved an analytic relation plotted in figure 28. This plot illustrates how the perceived effectiveness of the actuator changes with Mach number and energy deposited. For example it shows that the most effective case is high values of deposited energy and low Mach numbers and the least effective case is at low values of deposited energy and high Mach numbers. There are however limits on the flow control application that can be concluded from this study, based on the assumptions. The first assumption of concern is that the authors state the calculations only consider the

period of a single discharge of a PPSJ. Therefore it does not account for the losses in performance caused by repeated pulses of the actuator. Secondly, there is no validation of the CFD model mentioned in the paper. Therefore although the study presents interesting conclusions, further work is required to confirm the findings by considering the impact of multiple pulses and through better validation of the results.

Jin et al.[92] investigated the possible control effects of a PPSJ in a supersonic, Mach 2, flow. They showed, experimentally and numerically, that the plasma jet penetrates the boundary layer. Figure 29 shows both the experimental and numerical results. The oblique shock wave present in both sets of results is proof that the jet is capable of penetrating the supersonic boundary layer. From the numerical results plots of pressure and density downstream of the actuator are presented. Figure 30 shows the pressure and density plots which presents the impact of the pulsed plasma synthetic jet on the boundary layer downstream of the actuator. The dip in static pressure illustrates the momentum increase in the boundary layer as dynamic pressure has increased.

PPPSJ's are a promising technology for flow control. However further research is still required to better understand some of their characteristics such as the potential limitations of the actuator when operating at higher frequencies. This is a key element of the actuators operation if it is to be used to maintain the position of a shock wave for instance.

2. Future Work on Pulsed Plasma Synthetic Jets

These actuators have shown their capability to affect supersonic flows, particularly in the control of SBLI's.[86,92] However, based on the reviewed literature there are some areas that are important for the future development of these actuators and require further study.

One area of interest is the frequency limitation imposed by thermal effects of the discharge. It has been noted that, with continuous use, increasing temperatures can slow the refill time of the actuator cavity and thus place an upper limit on the operating frequency.[80,83] Depending on the scenario, higher frequencies may be a necessity for future applications e.g. position control of oscillating shock waves in high speed intakes. Therefore work needs to be done to determine precisely the frequency limitations with current models and, if possible, design new actuators that increase the maximum achievable frequencies.

The operating conditions of the actuators are another area which requires further research.

Emerick et al.[76] suggest that at lower ambient pressures these actuators produce a higher jet velocity indicating that at higher altitudes they may experience improved performance. However, as noted by the authors, the lower density at higher altitudes may counteract its impact due to the reduction in momentum. This is just one example of the impact the atmospheric condition may have on the performance of PPSJ's. Parameters such as temperature, flow speed and density could all have an effect on the operation of these actuators. Therefore detailed studies still need to be carried out to determine the effects of atmospheric parameters such as those mentioned above on the performance of the PPSJ actuators.

Finally, although there have been studies carried out on the effects of actuator geometry on performance,[76,77,80] no definitive criterion for the most efficient/effective actuator design has been proposed.

D. Laser Generated Plasma

Laser induced gas breakdown was first observed by Damon et al.[93] in 1963. Laser energy deposition control flows either through the interaction of generated blast waves with the flow or through its heating effects on other flow characteristics.

There are four steps in the process of laser induced breakdown. The process of laser induced gas breakdown is shown graphically in figure 31. Step 1 is the initial electron release due to multi-photon ionisation. Ionisation of the gas molecules often requires multi-photon hits as the ionisation energy of the atom/molecule is greater than the photon energy.[94] Equation 18[95] illustrates that the ion density (N_i) is directly proportional to a function of laser light intensity (I). This is the reason for the focusing of the laser, the greater the laser energy density, the greater the number of gas ions (plasma).

$$N_i \propto N_a(Ihv)^{N_0} \tag{18}$$

Step 2 is the cascade ionisation of gas molecules. In order to ionise other atoms/molecules, the free electrons absorb light energy through collisions with atoms in a process which is the opposite of Bremsstrahlung radiation (the process of charged particles emitting radiation through collisions with other particles). These "energised" electrons can then ionise the atoms creating two free slow electrons from one fast electron from which point the process

starts again. It is also possible for the cascade ionisation to be a combination of the multi-photon ionisation described previously and the electron ionisation.[96] Step 3 is the formation of the plasma (ionised gas) and the rapid heating of the region due to absorption of light energy. The plasma region formed is in the shape of a tear drop. If the area of plasma, the region which the light is absorbed by, is considered a layer, the next step is for the region between that and the laser to be ionised. This layer then starts to absorb the light and another layer forms between this and the laser which is then ionised. This process is repeated during the laser pulse causing the teardrop shaped plasma discharge.[96] Step 4 is the creation of a blast wave. This pressure wave is created by the rapid temperature increase in the region which in turns causes a rapid increase in pressure.[97] The final point for this process is the formation of a vortical structure following the blast wave. Adelgren et al.[98] and Dors et al.[99] observed this phenomenon during experiments. This vorticity is produced by the Richtmeyer-Meshkov instability[100,101] which, in turn, is a result of the baroclinic effect.[102,103] Figure 32 illustrates the process of the Richtmeyer-Meshkov instability which occurs when two fluids of different densities are impulsively accelerated. Ali[104] showed that equation 19 can be used to approximate the laser power needed for breakdown:

$$P_t = \frac{K_c I_i (w^2 + \nu_m^2)}{0.11 \tau \nu_m} \tag{19}$$

where P_t is the threshold power, K_c is the critical number of electron generations, I_i is the energy spent per ion pair generation, ν_m is the collision frequency for momentum transfer, w is the frequency of the radiation field, and τ is the duration of the laser pulse.

There are two different methods which laser energy deposition can be used as an active flow control device. The laser can either be operated in a repetitive pulsing mode or in a continuous mode. The former is the more commonly researched topic and functions on the basis described above. The continuous mode of operation was first studied by Generalov et al.[105] in 1970. The continuously operated laser energy deposition technique functions by first using a pulse of high energy laser radiation to generate the initial plasma. The plasma is then maintained by the continuous laser beam due to the absorption of the laser radiation by the plasma (explained above). The energy absorbed by the plasma (heat) is then convected downstream of the laser focal point (in the presence of high speed flows) and forms a heated wake. This type of operating mode of the laser functions in a similar manner to other energy deposition techniques applied in a steady manner such as steady DC discharge,[106,107] it acts

as a form of heat addition to the flow. This method does not generate a blast wave itself but instead the heated wake behind the focal point generates a shock structure. The interest in this mode of operation is focused on drag reduction as the shock structure generated by the heated wake can interact with bluff body bow shocks with the aim of reducing profile drag. Figure 33 provides an illustration of the modified shock structure encountered when applying continuous laser energy deposition to a bluff body flow. It shows the heated wake generated by the plasma and also the shock structure generated by the heated wake that interacts with the bow shock of the bluff body.

1. Applications of Laser Energy Deposition

The only application for continuous laser optical discharge that has been studied in any detail is bluff body drag reduction. Sperber at al.[108] demonstrated this by achieving a drag reduction of approximately 60% at Mach 2.7. They suggest that the drag reduction occurs due to the low speed heated wake, which trails from the laser focal point, creating a recirculation region upstream of the body. This has the effect of artificially decreasing the "bluntness" of the body (as perceived by the oncoming flow) and reducing the drag. Figure 34 shows the drop in peak static pressure of approximately 66% that was observed over the period that the plasma discharge was maintained. It also illustrates the heated wake behind the focal point of the laser and how this engulfs the cylinder face in figure 34b. The main limitation of continuous laser energy deposition in comparison to pulsed laser energy deposition is its lack of diversity.

Sasoh et al.[109] achieved a drag reduction of 3% and an efficiency of energy deposition, ratio of energy saved (drag reduction) to energy deposited (laser energy),[110] of 10. However, it was suggested that a higher reduction in drag could be achieved with higher repetition rates and an improvement to the laser optics in order to maintain laser efficiency at these higher repetition rates. They also carried out simulations to gain a better understanding of the fundamental reasons for the drag reduction. Further work by Sasoh et al.[111] proved that increasing the frequency of the laser pulses would lead to improvements in the drag reduction. The reduction of 3% at a laser pulse frequency of 10kHz[109] improved to approximately 21% at 80kHz.[111] The latter study showed that drag reduction from laser energy deposition became less effective as the body in question was made less blunt. Figure 35 illustrates both of these

conclusions. The reasoning for the technique being less effective for less blunt bodies was explained to be due to the decreased amount of time that the vortex rings created by the shock interactions are present upstream of the body. When the vortex rings are resident upstream of the body for longer, a "virtual" spike is created upstream of the body. This phenomenon is the reason for the reduction in drag and explains why the drag reduction is less significant for less blunt bodies where the vortex rings are resident for less time. Sasoh et al.[112] went on to further investigate this. It was found that introducing a concave face at the upstream face of the model further increased the vortex ring residence time. They also showed that the radius of the concave face was important and should match the vortex motion otherwise it can be detrimental to drag characteristics. Ultimately it was found that, with a time-averaged laser power of 400W, the increased drag reduction for a blunt cone did not lead to an improvement in drag in comparison to the sharp cone.

Adelgren et al.[113] investigated the use of laser energy deposition to influence bow shocks and also the Edney IV shock-shock interaction. The Edney shock interactions are a set of interactions between bow shocks and impinging oblique shock waves that were first documented by Edney[114] in 1968. There are 6 types of this interaction based on where the oblique shock interacts with the bow shock with the type IV being the most severe. Figure 36 provides a representation of the different Edney shock-shock interactions. The reason for the interest in this phenomenon is that the interaction of the oblique shock with the bow shock leads to a supersonic jet impinging on the surface of the blunt object in the subsonic region downstream of the bow shock. This leads to a dramatic increase in local surface pressure and heat transfer that could be catastrophic for a hypersonic vehicle. Figure 37 provides schlieren images showing the resultant interaction between the Edney type IV shock-shock structure and the laser induced blast wave. Adelgren et al.[113] were able to achieve a surface pressure reduction of 30% and 40% respectively for the simple bow shock case and the shock-shock interaction case.

Although both of these studies investigated the use of pulsed laser energy deposition for bow shock control, Adelgren et al.[113] base their conclusions on a single laser pulse. Sasoh et al.[112] includes the effects of repetitive pulsing, however the fundamental behaviour due to the pulse-pulse interactions is still not fully understood and requires further study.

Hong et al.[115] performed a similar study to Sasoh et al.[112] examining the drag reduction observed when introducing pulsed laser energy, both experimentally and numerically.

The computational model solved the compressible 3D Navier-Stokes equations. The laser energy was incorporated into the model as part of the specific internal energy as shown in equation 20[115] which can then be rearranged for the total energy:

$$e = \frac{Q_{in}}{\rho V} + E - \frac{1}{2}(u^2 + v^2 + w^2) \tag{20}$$

where Q_{in} is the total laser energy in the deposition area, V is the volume of the deposition area, E is the total energy of the gas per unit volume and u, v and w are the velocity components of the gas. Figure 38 shows the quasi-stationary wave that forms upstream of the body as a results of the multiple pulse interactions. The lower density region in the quasi-stationary wave causes the bow shock to "lens" forward increasing the shock stand-off distance. Kim et al.[116] presented an earlier experimental study that confirms the same phenomenon as Hong et al.[115] Figure 39,taken from Kim et al.,[116] shows the build up of vortex structures upstream of the body and how the shock stand-off distance increases in comparison to the baseline flow in figure 39(a). This same feature was found in a numerical study by Sakai.[117] It was found that the pulse-pulse interactions created a quasi-steady virtual spike supported by a re-circulation zone in front of a cone. The recirculation zone is created as a result of the vortical structures generated from the baroclinic interaction between the bow shock and the laser generated blast waves. Figure 40 illustrates the improved drag reduction as pulse frequency is increased from 1kHz up to 50kHz. This confirms the findings of Sasoh et al.[111] showing the effectiveness of repetitive laser pulsing at increasing bow shock stand-off distance and reducing drag.

Osuka et al.[118] used pulsed laser energy deposition to prevent flow separation over a flared cylinder in a flow at Mach 1.92 with a Reynolds number of 3.2 x 10^5. It was shown that the laser energy deposited prevented separation due to the production of toroidal vortices due to the baroclinic effect. These vortices interact with the boundary layer, enhancing mixing and causing the transition to a turbulent boundary layer which is more resistant to flow separation. More analysis was required to confirm this conjecture. Figure 41 provides schlieren images that show the improvement to the separation characteristics. With increasing frequency the bright region upstream of the flare decreases which indicates a reduction in the size of the separation zone. The angle of the slip line (border between bright region of conical segment of the cylinder mentioned previously) also decreases. The re-attachment shock is also visible in the 60kHz image. Another indicator that the flow separation charac-

teristics have improved is the increase in drag. This may not seem sensible initially however, as the separation region is on the flared section, a less separated flow will increase surface pressure. This in turn will increase the drag of the object.

Another interesting outcome of the work by Osuka et al.[118] is their demonstration that unsteadiness in the flow can be suppressed by laser energy deposition. Figure 42a shows the motion of the shock wave from approximately midway along the cylindrical section of the model to the 90° flare section back again under no laser energy deposition. Figure 42b shows that this oscillation of the shock wave is suppressed by laser energy deposition with a 60kHz repetition rate. This is another important result of this paper as it shows that laser energy deposition can be used to control supersonic flowfield unsteadiness.

The paper by Erdem et al.[119] investigated a very similar research case. The general understanding of the phenomenon of laser interaction with the bow shock generating a toroidal vortex, due to the baroclinic instability, is explained similarly to the paper by Osuka et al.[118] However Erdem et al.[119] show clearly the impact that different laser pulse frequencies have on the flow around the flared cylinder. Figure 43 displays the rms of schlieren images taken at different laser pulse frequencies. It is clear that the light area which indicates the SBLI region increases from the baseline case to 15kHz, but then decreases from the 15kHz image to a minimum in the 60kHz image. Therefore this indicates that the frequency of laser energy deposition is key for this method of flow control. In this case the lower frequency caused an increase in the region over which the SBLI was apparent, while higher frequencies resulted in a more stabilised flow thus reducing the size of the SBLI region. This trend may not be the same for all cases however as the frequency of the laser energy deposition may be exciting instabilities in the flow which in turn cause this behaviour. Therefore further research in this area would prove worthwhile to better understand this relationship.

Yan et al.[120] present a numerical study on the control of the position of a normal shock using laser energy deposition. They modelled the interaction using both the perfect and real gas models. This application is of interest as the terminating normal shock in mixed compression inlets are of great importance in high speed aircraft intakes. To minimise the total pressure loss it is desirable for the shock to be positioned close to the throat. However, disturbances upstream/downstream (e.g. atmospheric disturbances, combustion chamber overpressure) of the throat can cause the normal shock to move either upstream or downstream which can result in unstart or significant total pressure loss respectively.

They showed that the shock position can be altered significantly, however this came at the cost of increasing the area of separation downstream of the shock. Figure 44 illustrates the movement downstream of the re-attachment location. The reason for the increase in the separation region is the interaction between the compression waves generated by the laser pulse and the normal shock wave. It was shown however that this did not have an impact on the total pressure downstream of the shock.

2. Future Work on Laser Energy Deposition

Unlike the energy deposition methods previously discussed, there has been little work reported on the optimisation of the operating characteristics of the laser such as: pulse length, frequency, laser power and on the flow conditions such as: pressure, temperature and Mach number. More work is required to better understand the fundamentals of this technique so that its efficacy can be optimised.

An interesting area that deserves further research is the application of laser energy deposition to SBLI's, particularly the controlling of shock positions. It has been shown that the interaction between the heated bubbles from laser energy deposition and bow shock causes the shock to lens in the direction of the bubble. It may be possible for the same phenomenon to control the impinging location of an oblique shockwave. This is useful as it can be used, for example, to maintain the position of a shock wave in high speed intakes experiencing back pressure fluctuations.

E. Microwave Generated Plasmas

The concept of using microwaves to couple energy into a gas flow from a distance is not new. The first published microwave discharge was carried out by Khodataev in 1957.[121] However it did not gain much interest until the late 1970's/early 1980's with the appearance of this new area of research, namely, plasma aerodynamics.[122] Although it is not the most straightforward method of generating plasma, compared to surface plasmas for instance, it is of interest as it allows the possibility of generating plasma from a distance rather than the location of the hardware being restricted to the desired energy deposition location. Microwave energy deposition is used for flow control in much the same way as laser energy

deposition, either blast waves generated interact with the flow or the rapid heating alters flow field characteristics.

The basic principle of microwave plasma generation is simple, the first step is that the initial microwave pulse accelerates the ambient electrons. These electrons collide with heavy particles (Nitrogen and Oxygen molecules for example) and transfer energy through these collisions. The three main modes of energy transfer from the electrons to the heavy particles kinetic energy (increasing kinetic energy increases gas temperature) are: (i) rotational excitation, (ii) excitation of the particles to higher electronic states, and (iii) electron-ion recombination.[123,103] The latter two modes are synonymous with Joule heating described in Section 2.2.

Knight et al.[123] developed a three dimensional gas dynamics code to model microwave energy deposition. They present the governing equations of the simulation in the study with the equation of greatest interest here being the energy equation shown in equation 21,

$$\frac{\partial \rho\epsilon}{\partial t} + \frac{\partial}{\partial x_j}(\rho\epsilon + p)u_j = \dot{q} + \frac{\partial q_j}{\partial x_j} + \frac{\partial \tau_{ij} u_i}{\partial x_j} \tag{21}$$

where ϵ is the total energy per unit mass, τ_{ij} are the viscous stresses and $\dot{q}$ is the heat flux. The main term of interest in equation 21 with regard to microwave gas heating is $\dot{q}$, which is the rate of gas heating per unit volume. This variable can be split into a number of contributions, one for each of the modes of energy transfer described previously. First, is the contribution to $\dot{q}$ from energy transfer due to the collisions between electrons and heavy particles (equation 22):[123]

$$\dot{q}_{elastic} = \frac{3}{2} k_B T_e \delta \nu_e N_e \tag{22}$$

where k_B is the Boltzmann constant, T_e is electron temperature, δ is a mass ratio of electrons and neutrals/ions, ν_e is the effective collision frequency and N_e is the electron concentration. Secondly, there is a portion of the energy from the quenching of particles at excited states that is assumed to be completely transferred to the heating of the gas. This forms another contribution to the total $\dot{q}$ (equation 23):[123]

$$\dot{q}_{reaction} = \sum_{i=1}^{m} \alpha_i \Delta h_i \tag{23}$$

where Δh_i is the rate of change of enthalpy per unit volume for reaction i and α_i is the fraction of this that heats the gas. Finally, there is the contribution of the rotational heating

of the gas (equation 24):[123]

$$\dot{q}_{rotational} = \nu e \frac{E}{N}\bigg|_r N V_{dr} N_e \tag{24}$$

where ν is the rotational relaxation factor, e is the electron charge, $\frac{E}{N}\Big|_r$ is the reduced field, N is the total concentration of the species (excluding electrons) and V_{dr} is the electron drift velocity. All of these contributions are brought together to form the total rate of gas heating per unit volume due to microwave energy deposition:[123]

$$\dot{q} = \frac{3}{2} k_B T_e \delta \nu_e N_e + \sum_{i=1}^{m} \alpha_i \Delta h_i + \nu e \frac{E}{N}\bigg|_r N V_{dr} N_e \tag{25}$$

The study by Knight et al.[123] goes into much more detail regarding the constituents of each of these equations such as electron temperature, electron drift velocity and reduced field strength. The equations that are presented give an understanding of the different sources of the heating due to microwave energy deposition and they are incorporated into a gas dynamics numerical model.

There are two distinct categories of microwave discharge: overcritical and subcritical.[124] Overcritical discharges occur if the electric field strength exceeds the breakdown voltage of the gas in question on the other hand, the electric field strength for subcritical discharges is not greater than the breakdown voltage, therefore an initiator of some sort is required e.g. laser energy deposition. A Paschen curve, plot of breakdown voltage according to Paschen's law (empirical formula determined by Friedrich Paschen in 1889[125]), can be used as a simple graphical classification of overcritical and subcritical discharges as shown in figure 45. The formula related to Paschen's law that can be used to create a curve of breakdown voltage similar to figure 45 was shown in equation 9. Voltages below the curve will only trigger breakdown when used with some external "trigger" (subcritical) while voltages above the curve will trigger breakdown without an external "trigger" (overcritical). The following section examines each class of discharge in more depth.

1. Overcritical Plasma Generation

As stated previously, overcritical discharge occurs when the electric field strength is greater than the gas breakdown voltage. Therefore, no external stimuli are needed and

the discharge can be of two forms: either a diffusion discharge or a streamer discharge (figure 46 shows an example of each type). Diffusion discharge occurs at lower pressures with the boundary point between diffusion and streamer discharges defined by equation 26:[124]

$$P_{ds} \approx \frac{20}{\lambda} torr \tag{26}$$

where P_{ds} is the threshold pressure at which the discharge is streamer in nature and λ is the radiation wavelength. Above this pressure the discharge is streamer in nature. Shibkov et al.[126] agree, qualitatively, with the relation given in Eq(26). At low pressures they found that the discharge took the form of a chain of closely spaced plasma filaments i.e. diffusion discharge. At higher pressures the discharge instead consisted of an irregular display of plasma channels i.e. streamer discharge. They noted that the initial heating of the plasma was rapid however it began to noticeably slow down after 10μs to 20μs. This is caused by the tendency of the discharge of a converging microwave source to move towards the source. It is also caused by the "skin effect", this is the damping of an electromagnetic field inside a conductor,[127] the conductor in this case being the plasma. They also noted that microwave discharge could be maintained in supersonic flow if either the supersonic flow was started before the microwave discharge or vice versa. The power required to initiate a microwave discharge was found to only marginally depend on the flow velocity i.e. the discharge occurred on a time-scale faster than that of the flow speed.

There are two primary methods for the creation of an overcritical microwave discharge. The first, an example of which is presented by Shibkov et al,[128] is to focus the microwaves using a mirror and lens arrangement. This method is simple to implement and creates a focused spot of electromagnetic radiation at the focal point of the reflecting mirror where the plasma is generated. Figure 47 shows a schematic of this setup. The main concern with this form of microwave focusing is to ensure the containment of the microwaves. Therefore this type of experiment has to take place in some form of microwave containment chamber. The second common method for focusing microwaves to create an overcritical discharge is to create a tapered waveguide. This creates a standing wave at the point where the tapered dimension reaches the cutoff dimension. At the cutoff dimension, a function of the microwave wavelength, the microwaves can no longer travel along the waveguide and are reflected backwards. If a stub tuner is then used, a resonant cavity is formed between the cutoff dimension and the stub tuner. This increases the electromagnetic field strength at the

cutoff dimension which, if the microwave source is powerful enough, will cause overcritical breakdown. This type of system is described in detail by McAndrew et al.[129](see figure 48). The advantage of using the second method is that the microwaves are already contained within the waveguide and thus the experiment does not need to be carried out in a microwave chamber, however this method is more complex and less adaptable. The mirror and lens focusing setup can be used to create a discharge in any number of locations in the test section unlike the waveguide microwave focusing technique. The mirror and lens setup can also be used with any existing wind tunnel available unlike the waveguide method which requires a custom designed test section in order to create a resonant microwave cavity.

The advantages of an overcritical microwave discharge is the simplicity of the system requirements. The only energy source is the microwave itself and it can act from a distance. However there is the significant disadvantage when compared to other methods, such as subcritical, initiated microwave discharges, of the large power required.

a. Applications

Using the tapered waveguide, McAndrew et al.[129] generated a plasma discharge using solely microwaves in an air flow at Mach 3. Figure 48 provides a schematic of their setup. They found that the discharge would tend to form on one side of the wind tunnel, either the top or the bottom. This was due to the boundary layer being at a higher temperature than the rest of the flow, therefore plasma would form there first. This means that the results of the study are not necessarily useful as the manner in by which the plasma is formed is dependant on the experimental setup. The objective of their study was to show that the plasma could be used to change the lift and drag of a cone model. From the results presented, the concept of changing lift and drag by microwave driven plasma discharges was proven. However some important factors need to be considered form their study. Firstly, the study only showed the decrease in drag (figure 49) and not the baseline drag. This means that although it is clear that there is a drag reduction, it is not clear how significant this reduction is as there is no baseline case to compare it to. Secondly, the plot showing lift versus microwave power was ambiguous as, based on the drag plot, it is difficult to say whether this is the increase in lift or the total lift. Again, if it is the increase in lift there is no way to determine its significance as no baseline values were provided. Thus is it difficult

to fully quantify the effectiveness of microwave driven plasma discharges from this paper.

Lashkov et al.[130] demonstrated experimentally that a bow shock could be controlled by upstream microwave generated plasma discharge. Their experimental study used the parabolic mirror method to focus the microwave radiation to a spot in the supersonic flow. Schlieren, luminescence measurements, and pressure measurements were used to show that focused microwave energy deposition and the associated plasma discharge can be used to reduce drag through modification of the bow shock. The movement of the shock wave upstream, increasing the stand off distance, and the formation of a vortex structure between the bow shock and the body itself were captured. Schlieren images of this and an associated schematic of the shock structure is shown in figure 50. These physical observations were assumed to be the reason for the decrease in stagnation pressure at the body and thus the decrease in drag. By comparing the results from different geometries Lashkov et al.[130] demonstrated that the impact on drag scaled linearly with the spanwise dimension of the object i.e. more slender bodies had a lower reduction in drag.

The two methods commonly used to focus microwaves in literature, are not readily applicable to real world applications. This is because both of these methods require equipment that at the moment are large in size and have significant mass. In order for this method to be considered feasible a new simple and effective method of focusing microwave beams would be necessary.

2. Subcritical Plasma Generation (Laser Sparked)

This type of dicharge involves the use of a microwave field that doesn't reach the breakdown electric field strength. Therefore an "initiator" is required. An initiator refers to anything that can create a discharge in a microwave field with subcritical electric field strength. The initiator can take many forms, both physical items as well as other energy deposition sources. If a physical item is used it is known as a "vibrator" and usually takes the form of a metallic rod.[131] This has the effect of increasing the electric field strength around the rod to a point above the breakdown voltage. This type of initiator however is not overly useful as it will be intrusive and change the flow characteristics which is undesirable. The method of using energy deposition however would appear to be more useful. The two common types of energy deposition used for microwave initiation are electron beam radiation and laser

pulses. Here, the focus is on the laser pulse method due to its potential and practicality in real world applications compared to electron beam radiation (as this is ionising radiation).

The physical concept behind laser initiated microwave discharge is that the laser pulse creates an initial spark discharge through multi-photon ionisation and cascade ionisation leading to rapid thermal heating of the focal region. This process is explained in depth in the following section on laser generated plasma. This allows the discharge to be maintained by a microwave source of lower intensity than would be required to initiate the discharge. This is because it requires less energy to maintain a discharge than to initiate one.[132] There are a number of benefits of laser sparked discharge when compared to the overcritical microwave discharge previously discussed. As mentioned previously current methods for the focusing of microwaves are cumbersome and heavy, characteristics which do not lend themselves to aerospace applications. The difficulty in focusing microwaves stems from their long wavelength.[132] The difficulties described above mean that not only does overcritical discharge require large quantities of power, but there are also problems with defining the location of the discharge. Laser initiated microwave discharge solves this issue. Using a microwave source with an intensity below breakdown in conjunction with a pulsed laser energy source can create a discharge in the laser focal region and nowhere else.

Using a laser pulse, 200 femtoseconds in duration, Michael et al.[133] were able to generate microwave a discharge at a specified location i.e. the laser focal region. This was taken one step further in the same study by using beam splitters and spherical reflectors to create a focal "volume" in a rectangular shape. Figure 51 illustrates the effectiveness of this technique with the plasma discharge showing clear preference to the pre-ionised rectangular region. The ability to locate the microwave plasma discharge through focused laser energy deposition is further shown by Khoronzhuk et al.[134] The authors compared single laser pulse sparked microwave discharge with double pulse microwave discharge. They showed that elongation of the plasma discharge that can be achieved through multiple laser pulses. A similar study was carried out by Mashek et al.[135] with figure 52 showing similar results to those described by Khoronzhuk et al.[134] This seemingly simple observation is important as it has been shown that plasma spikes, elongated regions of plasma discharge, are effective at reducing bow shock strength and therefore the associated drag.[136] The study also found that a femtosecond pulse duration laser is not necessary and a nanosecond duration laser pulse is sufficient to create the same laser initiated discharge.

3. Numerical Modelling of Microwave Discharges

Experimental studies involving microwave energy deposition can be difficult and costly to run. Therefore computational studies have been very popular in order to study the fundamentals of these interactions. There are two methods of simulating the microwave energy deposition into the flow: ideal gas simulations and thermochemistry models.

The ideal gas simulations are the more computationally straightforward method of the two. Using ideal gas simulations the region of microwave energy deposition can be modelled as a rarified channel of infinite length as was shown by Azarova et al.[137] Equations 27-29 show the system of Euler equations solved:

$$\frac{\partial \mathbf{U} r^{\omega}}{\partial t} + \frac{\partial \mathbf{F} r^{\omega}}{\partial t} + \frac{\partial \mathbf{G} r^{\omega}}{\partial t} = \mathbf{H} \tag{27}$$

$$\mathbf{U} = \begin{bmatrix} \rho \\ \rho u \\ \rho v \\ E_s \end{bmatrix} \mathbf{F} = \begin{bmatrix} \rho u \\ p + \rho u^2 \\ \rho uv \\ u(E_s + p) \end{bmatrix} \mathbf{G} = \begin{bmatrix} \rho v \\ \rho uv \\ p + \rho v^2 \\ v(E_s + p) \end{bmatrix} \mathbf{H} = \begin{bmatrix} 0 \\ 0 \\ \boldsymbol{\omega} r^{\omega - 1} p \\ 0 \end{bmatrix} \tag{28}$$

$$E_s = \rho(\epsilon + 0.5(u^2 + v^2)) \tag{29}$$

where ω has a value of 0 or 1 for plane or cylindrical flow respectively and E_s is the total energy density of the gas. The rarified channel is set to have the same static pressure and velocity as the rest of the domain thus, based on the ideal gas law, the temperature is increased due to the lower density. This methodology has been used in a number of studies by Azarova et al.[138–140] to study flow instabilities induced by microwave energy deposition and its efficacy for flow control. Azarova et al.[137] corroborated what other studies have shown with the use of energy deposition (laser, microwave or DBD based) to reduce the wave drag of bow shocks. Objects with a wider cross-section, i.e. less "streamlined", experience a greater reduction in drag in comparison with those that have a narrower cross-section. This study also went some way to validate the results of the computations by comparing them to experimental results of Lashkov et al.,[130] however this was limited to the generated microwave filament and not its effects on the flow.

In a later study however, Azarova et al.[138] present a more in-depth validation of the model. They compared the shock stand-off distance, pressure and density of the computational model with known experimental data. Figure 53 shows a representation of the computational domain used in the study. The study also examined the effect of moving the microwave deposition location away from the axis of symmetry of the object. This was found to increase the drag as a result of the "heat piston" effect. This is the effect of the vortex compressing the flow between it and the body surface creating a region of higher pressure at the body surface. This, in turn, increases the drag force of the body. A more in depth explanation of this phenomenon is provided by Knight et al.[141] A further study of this interaction by Azarova[140] focused on the instant at which the heated microwave filament interacts with the bow shock. Part of this study illustrated the region in which baroclinic effects, resulting from misaligned density and pressure gradients, were active and produced vorticity. Figure 54 presents results from the numerical model that illustrates this misalignment in the pressure and density gradients.

The other method of modelling microwave energy deposition is the use of a gas dynamics model with detailed kinetics and thermochemistry modelling as was used by Knight et al.[142] Although the simplistic ideal gas model is capable of modelling the microwave discharge, it ignores some of the details of the phenomenon. An ideal gas simulation sets an initial assumed spatial distribution of temperature and velocity, however these are not the experimental parameters. The experimental parameters are the microwave frequency, pulse duration, and the electric field strength and distribution. So in effect, the ideal gas simulations are defining inputs based on previous experimental conditions rather than using the actual energy deposition input parameters themselves.[143] This would seem to indicate that the ideal gas simulations, although useful for the general study of microwave energy deposition, are somewhat limited by their inputs.

A thermochemistry model incorporates the modelling of reactions and different "species" of ions and molecules. This more robust approach allows more refined modelling of the microwave discharge. This is important depending on the study as it has been shown that microwave streamers can cause either an increase or a decrease in drag depending on their orientation.[130] The thermochemistry model also allows the gas processes which result in the rapid heating to be better understood. The findings of Knight et al.,[143] as shown in Figure 55, validated against experimental results show that this type of model can accurately model

the impact of microwave energy deposition on high speed flows. The same model is used in a study by Knight et al.[123] in an effort to replicate the experimental results of Kolesnichenko et al.[122] The minimum achieved surface pressure of the numerical model showed excellent comparison to the experimental data, however the duration of this feature was debated. Two cases were run, each with a different streamwise length for the electric field. This is because the length of the plasma is sensitive to the length of the electric field. The second case, with an increased streamwise length, showed a good comparison however the shorter electric field case did not.

Comparing both aforementioned numerical approaches, it is clear that they both can accurately predict the flowfield structure caused by the interaction of microwave energy deposition and a supersonic flowfield. Studies have illustrated that both predict key flow features, such as the lensing of the bow shock wave and the recirculation region between the body and the bow shock. Therefore for studies where the objective is to study the impact of microwave discharge on the flow, ideal gas simulation is sufficient. However if resources are available, the thermochemistry model provides more in-depth details of the microwave discharge.

4. Future Work on Microwave Discharges

The most important issue that needs to be addressed for this technology to implemented is the method of focusing the microwave radiation. The current methods involve the use of heavy and cumbersome equipment which make them infeasible to use in real-world applications such as high speed aircraft intake flow control. Therefore further research needs to be carried out to discover a new and improved method of microwave focusing that can be applied to real-world applications.

Further work is also necessary to provide a better understanding of the parameters of the microwave energy source and their impact on system performance. There has been very little to no work reported on understanding the effects of microwave frequency/wavelength and microwave power have on the performance of this flow control technique.

III. ENERGY DEPOSITION METHODS FOR SBLI AND BOUNDARY LAYER SEPARATION CONTROL IN HIGH SPEED INTAKES

A key area in high-speed propulsion is the intake/compression system. One of the most researched topics of a supersonic/hypersonic propulsion system which will be used as an example for this review is the dual-mode ram-scramjet (DMR), see figure 56. This is a design that operates as a ramjet system at lower supersonic Mach numbers with subsonic combustion and as a scramjet system at higher Mach numbers with supersonic combustion. In the ramjet system the isolator, the duct between the inlet and the combustion chamber, will contain a series of shocks known as a shock train. These can either be a series of bifurcated normal shocks or a series of oblique shocks depending on the isolator entrance condition.[144] If the duct is long enough then a mixing region of adverse pressure gradient will follow the shock train, this is shown in figure 57.[145] In the scramjet mode of operation the isolator is also important as the rate of area increase in the combustion chamber is often not large enough to relieve the thermal blockage from the heat addition to a supersonic flow and an adverse pressure gradient occurs.[33] This can lead to boundary layer separation which in turn will result in an oblique shock train forming in the isolator with a supersonic core flow.[33]

A key concern currently with DMR operation is isolator unstart. Unstart is the ejection of the shock train upstream of the inlet which can eventually lead to a detached bow shock upstream of the propulsion system intake.[146,147] This could be catastrophic to the aircraft as the mass flow rate spillage due to the bow shock will drastically reduce thrust from the propulsion system. The most common cause of unstart is a rapid increase in back pressure at the combustor. This causes an adverse pressure gradient which in turn can lead to boundary layer separation in the isolator. The separation results in a reduction in core flow area which forces the internal flow subsonic and thus forces the shock system upstream of the isolator.

The flow control methods discussed above have the potential to be used for SBLI and separation control in DMR's. The pressure waves created by these methods can be used either to alter the shock waves themselves (position, strength etc.) or to mitigate the level of separation downstream of the shock wave. It has been documented that bow shocks can be controlled through interaction of the bow shocks with ns-DBD generated pressure waves[30] on the model surface or interaction with heated bubbles from focused laser/MW

energy deposition.[112] It follows that the same techniques can be used to control the location of an impinging shock wave in a supersonic/hypersonic isolator. Thomas et al.[148] showed that there is a strong correlation between oscillations in the shock wave and the proceeding separation region. Therefore it is thought that if the motion of the shock wave can be controlled so could the separation region.

Another method by which energy deposition flow control methods have to the potential to be used is to reduce the impact the SBLI's have on flow separation. It has been shown in a number of the aforementioned studies that these flow control methods can prevent or delay separation. Osuka et al.[118] showed that laser energy deposition can delay the shock induced separation over a flared cylinder. While Im et al.[32] demonstrated the control of a supersonic boundary layer over a flat plate using ns-DBD's. As previously stated, separation of the boundary layer in high-speed engines is a major factor in unstart and thus controlling the boundary layer and preventing boundary layer separation are key in preventing or delaying unstart. These studies have shown that there is the potential to control the unstart phenomenon through boundary layer and separation control. However further work is required to investigate other configurations that could provide a beneficial effect on the SBLI and separation characteristics. Consider laser energy deposition focused near the surface close to the location of an impinging oblique shock wave as an example. The vorticity generated through the interaction of the oblique shock and the heated gas "bubble" has the potential reduce the degree of separation downstream of the shock wave. Another interesting future study is based on the position control of impinging oblique shock waves through pressure waves generated by ns-DBD's, based on a similar outcome shown by Nishihara et al.[30] examining bow shocks. Of course, these are just two examples of possible areas of future research that can be conducted.

IV. CONCLUSIONS

This review has shown that there has vast growth in research and interest in EHD and Joule heating flow control techniques over the past 15 to 20 years. These studies have provided a good base of knowledge on energy deposition based flow control methods. They have shown that the actuators/techniques are capable of influencing supersonic/hypersonic flows. They have been proven capable of preventing/delaying some of the most adverse fluid

dynamics phenomena such as: separation, bluff body drag reduction, and SBLI control. There is however significant scope for further work to be carried out for all of the EHD/Joule heating flow control methods discussed above.

Considering ns-DBD actuators, there has been significant work in optimising the actuator geometry and electrical system characteristics (frequency, pulse width, voltage etc.). However, this has all been done for a simple 1D linear actuator. Future research must examine more complicated actuator designs e.g. multiple high voltage/ground electrodes, 2D actuators (sine wave/serpentine, sawtooth shapes). The impact of the flow conditions e.g. ambient pressure, temperature, Mach number, Reynolds number on ns-DBD actuators should also be investigated. An area, highlighted earlier, that should be investigated is the efficiency of these actuators. A number of processes can be examined with regards to efficiency: conversion of electrical energy to heat energy, conversion of heat energy to mechanical energy of shockwave and overall efficiency of the system i.e. ratio of energy saved by energy deposition to the energy used by the actuator. Industrial applications of new technology, however effective it may be, is, more often than not, ultimately based on efficiency. The actuators will no doubt improve performance, but if they use more energy than is saved by the improved aerodynamic performance then they are most likely not viable. It is therefore important that studies are conducted to determine the efficiency of actuators and how to optimise this efficiency.

PPSJ actuators can be considered to be one stage behind ns-DBD's in their development. The research published thus far has proven their capability to control flow separation and SBLI's. However, their has only been limited work published on the optimisation of these actuators. Research is required to achieve a better understanding of the optimal geometric configuration for PPSJ's (cavity size and shape, jet orifice size, electrode separation). Another important parameter is the frequency limitations of the actuators. It has been shown that at higher frequencies the slower refill times due to thermal effects starts to limit the operation.

The current state-of-the-art of laser energy deposition is at a similar point to PPSJ actuators. Its potential to be used to affect supersonic/hypersonic flows has been proven. Research covered here has shown that it can be used to reduce drag of bluff bodies and control SBLI's. However, there is limited/no published research on the optimisation of laser energy deposition. Therefore research must be conducted regarding both the effects of laser

parameters (frequency, pulse length and laser power) and the effects of the environment (Mach number, temperature and pressure) on performance.

Microwave energy deposition is at a similar stage to laser energy deposition in terms of the maturity of the technology. There are however some key issues that require further study. The significant issue currently with microwave energy deposition is the ability to apply it to real-world situations. The currently available methods for focusing microwave radiation are unsuitable for aerospace applications. Thus the most urgent work required for microwave energy deposition is to determine a method for its application in a manner that is suitable for aerospace.

Acknowledgments

The authors are grateful to the various staff at Glasgow University.

[1] M. R. Saad, H. Zare-Behtash, A. Che-Idris, and K. Kontis. Micro-ramps for hypersonic flow control. *Micromachines*, 3:364–378, 2012.

[2] W. F. Wong. The application of boundary layer suction to suppress strong shock-induced separation in supersonic inlets. *AIAA 1974-1063*, 1974.

[3] T. J. Troia, A. A. Patel, D. Crouse, and G. R. Hall. Passive Device Flow Control for Normal Shock / Boundary Layer Interactions in External Compression Inlets. In *41st AIAA Fluid Dynamics Conference and Exhibit*, number June, pages 1–20, 2011.

[4] H. A. Holden and H. Babinsky. Effect of Microvortex Generators On Seperated Normal Shock/ Boundary Layer Interactions. *Journal of Aircraft*, 44(1):170–174, 2007.

[5] L. Prandtl. Ober Fffissigkeitsbewegung bei sehr kleiner Reibung. In *Third International Congress of Mathematicians*, 1904.

[6] J. Flatt. The History of Boundary Layer Control Research in the United States of America. *Boundary Layer and Flow Control*, 1, 1961.

[7] L. N. Cattafesta and M. Sheplak. Actuators for Active Flow Control. *Annual Review of Fluid Mechanics*, 43:247–272, 2011.

[8] K. W. Yung, P B. Landecker, J. Ketcham, and H. R. Velkhoff. Effect of an electrostatic field on boundary- layer transition., 1968.

[9] J. R. Roth, D. M. Sherman, and S. P. Wilkinson. Boundary layer flow control with a one atmosphere uniform glow discharge surface plasma. In *36th Aerospace Sciences Meeting & Exhibit January*, volume 28, 1998.

[10] W. Siemens. Ueber die elektrostatische Induction und die Verzögerung des Stroms in Flaschendrähten. *Poggendorffs Annalen der Physik und Chemie*, 1857.

[11] A. Fridman, A. Chirokov, and A. Gutsol. Non-thermal atmospheric pressure discharges. *J. Phys. D*, 38:1, 2005.

[12] E. Moreau. Airflow control by non-thermal plasma actuators. *Journal of Physics D: Applied Physics*, 40:605–636, 2007.

[13] S. O. Macheret, M. N. Shneider, and R. B. Miles. Scramjet Inlet Control by Off-Body Energy Addition: A Virtual Cowl. *AIAA Journal*, 42(11):2294–2302, 2004.

[14] S. Pal, R. Sriram, M. Rao, and G. Jagadeesh. Effect of Dielectric Barrier Discharge Plasma in

Supersonic Flow. *28th International Symposium ...*, 2:867–872, 2012.

[15] A. V. Likhanskii, M. N. Shneider, S. O. Macheret, and R. B. Miles. Modeling of Interaction Between Weakly Ionized Near-Surface Plasmas and Gas Flow. *44th AIAA Aerospace Sciences Meeting and Exhibit*, pages 1–26, 2006.

[16] D. F. Opaits, G. Neretti, A. V. Likhanskii, S. Zaidi, M. N. Shneider, and R. B. Miles. Experimental Investigation of DBD Plasma Actuators Driven by Repetitive High Voltage Nanosecond Pulses with DC or Low-Frequency Sinusoidal Bias. In *38th AIAA Plasmadynamics and Lasers Conference*, number June, pages 1–21, 2007.

[17] D. V. Roupassov, A. A. Nikipelov, M. M. Nudnova, and A. Y. Starikovskii. Flow Separation Control by Plasma Actuator with Nanosecond Pulsed-Periodic Discharge. *AIAA Journal*, 47 (1):168–185, 2009.

[18] N. A. Popov. Investigation of the mechanism for rapid heating of nitrogen and air in gas discharges. *Plasma Physics Reports*, 27(10):886–896, 2001.

[19] N Bohr. On the Constitution of Atoms and Molecules, Part II Systems Containing Only a Single Nucleus. *The London, Edinburgh, and Dublin Philosophical*, 26:1–25, 1913.

[20] K. Takashima, Y. Zuzeek, W. R. Lempert, and I. V. Adamovich. Characterization of a surface dielectric barrier discharge plasma sustained by repetitive nanosecond pulses. *Plasma Sources Science and Technology*, 20:055009, 2011.

[21] N. Benard, N. Zouzou, A. Claverie, J. Sotton, and E. Moreau. Optical visualization and electrical characterization of fast-rising pulsed dielectric barrier discharge for airflow control applications. *Journal of Applied Physics*, 111(2012), 2012.

[22] R. Dawson and J. Little. Effects of pulse polarity on nanosecond pulse driven dielectric barrier discharge plasma actuators. *Journal of Applied Physics*, 115(2014), 2014.

[23] K. Takashima, Y. Zuzeek, W. Lempert, and I. Adamovich. Characterization of Surface Dielectric Barrier Discharge Plasma Sustained by Repetitive Nanosecond Pulse. *41st AIAA Plasmadynamics and Lasers Conference*, (July):1–26, 2010.

[24] R. Dawson and J. Little. Characterization of nanosecond pulse driven dielectric barrier discharge plasma actuators for aerodynamic flow control. *Journal of Applied Physics*, 113, 2013.

[25] A. C. Aba'a Ndong, N. Zouzou, N. Benard, and E. Moreau. Geometrical optimization of a surface DBD powered by a nanosecond pulsed high voltage. *Journal of Electrostatics*, 71(3): 246–253, 2013.

[26] Z. Zhao, J. Li, J. Zheng, Y. D. Cui, and B. C. Khoo. Study of Shock and Induced Flow Dynamics by Nanosecond Dielectric-Barrier-Discharge Plasma Actuators. *AIAA Journal*, pages 1–13, 2014.

[27] Y. Wu, Y. H. Li, H. Liang, M. Jia, and H. M. Song. On mechanism of plasma-shock-based flow control. *AIP Conference Proceedings*, 1376(2011):521–523, 2011.

[28] Z. Chen, L. Hao, and B. Zhang. A model for Nanosecond Pulsed Dielectric Barrier Discharge (NSDBD) actuator and its investigation on the mechanisms of separation control over an airfoil. *Science China Technological Sciences*, 56(5):1055–1065, 2013.

[29] M. Nishihara, D. Gaitonde, and I. Adamovich. Effect of Nanosecond Pulse DBD Plasma Actuators on Oblique Shocks and on Shock / Boundary Layer Interaction. *51st AIAA Aerospace Sciences Meeting including the New Horizons Forum and Aerospace Exposition*, (January):1–17, 2013.

[30] M. Nishihara, K. Takashima, J. W. Rich, and I. V. Adamovich. Mach 5 bow shock control by a nanosecond pulse surface dielectric barrier discharge. *Physics of Fluids*, 23(2011), 2011.

[31] N. J. Bisek and J. Poggie. Hypersonic Flow over a Cylinder with a Nanosecond Pulse Electrical Discharge. *Journal of Thermophysics and Heat Transfer*, 28(1):18–26, 2014.

[32] S. Im, H. Do, and M. A. Cappelli. Plasma Control of an Unstarting Supersonic Flow. In *17th AIAA International Space Planes and Hypersonic Systems and Technologies Conference*, number January, pages 1–8, 2011.

[33] E. Curran. Fluid Phenomena in Scramjet Combustion Systems. *Annual Review of Fluid Mechanics*, 28:323–360, 1996.

[34] S. Roy and C. Wang. Bulk flow modification with horseshoe and serpentine plasma actuators. *Journal of Physics D: Applied Physics*, 42:032004, 2008.

[35] R. Durscher and S. Roy. Induced Flow from Serpentine Plasma Actuators Acting in Quiescent Air. *49th AIAA Aerospace Sciences Meeting*, AIAA 2011-(January):4–14, 2011.

[36] C. C. Wang, R. Durscher, and S. Roy. Three-dimensional effects of curved plasma actuators in quiescent air. *Journal of Applied Physics*, 109:1–9, 2011.

[37] M. Riherd and S. Roy. Numerical Investigation of Serpentine Plasma Actuators for Separation Control at Low Reynolds Number. *41st AIAA Fluid Dynamics Conference*, (June):AIAA–2011–3990, 2011.

[38] C. C. Wang and S. Roy. Combustion stabilization using serpentine plasma actuators. *Applied*

Physics Letters, 99:4–6, 2011.

[39] R. J. Durscher and S. Roy. Three-dimensional flow measurements induced from serpentine plasma actuators in quiescent air. *Journal of Physics D: Applied Physics*, 45:035202, 2012.

[40] P. Riherd and S. Roy. Simulations of Serpentine Plasma Actuators in a Laminar Boundary Layer. *51st AIAA Aerospace Sciences Meeting including the New Horizons Forum and Aerospace Exposition*, pages 1–11, 2013.

[41] K. Kontis, H. Zare-Behtash, and S. Roy. Flow Control at Subsonic Speeds using Serpentine Plasma Actuators. In *45th AIAA Plasmadynamics and Lasers Conference*, 2014.

[42] C. Hale, R. Erfani, and K. Kontis. Plasma Actuators with Multiple Encapsulated. *48th AIAA Aerospace Sciences and Meeting Including the New Horizons Forum and Aerospace Exposition*, 2010.

[43] R. Erfani, T. Erfani, C. Hale, K. Kontis, and S. V Utyuzhnikov. Optimization of Induced Velocity for Plasma Actuator Surface Methodology. *49th AIAA Aerospace Sciences Meeting including the New Horizons Forum and Aerospace Exposition*, (January), 2011.

[44] R. Erfani, C. Hale, and K. Kontis. The Influence of Electrode Configuration and Dielectric Temperature on Plasma Actuator. *49th AIAA Aerospace Sciences Meeting including the New Horizons Forum and Aerospace Exposition*, (January), 2011.

[45] C. Hale. Development of Dielectric Barrier Discharge Plasma Actuators and Their Application At Subsonic Speeds. 2012.

[46] R. Erfani, H. Zare-Behtash, C. Hale, and K. Kontis. Development of DBD plasma actuators: The double encapsulated electrode. *Acta Astronautica*, 109:132–143, 2015.

[47] Ryan (Univeristy of Florida) Durscher and Subrata (Univeristy of Florida) Roy. Novel Multi-Barrier Plasma Actuators for Increased Thrust. In *48th AIAA Aerospace Sciences Meeting including the New Horizons Forum and Aerospace Exposition*, pages 2010–965, 2010. ISBN 9781600867392.

[48] R. Durscher and S. Roy. On Multi-Barrier Plasma Actuators. pages 1–11, 2011.

[49] P. Versailles, V. Gingras-Gosselin, and H. D. Vo. Impact of Pressure and Temperature on the Performance of Plasma Actuators. *AIAA Journal*, 48:859–863, 2010.

[50] J. A. Valerioti and T. C. Corke. Pressure Dependence of Dielectric Barrier Discharge Plasma Flow Actuators. *AIAA Journal*, 50:1490–1502, 2012.

[51] R. Erfani, H. Zare-Behtash, and K. Kontis. Plasma actuator: Influence of dielectric surface

temperature. *Experimental Thermal and Fluid Science*, 42:258–264, 2012.

[52] R. Erfani, H. Zare-Behtash, and K. Kontis. Influence of shock wave propagation on dielectric barrier discharge plasma actuator performance. *Journal of Physics D: Applied Physics*, 45, 2012.

[53] M. Samimy, I. Adamovich, B. Webb, J. Kastner, J. Hileman, S. Keshav, and P. Palm. Development and characterization of plasma actuators for high-speed jet control. *Experiments in Fluids*, 2004.

[54] Y. G. Utkin, S. Keshav, J. Kim, J. Kastner, I. V. Adamovich, and M. Samimy. Development and use of localized arc filament plasma actuators for high-speed flow control. *Journal of Physics D: Applied Physics*, 2007.

[55] C. Hahn, M. Kearney-Fischer, and M. Samimy. On factors influencing arc filament plasma actuator performance in control of high speed jets. *Experiments in Fluids*, 2011.

[56] K. B. M. Q. Zaman, M. F. Reeder, and M. Samimy. Control of an axisymmetric jet using vortex generators. *Physics of Fluids*, 1994.

[57] J. Hileman and M. Samimy. Effects of vortex generating tabs on noise sources in an ideally expanded mach 1.3 jet. *International Journal of Aeroacoustics*, 2003.

[58] V. Kibens, J. Dorris, III, D. Smith, and M. Mossman. Active flow control technology transition - The Boeing ACE program. In *30th Fluid Dynamics Conference*, 1999.

[59] M. Samimy, J.-H. Kim, J. Kastner, I. Adamovich, and Y. Utkin. Active control of high-speed and high-Reynolds-number jets using plasma actuators. *Journal of Fluid Mechanics*, 2007.

[60] M. Samimy and I. Adamovich. Active Control of High Reynolds Number Supersonic Jets Using Plasma Actuators. 2010.

[61] M. Samimy, N. Webb, and C. Clifford. Supersonic Inlet Flow Control Using Localized Arc Filament Plasma Actuators. Technical report, 2011.

[62] E. Caraballo, N. Webb, J. Little, J.-H. Kim, and M. Samimy. Supersonic Inlet Flow Control Using Plasma Actuator. In *47th AIAA Aerospace Sciences Meeting Including The New Horizons Forum and Aerospace Exposition*, pages 1–14, 2009.

[63] B. H. Anderson, J. Tinapple, and L. Surber. Optimal Control of Shock Wave Turbulent Boundary Layer Interactions Using Micro-Array Actuation. *3rd AIAA Flow Control Conference*, pages 1–14, 2006.

[64] M. Samimy, K. B. M. Q. Zaman, and M. F. Reeder. Effect of tabs on the flow and noise field

of an axisymmetric jet. *AIAA Journal*, 31:609–619, 1993.

[65] P. Dupont, C. Haddad, and J. F. Debiève. Space and time organization in a shock-induced separated boundary layer. *Journal of Fluid Mechanics*, 2006.

[66] N. Webb, C. Clifford, and M. Samimy. Control of oblique shock wave/boundary layer interactions using plasma actuators. *Experiments in Fluids*, 54, 2013.

[67] V. Jaunet, J. Debiève, and P. Dupont. Experimental Investigation of an Oblique Shock Reflection with Separation over a Heated Wall. In *50th AIAA Aerospace Sciences Meeting*, 2012.

[68] H. Zare-Behtash, K.H. Lo, K. Kontis, T. Ukai, and S. Obayashi. Transverse jet-cavity interactions with the influence of an impinging shock. *International Journal of Heat and Fluid Flow*, 2015.

[69] T. Ukai, H. Zare-behtash, E. Erdem, K.H. Lo, and K. Kontis. Effectiveness of jet location on mixing characteristics inside a cavity in supersonic flow. *Experimental Thermal and Fluid Science*, 2014.

[70] Takahiro Ukai, Hossein Zare-behtash, Erinc Erdem, Kin Hing, and Konstantinos Kontis. Effectiveness of jet location on mixing characteristics inside a cavity in supersonic flow. *Experimental Thermal and Fluid Science*, 52:59–67, 2014.

[71] N. Webb and M. Samimy. Supersonic Cavity Control Using Plasma Actuators. *53rd AIAA Aerospace Sciences Meeting*, 2015.

[72] N Webb and M Samimy. Control of a Non-Resonating Supersonic Cavity Using Plasma Actuators. *54th AIAA Aerospace Sciences Meeting*, 2016.

[73] N Webb and M Samimy. Shock-Trapping Capability of a Cavity in a Supersonic Flow. *46th AIAA Plasmadynamics and Lasers Conference*, 2015.

[74] B. Z. Cybyk, K. R. Grossman, J. T. Wilkerson, J. Chen, and J. Katz. Single-Pulse Performance of the SparkJet Flow Control Actuator. In *AIAA Paper*, pages 1–12, 2005.

[75] A. Glezer, M. G. Allen, D. J. Coe, B. L. Smith, M. A. Trautman, and J. W. Wiltse. Synthetic Jet Actuator and Application thereof, 1998.

[76] T. Emerick, M. Y. Ali, C. Foster, F. S. Alvi, and S. Popkin. SparkJet characterizations in quiescent and supersonic flowfields. *Experiments in Fluids*, 55, 2014.

[77] L. Wang, Z. Xia, Z. Luo, and J. Chen. Three-Electrode Plasma Synthetic Jet Actuator for High-Speed Flow Control. *AIAA Journal*, 52(4):1–4, 2014.

[78] M. A. Lieberman and A. J. Lichtenberg. *Principles of Plasma Discharges and Materials Pro-*

cessing. Wiley, New jersey, 2nd edition, 2005.

[79] S. H. Popkin, T. M. Taylor, and B. Z. Cybyk. Development and application of the Sparkjet actuator for high-speed flow control. *Johns Hopkins APL Technical Digest (Applied Physics Laboratory)*, 32(1):404–418, 2013.

[80] G. Sary, G. Dufour, F. Rogier, and K. Kourtzanidis. Modeling and Parametric Study of a Plasma Synthetic Jet for Flow Control. *AIAA Journal*, 52(8):1591–1603, 2014.

[81] D. Caruana, J. P. Cambronne, P. Barricau, and A. Belinger. The Plasma Synthetic Jet Actuator for Separation Control. *ERCOFTAC Bulletin*, 94, 2013.

[82] P. Hardy. *Etude et qualification aérothermodynamique et électrique d'un actionneur plasma de type jet*. PhD thesis, University de Toulouse, 2011.

[83] V. Narayanaswamy, L. L. Raja, and N. T. Clemens. Characterization of a High-Frequency Pulsed-Plasma Jet Actuator for Supersonic Flow Control. *AIAA Journal*, 48(2):297–305, 2010.

[84] A. Belinger, P. Hardy, P. Barricau, J. P. Cambronne, and D. Caruana. Influence of the energy dissipation rate in the discharge of a plasma synthetic jet actuator. *Journal of Physics D: Applied Physics*, 44, 2011.

[85] A. Belinger, N. Naudé, J. P. Cambronne, and D. Caruana. Plasma synthetic jet actuator: electrical and optical analysis of the discharge. *Journal of Physics D: Applied Physics*, 47, 2014.

[86] V. Narayanaswamy, L. L. Raja, and N. T. Clemens. Control of unsteadiness of a shock wave/turbulent boundary layer interaction by using a pulsed-plasma-jet actuator. *Physics of Fluids*, 24, 2012.

[87] V. Narayanaswamy, L. L. Raja, and N. T. Clemens. Control of a Shock/Boundary-Layer Interaction by Using a Pulsed-Plasma Jet Actuator. *AIAA Journal*, 50(1):246–249, 2012.

[88] R. K. Lobb. *Experimental Measurement of Shock Detachment Distance on Spheres Fired in Air at Hypervelocities*. Defense Technical Information Center, 1962.

[89] H. Julian, A. Seiff, T. Canning, G. Goodwin, and J. Allen. *Gas Dynamics in Space Exploration*. National Aeronautics and Space Administration, 1962.

[90] H. G. Hornung. Non-equilibrium dissociating flow over spheres and circular cylinders, 1972.

[91] K. V. Anderson and D. D. Knight. Plasma Jet for Flight Control. *AIAA Journal*, 50(9): 1855–1872, 2012.

[92] D. Jin, W. Cui, Y. Li, F. Li, M. Jia, Q. Sun, and B. Zhang. Characteristics of pulsed plasma

synthetic jet and its control effect on supersonic flow. *Chinese Journal of Aeronautics*, 28(1): 66–76, 2015.

[93] E. K. Damon and R. G. Tomlinson. Observation of Ionization of Gases by a Ruby Laser. *Applied Optics*, 2:546, 1963.

[94] G. Leuchs. Multiphoton ionization of atoms. *Laser Physics*, 182:174–194, 1983.

[95] E. Panarella. Theory of laser-induced gas ionization. *Foundations of Physics*, 4:227–259, 1974.

[96] Y. P. Raizer. Heating of a Gas by a Powerful Light Pulse. *Soviet Physics JetP*, 21(5), 1965.

[97] H. Yan, R. Adelgren, M. Boguszko, G. Elliott, and D. Knight. Laser Energy Deposition in Quiescent Air. *AIAA Journal*, 41(10):1988–1995, 2003.

[98] R. G. Adelgren, Gregory S. Elliott, and D. Knight. Energy deposition in supersonic flows. *AIAA paper*, 0885, 2001.

[99] I. Dors, C. Parigger, and J. Lewis. Fluid dynamics effects following laser-induced optical breakdown. In *38th Aerospace Sciences Meeting and Exhibit*, 2000.

[100] E. E. Meshkov. Instability of the interface of two gases accelerated by a shock wave. *Fluid Dynamics*, 4:101–104, 1969.

[101] R. D. Richtmyer. Taylor Instability in Shock Acceleration of Compressible Fluids. *Communications on Pure and Applied Mathematics*, XIII:297–319, 1960.

[102] Y. Ogino, N. Ohnishi, S. Taguchi, and K. Sawada. Baroclinic vortex influence on wave drag reduction induced by pulse energy deposition. *Physics of Fluids*, 21(2009), 2009.

[103] D. Knight. A summary of laser and microwave flow control in high-speed flows. *Progress in Flight Physics*, 5:125–138, 2013.

[104] A. W. Ali. On Laser Air Breakdown, Threshold Power and Laser Generated Channel Length. Technical report, Naval Research Laboratory, 1983.

[105] N. A. Generalov, V. P. Zimakov, and G. I. Kozlov. Continuous Optical Discharge. *Soviet Physics JetP Letters*, 1970.

[106] E. Erdem, K. Kontis, and L. Yang. Steady energy deposition at Mach 5 for drag reduction. *Shock Waves*, 23:285–298, 2013.

[107] E. Schülein and A. Zheltovodov. Effects of steady flow heating by arc discharge upstream of non-slender bodies. *Shock Waves*, 21:383–396, 2011.

[108] D. Sperber, H. A. Eckel, S. Steimer, and S. Fasoulas. Objectives of Laser-Induced Energy Deposition for Active Flow Control. *Contributions to Plasma Physics*, 52(7):636–643, 2012.

[109] A. Sasoh, Y. Sekiya, T. Sakai, J. Kim, and A. Matsuda. Supersonic Drag Reduction with Repetitive Laser Pulses Through a Blunt Body. *AIAA Journal*, 48(12):2811–2817, 2010.

[110] Doyle D. Knight. Survey of Aerodynamic Drag Reduction at High Speed by Energy Deposition. *Journal of Propulsion and Power*, 24(6):1153–1167, 2008.

[111] A. Sasoh, J. H. Kim, K. Yamashita, T. Sakai, and A. Matsuda. Efficient supersonic drag reduction using repetitive laser pulses of up to 80 kHz. *AIP Conference Proceedings*, 1402 (2011):424–429, 2011.

[112] A. Sasoh, J. H. Kim, K. Yamashita, and T. Sakai. Supersonic aerodynamic performance of truncated cones with repetitive laser pulse energy depositions. *Shock Waves*, 24:59–67, 2014.

[113] R. G. Adelgren, H. Yan, G. S. Elliott, D. D. Knight, T. J. Beutner, and A. A. Zheltovodov. Control of Edney IV Interaction by Pulsed Laser Energy Deposition. *AIAA Journal*, 43(2): 256–269, 2005.

[114] B. E. Edney. Effects of shock impingement on the heat transfer around blunt bodies., 1968.

[115] H. Yanjii, D. Wang, Q. Li, and J. Ye. Interaction of single-pulse laser energy with bow shock in hypersonic flow. *Chinese Journal of Aeronautics*, 27(2):241–247, 2014.

[116] J. Kim, A. Matsuda, T. Sakai, and A. Sasoh. Wave Drag Reduction with Acting Spike Induced by Laser-Pulse Energy Depositions. *AIAA Journal*, 49(9):2076–2078, 2011.

[117] T. Sakai. Supersonic Drag Performance of Truncated Cones with Repetitive Energy Deposition. *International Journal of Aerospace Innovations*, 1:31–43, 2009.

[118] T. Osuka, E. Erdem, N. Hasegawa, R. Majima, T. Tamba, S. Yokota, A. Sasoh, and K. Kontis. Laser energy deposition effectiveness on shock-wave boundary-layer interactions over cylinder-flare combinations. *Physics of Fluids*, 26, 2014.

[119] E. Erdem, K. Kontis, T. Osuka, R. Majima, T. Tamba, and A. Sasoh. Laser Energy Deposition for Shock Wave Boundary Layer Control at Supersonic Speeds. In *29th International Symposium on Shock Waves*, pages 1411–1416, 2013.

[120] H. Yan, D. Knight, R. Kandala, and G. Candler. Effect of a Laser Pulse on a Normal Shock. *AIAA Journal*, 45(6):1270–1280, 2007.

[121] Y. V. Khodataev. Problems of discharge safety on the onboard antennas of high flying objects. *Nauchno-Proizvodstvennoe*, 1957.

[122] Y. Kolesnichenko, O. Azarova, V. Brovkin, D. Khmara, V. Lashkov, I. Mashek, and M. Ryvkin. Basics in Beamed MW Energy Deposition for Flow/Flight Control. In *42nd AIAA Aerospace*

Sciences Meeting and Exhibit, 2004.

[123] D. Knight and Y. F. Kolesnichenko. Interaction of Microwave-generated Plasma with Hemisphere-Cone-Cylinder. *48th AIAA Aerospace Sciences Meeting Including the New Horizons Forum and Aerospace Exposition*, (January):2010, 2010.

[124] K. V. Khodataev. Microwave Discharges and Possible Applications in Aerospace Technologies. *Journal of Propulsion and Power*, 24(5):962–972, 2008.

[125] F. Paschen. Ueber die zum Funkenübergang in Luft, Wasserstoff und Kohlensäure bei verschiedenen Drucken erforderliche Potentialdifferenz. *Annalen der Physik*, 273:69–96, 1889.

[126] V. M. Shibkov, A. F. Aleksandrov, V. A. Chernikov, A. P. Ershov, and L. V. Shibkova. Microwave and Direct-Current Discharges in High-Speed Flow: Fundamentals and Application to Ignition. *Journal of Propulsion and Power*, 25(1):123–137, 2009.

[127] V. I Kolobov and D. J. Economou. The anomalous skin effect in gas discharge plasmas. *Plasma Sources Science and Technology*, 6, 1997.

[128] V. M.. Shibkov, A. F. Aleksandrov, A. P. Ershov, I. B. Timofeev, V. A. Chernikov, and L. V. Shibkova. Freely localized microwave discharge in a supersonic gas flow. *Plasma Physics Reports*, 31(9):795–801, 2005.

[129] B. McAndrew, J. Kline, and R. B. Miles. Aerodynamic control of a symmetric cone in compressible flow using microwave driven plasma discharges. *41st Aerospace Sciences Meeting*, (January), 2003.

[130] V. Lashkov, I. Mashek, Y. Anisimov, V. Ivanov, Y. Kolesnichenko, and M. Ryvkin. Gas Dynamic Effect of Microwave Discharge on Supersonic Cone-shaped Bodies. In *42nd AIAA Aerospace Sciences Meeting and Exhibit*, 2004.

[131] L. P. Grachev, I. I. Esakov, G. I. Mishin, and K. V. Khodataev. The high frequency air breakdown in presence of a vibrator. *Zhurnal Tekhnicheskoi Fiziki*, 1995.

[132] R. B. Miles. Flow Control by Energy Addition into High-Speed Air. *AIAA Journal*, pages 1–14, 2000.

[133] J. B. Michael, M. R. Edwards, and R. B. Miles. Time-resolved temperature measurements of laser- designated , microwave driven ignition. In *49th AIAA Aerospace Sciences Meeting including the New Horizons Forum and Aerospace Exposition*, pages 1–7, 2011.

[134] R. S. Khoronzhuk, A. G. Karpenko, V. A. Lashkov, D. P. Potapeko, and I. Ch. Mashek. Microwave discharge initiated by double laser spark in a supersonic airflow. *Journal of Plasma*

Physics, 81:1–12, 2015.

[135] I. Mashek, V. Lashkov, R. Khoronzhuk, D. Potapenko, and V. Brovkin. Laser-Initiated Dipole Structures. *52nd Aerospace Sciences Meeting*, pages 1–6, 2014.

[136] D. Bivolaru and S. P. Kuo. Evidence of non-thermal plasma effect for supersonic drag reduction. *IEEE Conference Record - Abstracts. 2002 IEEE International Conference on Plasma Science*, 2002.

[137] O. Azarova, D. Knight, and Y. Kolesnichenko. Instabilities, Vortices and Structures Characteristics During Interaction of Microwave Filaments with Body in Supersonic Flow. *48th AIAA Aerospace Sciences Meeting Including the New Horizons Forum and Aerospace Exposition 4 - 7 January 2010, Orlando, Florida*, (January), 2010.

[138] O. Azarova, D. Knight, and Y. Kolesnichenko. Flow control via instabilities, vortices and steady structures under the action of external microwave energy release. *Proceedings of the Institution of Mechanical Engineers, Part G: Journal of Aerospace Engineering*, 227(9):1498–1515, 2012.

[139] O. Azarova. Supersonic Flow Control Using Combined Energy Deposition. *Aerospace*, 2: 118–134, 2015.

[140] O. A. Azarova. Generation of RichtmyerMeshkov and secondary instabilities during the interaction of an energy release with a cylinder shock layer. *Aerospace Science and Technology*, 42: 376–383, 2015.

[141] D. Knight, O. Azarova, and Y. Kolesnichenko. On Details of Flow Control via Characteristics and Location of Microwave Filament During Its Interaction with Supersonic Blunt Body. In *47th AIAA Aerospace Sciences Meeting including The New Horizons Forum and Aerospace Exposition*, 2009.

[142] D. Knight, Y. F. Kolesnichenko, V. Brovkin, and D. Khmara. High Speed Flow Control Using Microwave Energy Deposition. *16th Australasian Fluid Mechanics Conference*, (December): 199–206, 2007.

[143] D. Knight, V. Brovkin, D. Khmara, Y. Kolesnichenko, V. Lashkov, and I. Mashek. Interaction of a microwave-generated plasma with flow past a hemisphere cylinder at mach 2.1. *AIAA Journal*, (12):2996–3011, 2009.

[144] J. Wagner, K. Yuceil, N. Clemens, and D. Dolling. Experimental investigation of unstart in an inlet/isolator model in Mach 5 flow. *AIAA Journal*, 47(6):1528–1542, 2009.

[145] K. Matsuo, Y. Miyazato, and H. Kim. Shock train and pseudo-shock phenomena in internal

gas flows. *Progress in Aerospace Sciences*, 35:33–100, 1999.

[146] S. Emami, C. A. Trexler, A. H. Auslender, and John P.J. Weidner. Experimental investigation of inlet-combustor isolators for a dual-mode scramjet at a Mach number of 4. Technical Report May, 1995.

[147] J. L. Wagner, K. B. Yuceil, and N. T. Clemens. Velocimetry Measurements of Unstart of an Inlet-Isolator Model in Mach 5 Flow. *AIAA Journal*, 48(6):1875–1888, 2010.

[148] F. O. Thomas, C. M. Putnam, and H. C. Chu. On the mechanism of unsteady shock oscillation in shock wave/turbulent boundary layer interactions. *Experiments in Fluids*, 18:69–81, 1994.

[149] S. Chen, L. C. J. Heijmans, R. Zeng, S. Nijdam, and U. Ebert. Nanosecond repetitively pulsed discharges in N2 O2 mixtures: inception cloud and streamer emergence. *Journal of Physics D: Applied Physics*, 48, 2015.

[150] R. Dawson and J. Little. Characterization of Nanosecond Pulse Driven Dielectric Barrier Discharge Plasma Actuators for Aerodynamic Flow Control. In *6th AIAA Flow Control Conference*, 2012.

[151] R. G. Adelgren, H. Yan, G. Elliott, D. Knight, T. J. Beutner, and A. A. Zheltovodov. Localized flow control by laser energy deposition applied to Edney IV shock impingement and intersecting shocks. *AIAA Journal*, 2003.

[152] J. W. Jacobs and V. V. Krivets. Experiments on the late-time development of single-mode RichtmyerMeshkov instability. *Physics of Fluids*, 17(2005), 2005.

[153] D. Sperber, F. Schmid, and H. A. Eckel. Wave drag reduction of blunt bodies using laser sustained energy deposition in argon atmosphere. *6th AIAA Flow Control Conference*, pages 1–10, 2012.

[154] Tomáš Homola, Jindich Matoušek, Martin Kormunda, Linda Y L Wu, and Mirko Černák. Plasma treatment of glass surfaces using diffuse coplanar surface barrier discharge in ambient air. *Plasma Chemistry and Plasma Processing*, 33:881–894, 2013.

[155] G. A. Sullins. Demonstration of mode transition in a scramjet combustor, 1993.

[156] A. Weiss, A. Grzona, and H. Olivier. Behavior of shock trains in a diverging duct. *Experiments in Fluids*, 49:355–365, 2010.

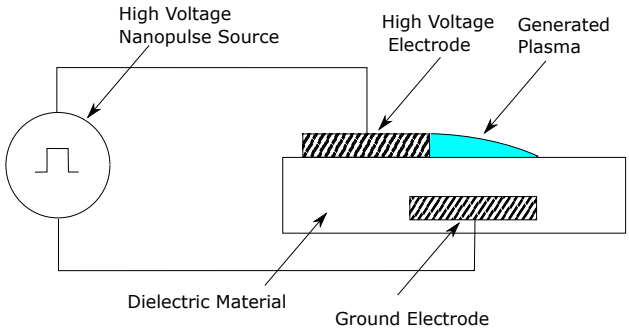

FIG. 1: Schematic of a basic dielectric barrier discharge setup

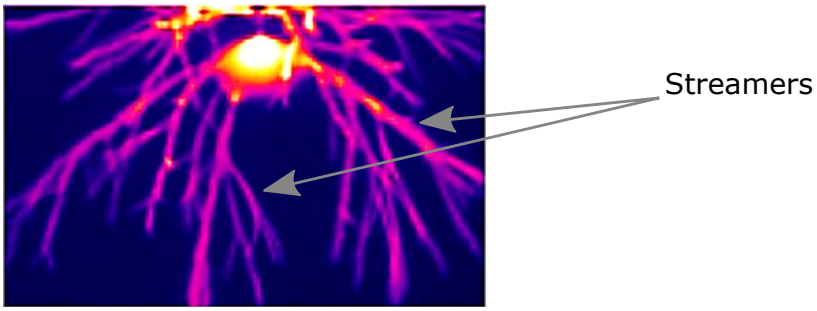

FIG. 2: Plasma discharge in streamer form[149]

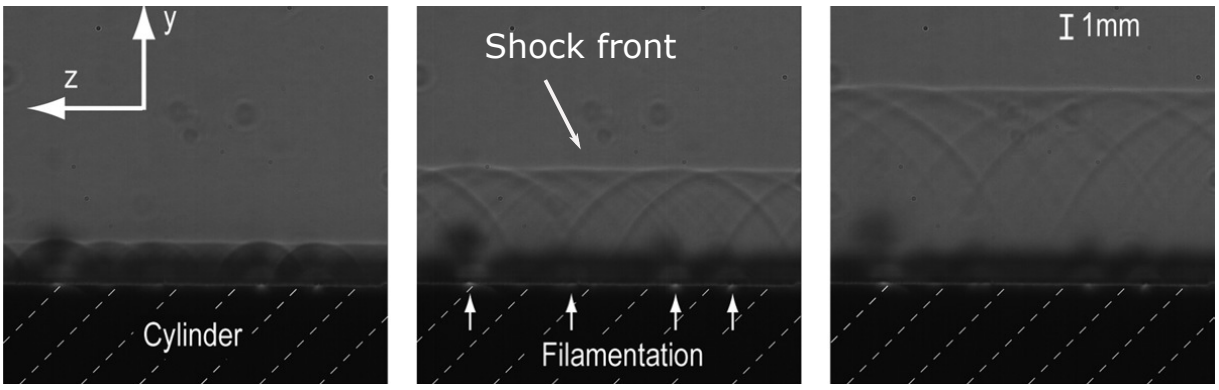

FIG. 3: Time history of compression waves generated by plasma filaments in quiescent conditions[20]

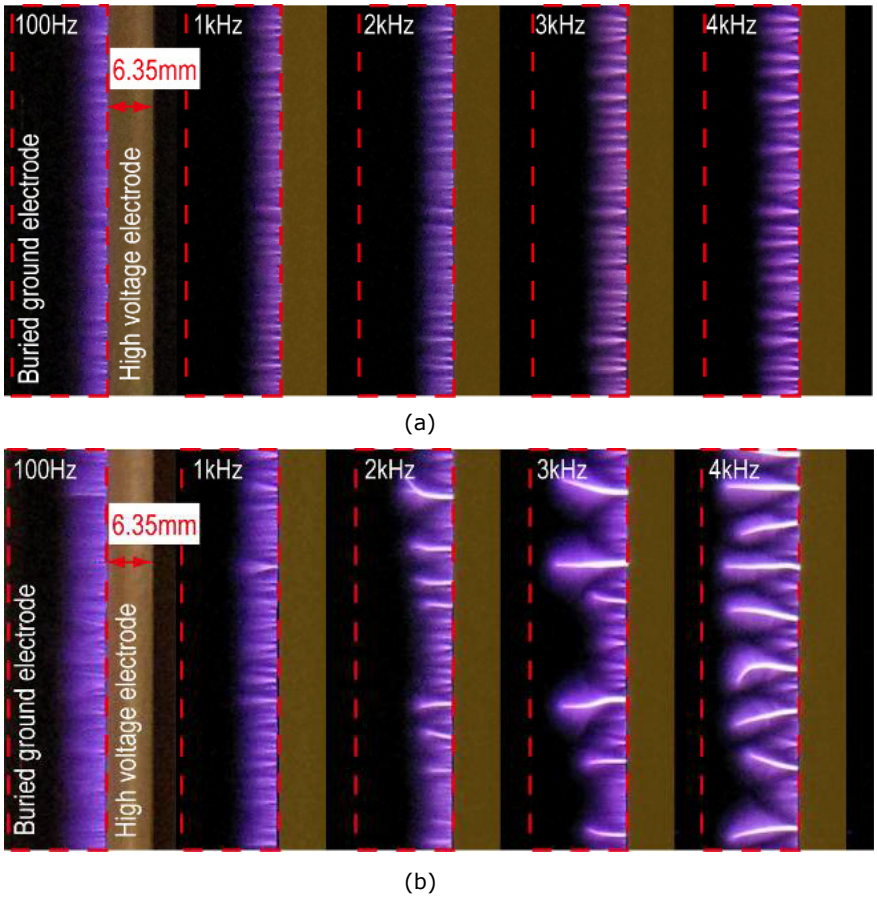

FIG. 4: Effect of pulse frequency on plasma generated by a) positive voltage pulses and b) negative voltage pulses[23]

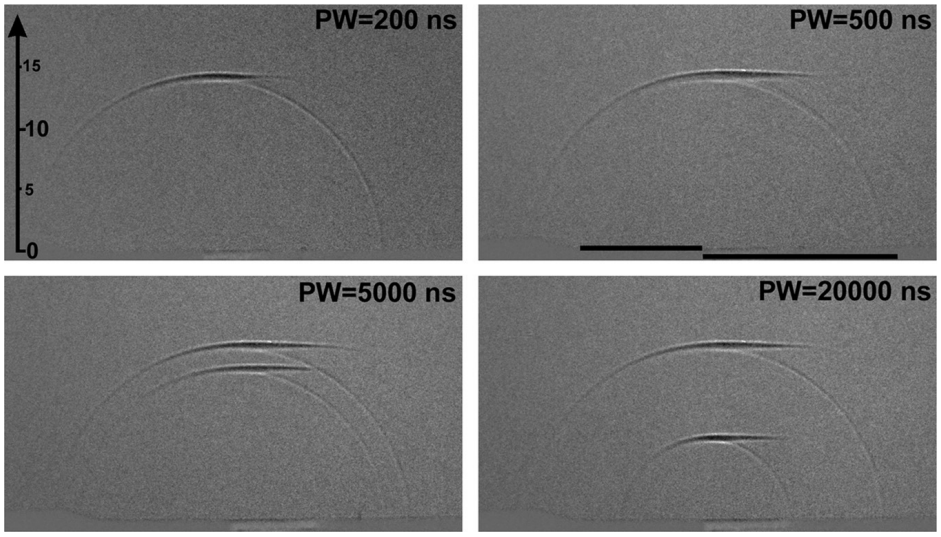

FIG. 5: Effect of pulse width on generated pressure waves[21]

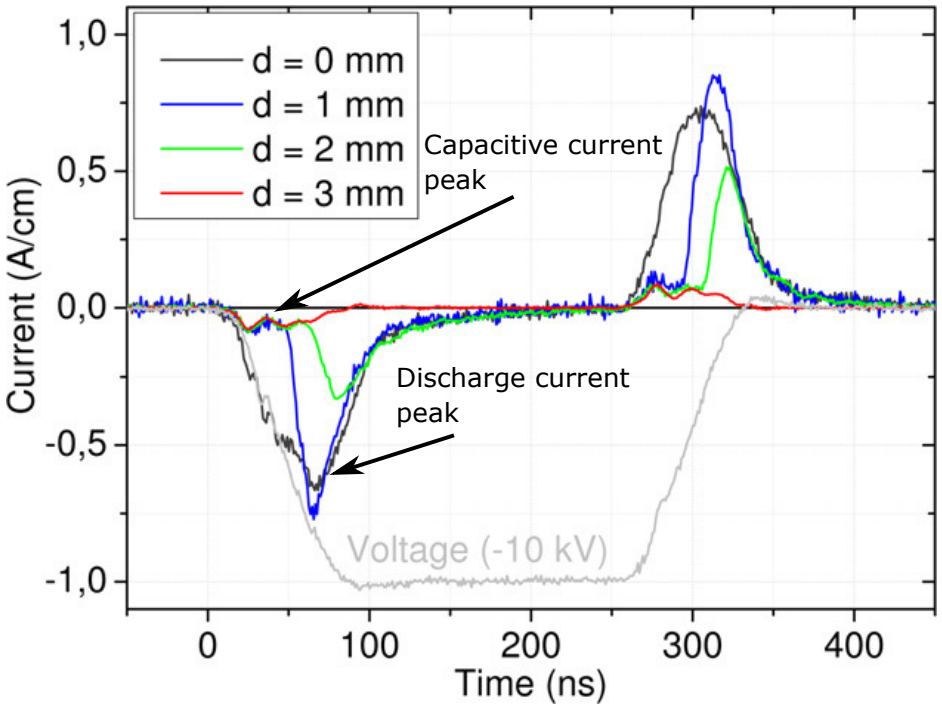

FIG. 6: Current waveforms for a range of electrode gap widths (10kV negative voltage pulse)[25]

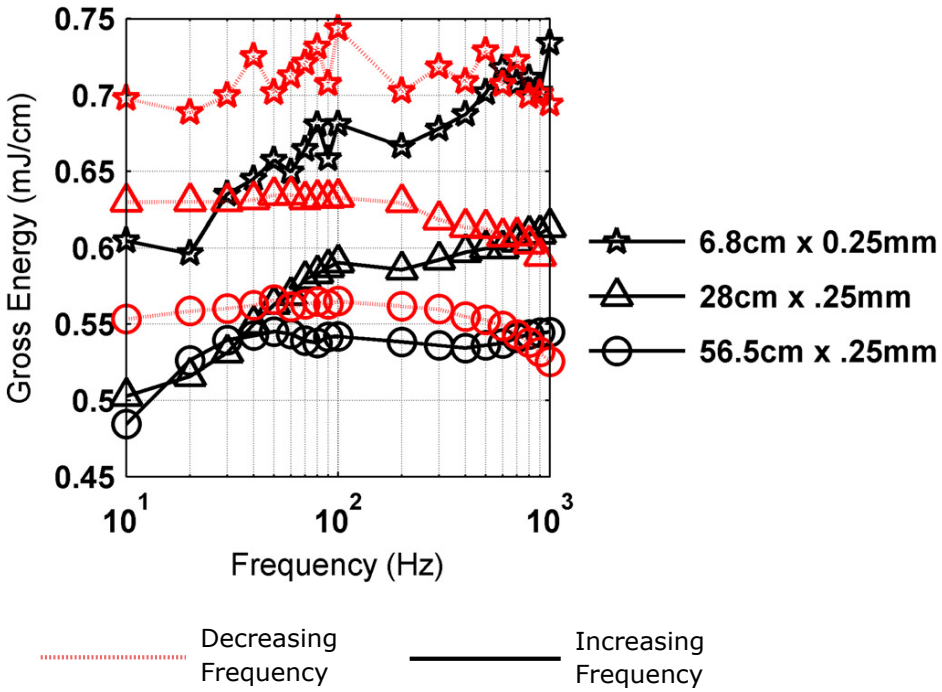

FIG. 7: Gross energy per pulse as a function of increasing (solid) or decreasing (dashed) frequency[150]

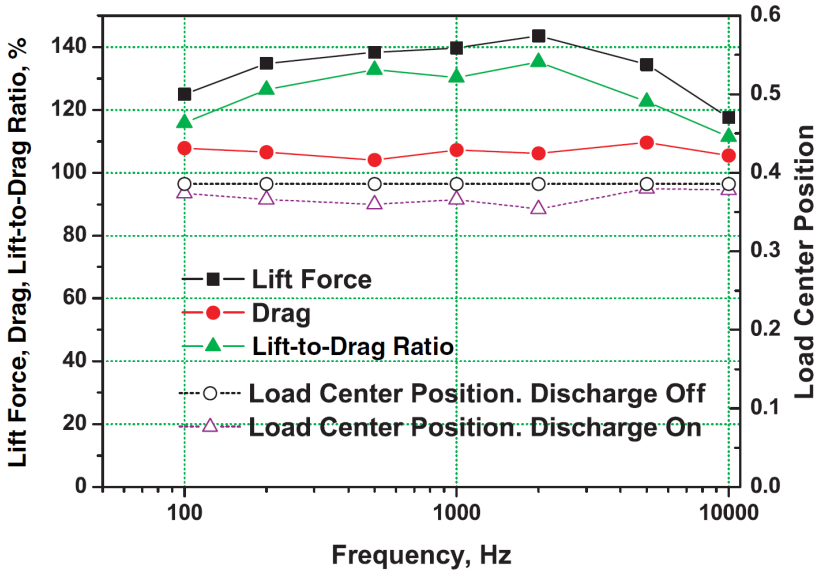

FIG. 8: Lift and drag force, lift-to-drag ratio, and load center location dependencies on discharge frequency[17]

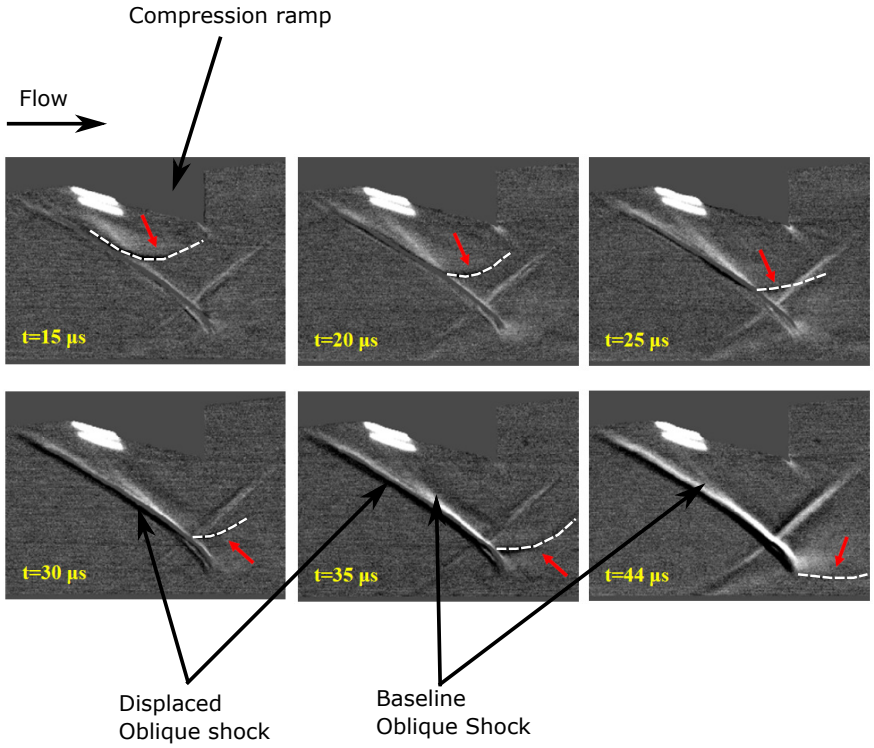

FIG. 9: Difference of two sets of Schlieren images, at time 35 and 44 μs the baseline shock is visible as the white region while the perturbed shock is the dark region (dotted white line and red arrows indicate blast wave from ns-DBD)[29]

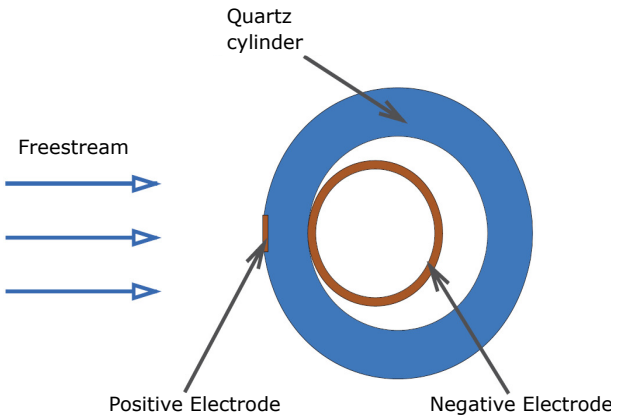

FIG. 10: ns-DBD schematic used for blunt body Mach 5 bow shock control (quartz cylinder is the blunt body)[31]

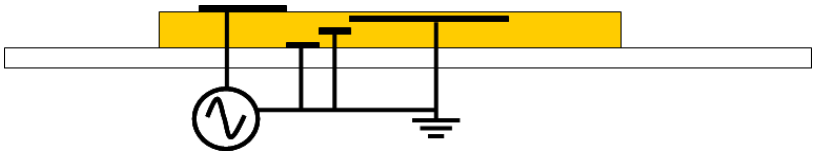

FIG. 11: Example schematic of multi encapsulated electrode DBD[42]

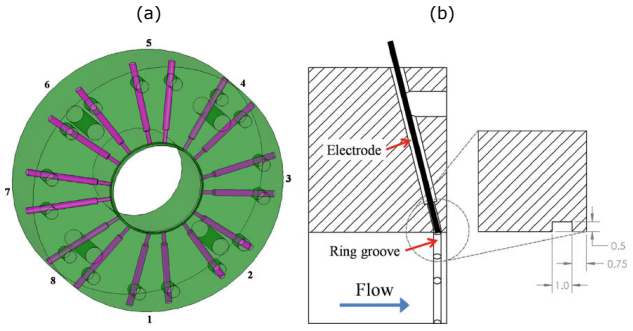

FIG. 12: Schematic of LAFPA's applied to a nozzle showing (a) entire nozzle section illustrating groove housing for actuator (b) cross section of nozzle to illustrate features[55]

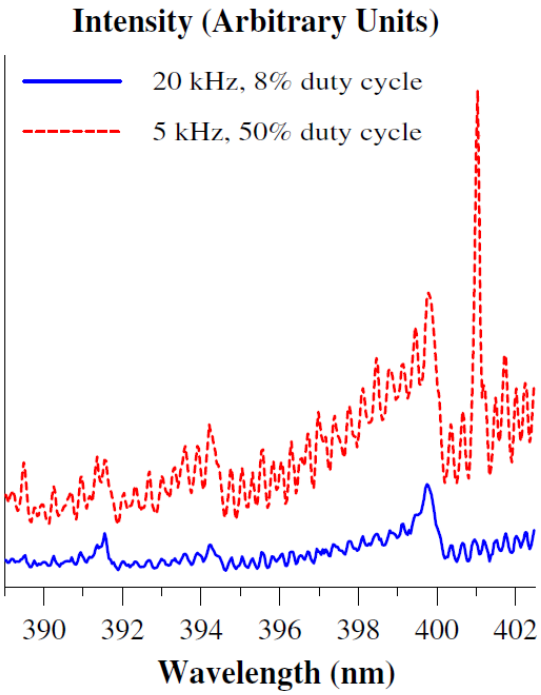

FIG. 13: Plasma visible emission spectra (N2 second positive system bands) of a LAFPA discharge for two different supply frequencies[54]

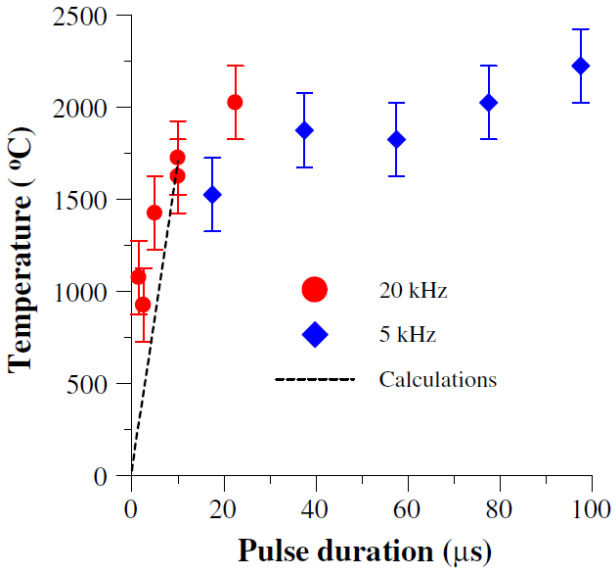

FIG. 14: Effect of supply voltage pulse duration on temperature of plasma discharge from LAFPA actuator[54]

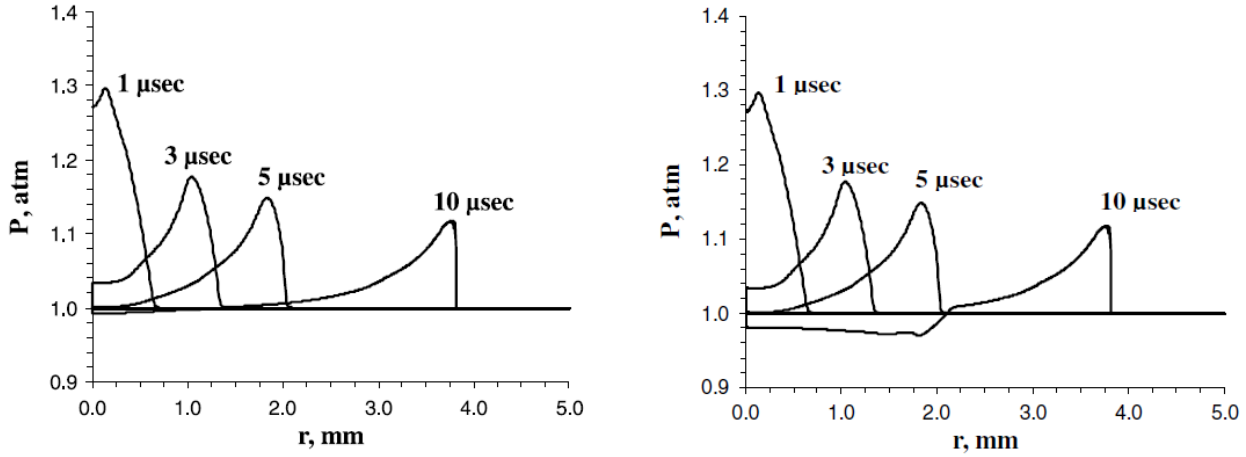

FIG. 15: Pressure profile near a modelled cylindrical arc filament at different time after initial discharge when (a) the discharge is active the entire time and (b) the discharge stops after $5\mu s$[54]

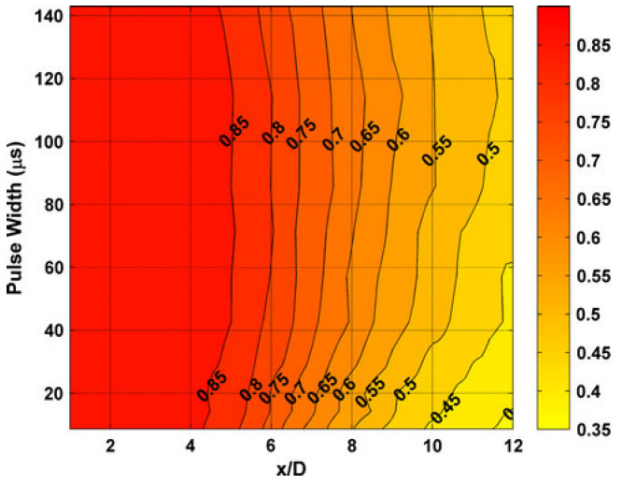

FIG. 16: Plot illustrating the effect of LAFPA supply voltage pulse width on high speed jet centreline Mach number[55]

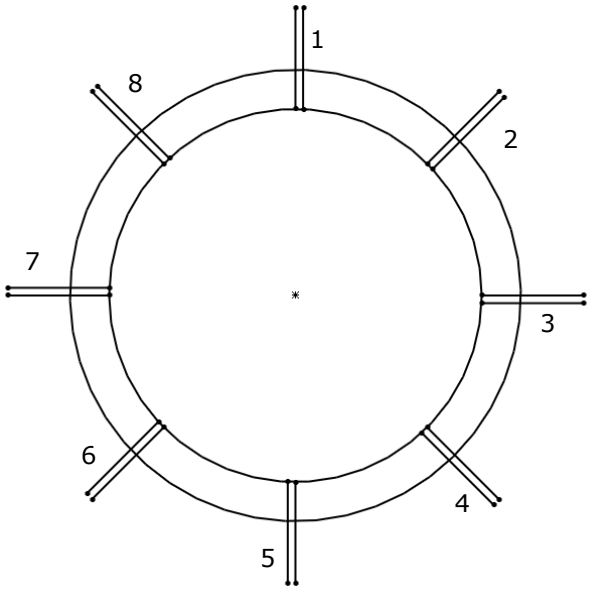

FIG. 17: Schematic of nozzle exit showing locations and numbering of LAFPA's around the circumference

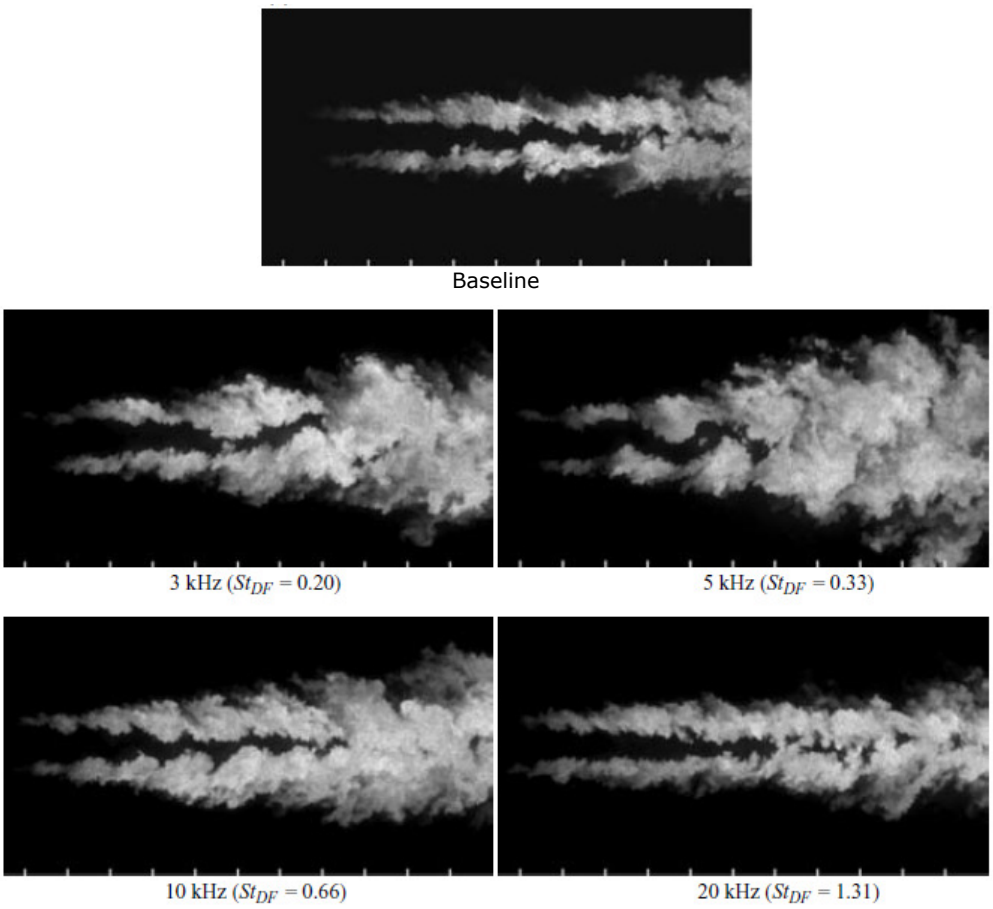

FIG. 18: Instantaneous images of laser light sheet scattered by mixing layer of a high speed jet forced by LAFPA's at different forcing frequencies[59]

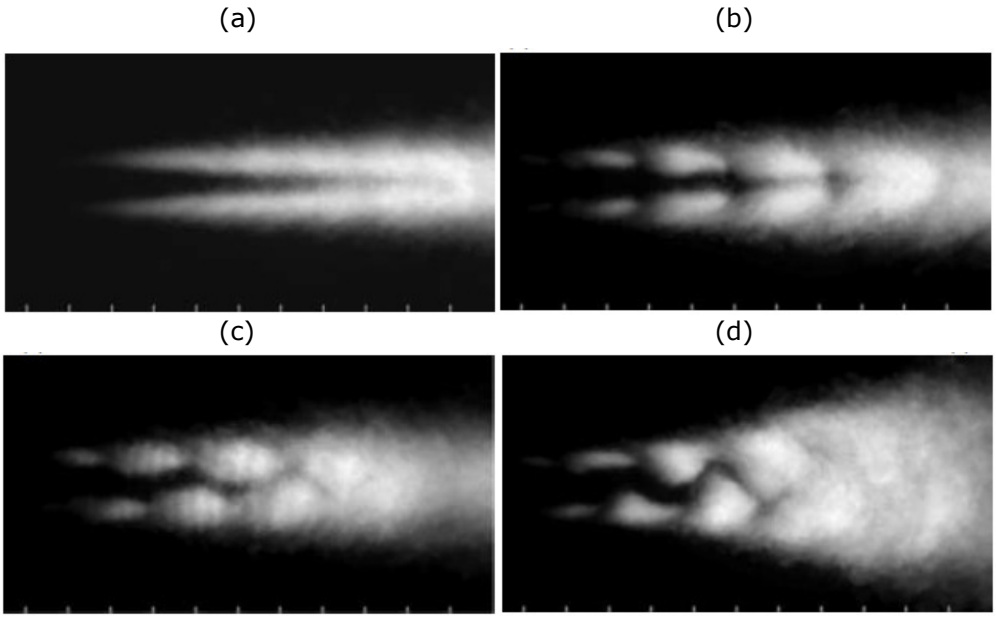

FIG. 19: Phase averaged images of laser light sheet scattered by mixing layer of a high speed jet forced by LAFPA's at different azimuthal forcing modes: (a) baseline (no forcing) (b) m = 0 (c) m = 1 (d) m = ±1[59]

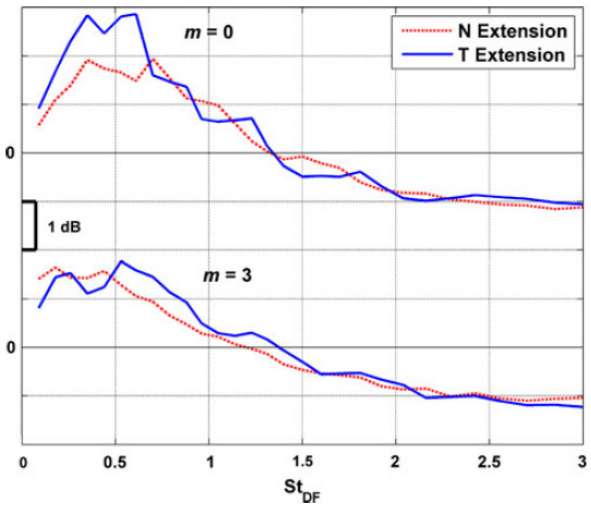

FIG. 20: The effect of LAFPA forcing frequency on the average acoustic energy[55]

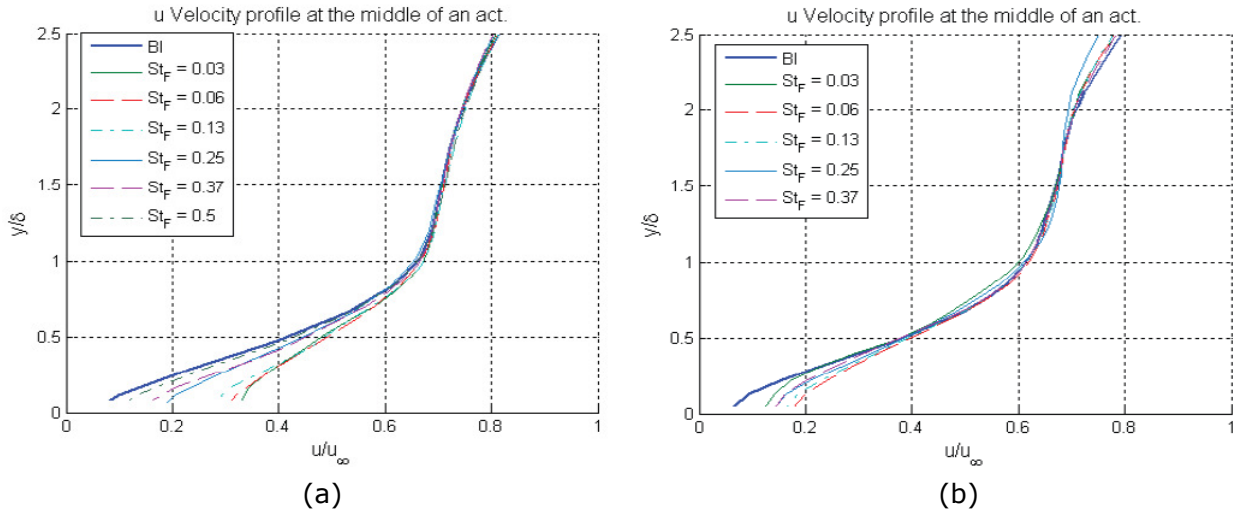

FIG. 21: The impact of LAFPA forcing frequency on boundary layer velocity profile at a SBLI for (a) upstream location and (b) downstream location[62]

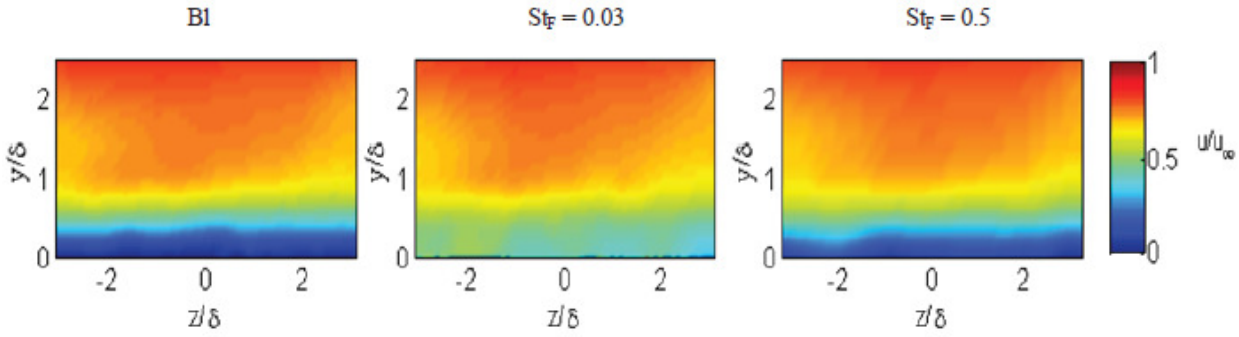

FIG. 22: PIV image showing a cross-section of the streamwise velocity in the boundary layer region for different LAFPA forcing frequencies with the actuators located upstream of the SBLI(z/δ represents the location of the actuators)[62]

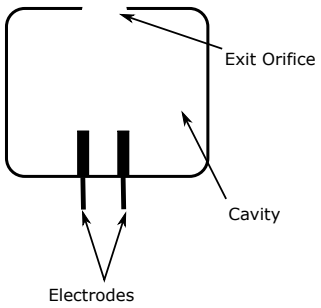

FIG. 23: Basic schematic of a simple PPSJ

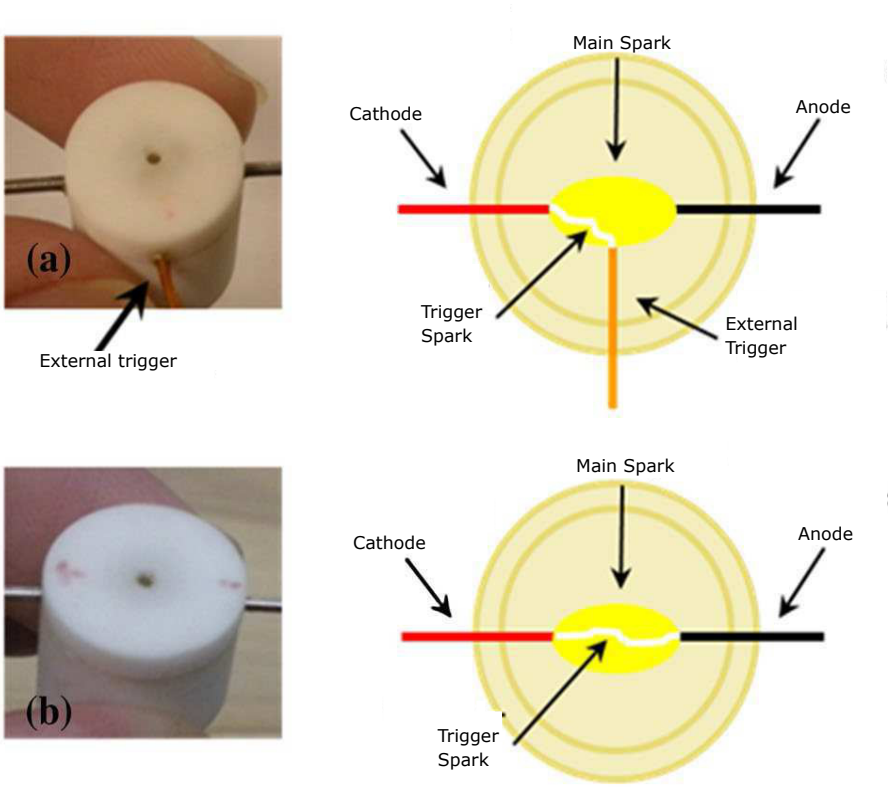

FIG. 24: Schematics of PPSJ actuator with a) external trigger electrode (3 electrodes) and b) pseudo trigger electrode (2 electrodes)[76]

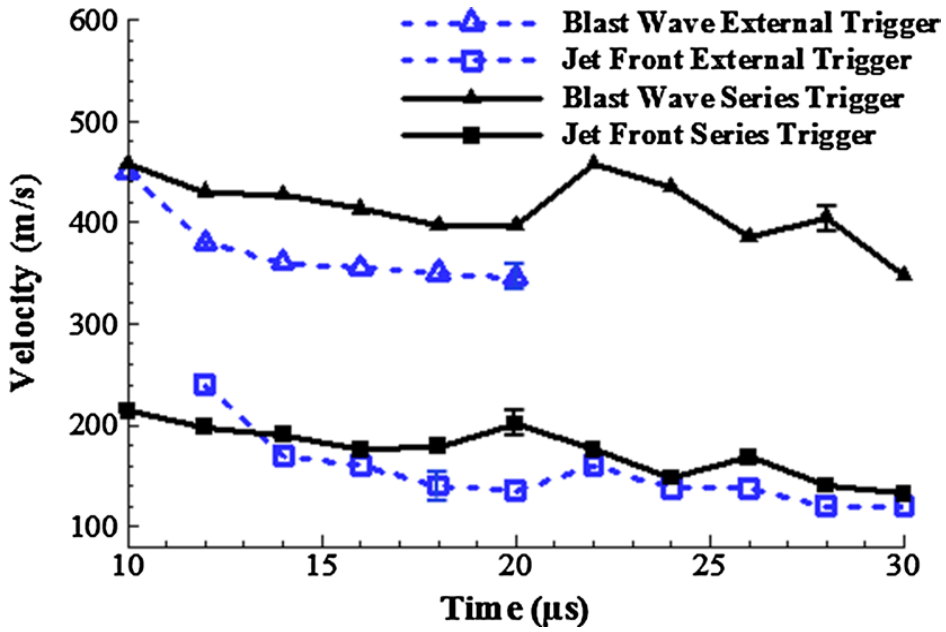

FIG. 25: Plot of blast wave/jet velocity against time of for a PPSJ using an external trigger (3 electrodes) and a PPSJ using a pseudo trigger (2 electrodes)[76]

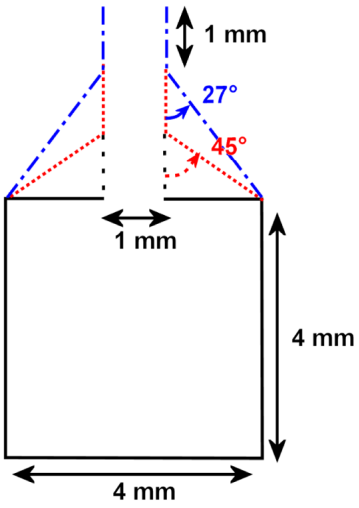

FIG. 26: Different geometries of the neck region used for the numerical model[80]

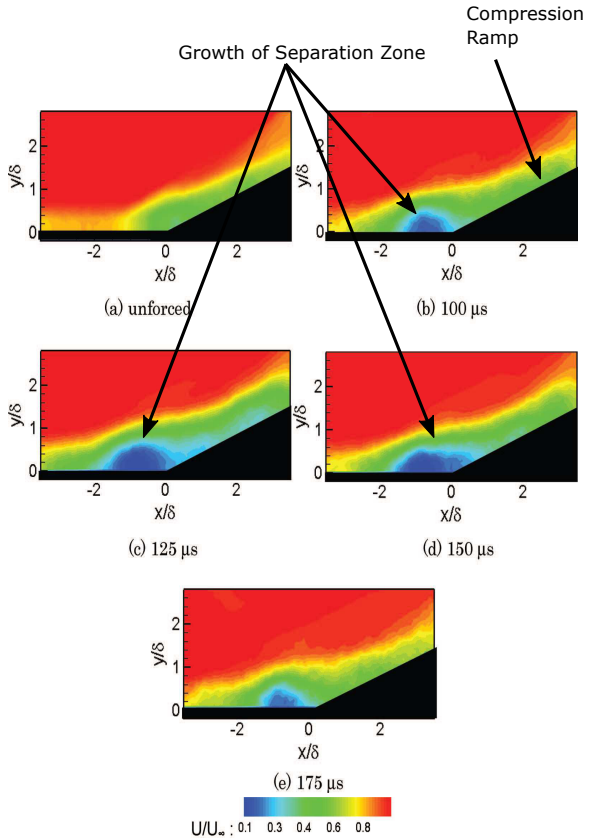

FIG. 27: Phase Averaged Streamwise Velocity Contours with and without plasma jet[86]

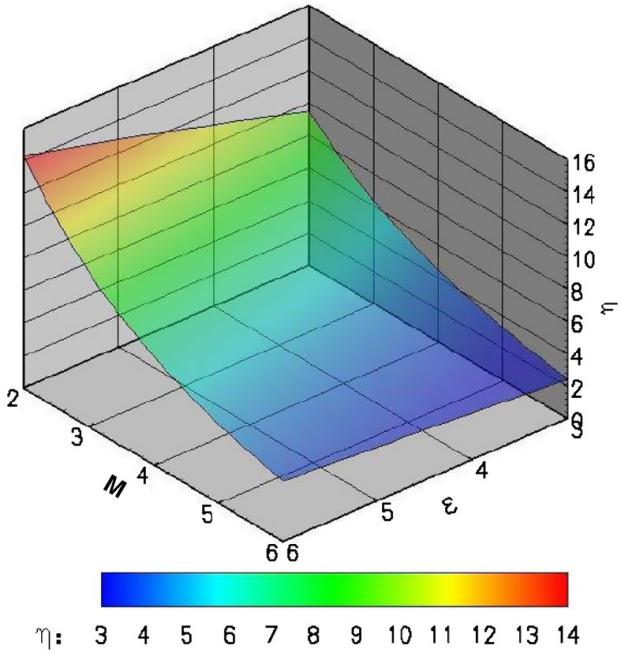

FIG. 28: 3D plot of Mach vs. dimensionless energy deposition vs. Effectiveness parameter[91]

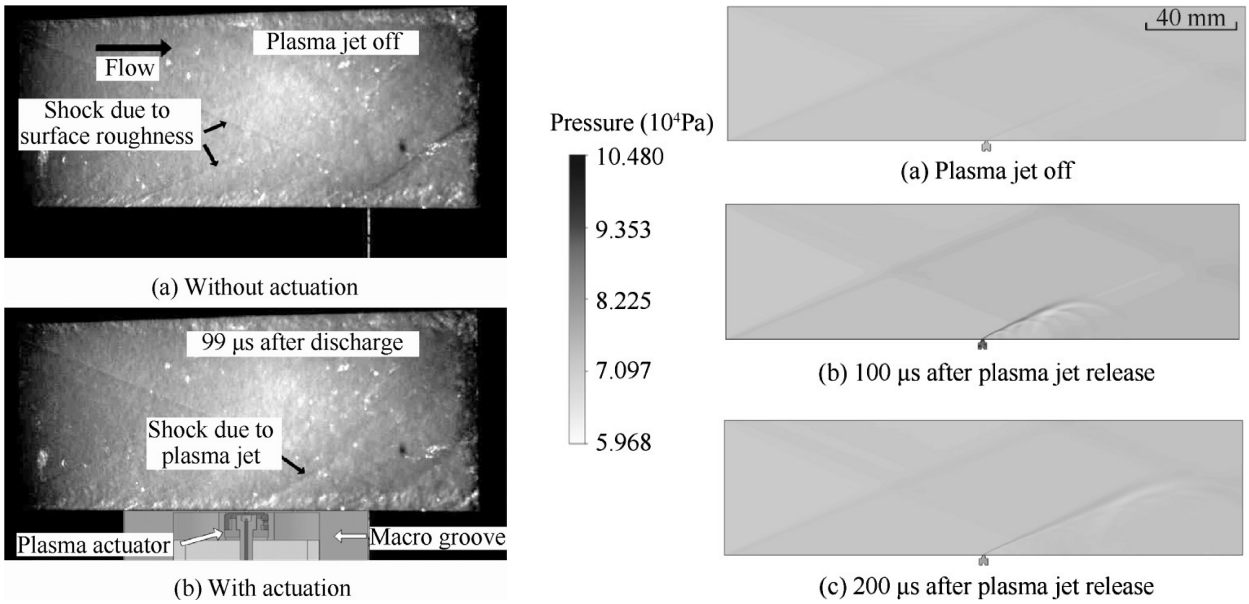

FIG. 29: Schlieren showing experimental (left) and computational (right) results of pulsed plasma synthetic jet operation in supersonic flow (Mach 2)[92]

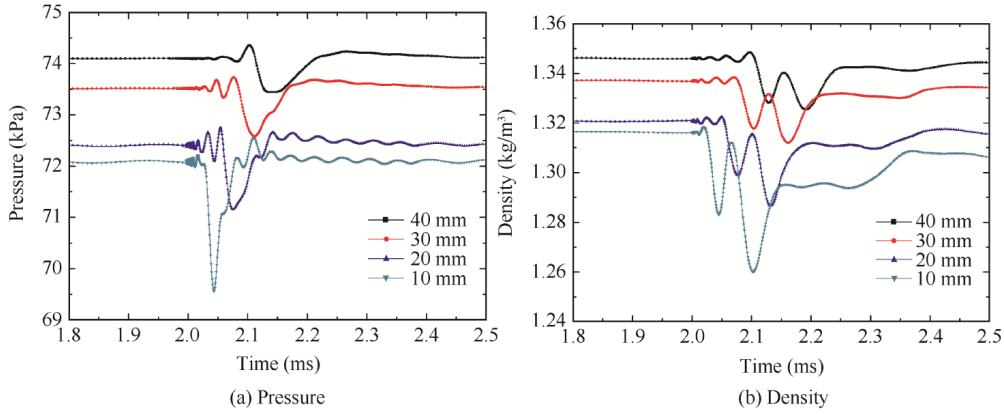

FIG. 30: Plots showing impact on boundary layer characteristics downstream of pulsed plasma synthetic jet: a) Pressure b) Density[92]

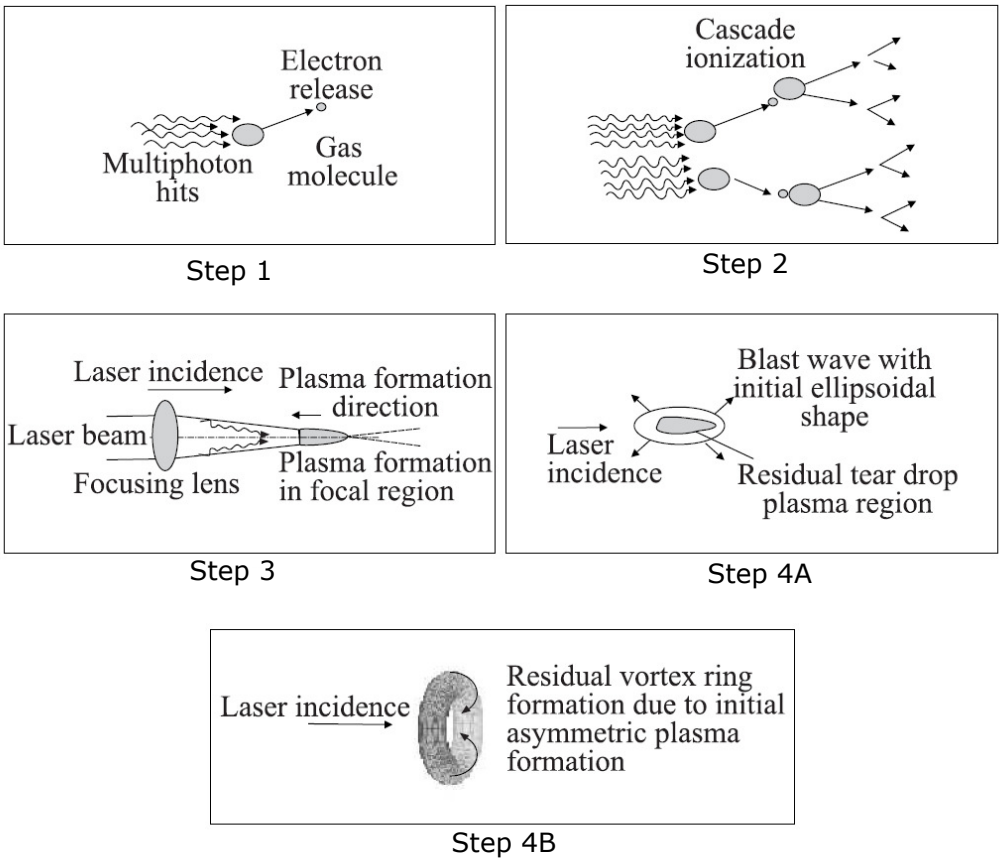

FIG. 31: 4 step process of laser induced gas breakdown[151]

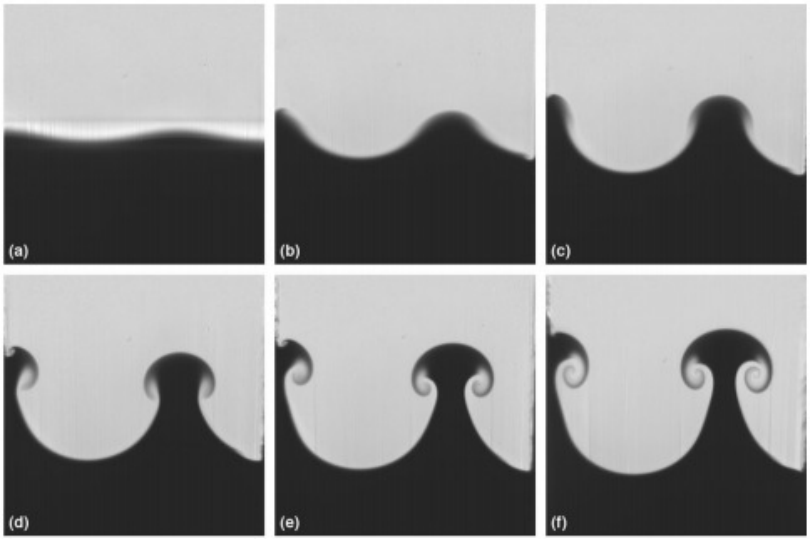

FIG. 32: Series of images showing the growth of Richtmeyer-Meshkov instability produced by an incident shock wave travelling at M = 1.11 over a period of 5.2ms[152]

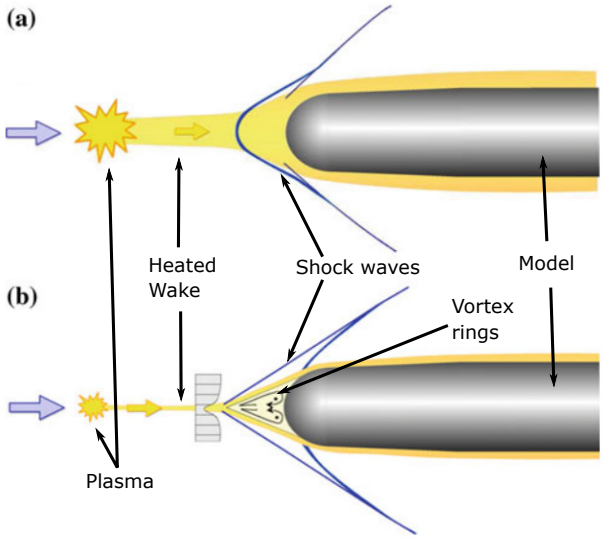

FIG. 33: Example of possible shock structure for continuous laser energy deposition applied to bluff body flows a) global effect b) localised effect[107]

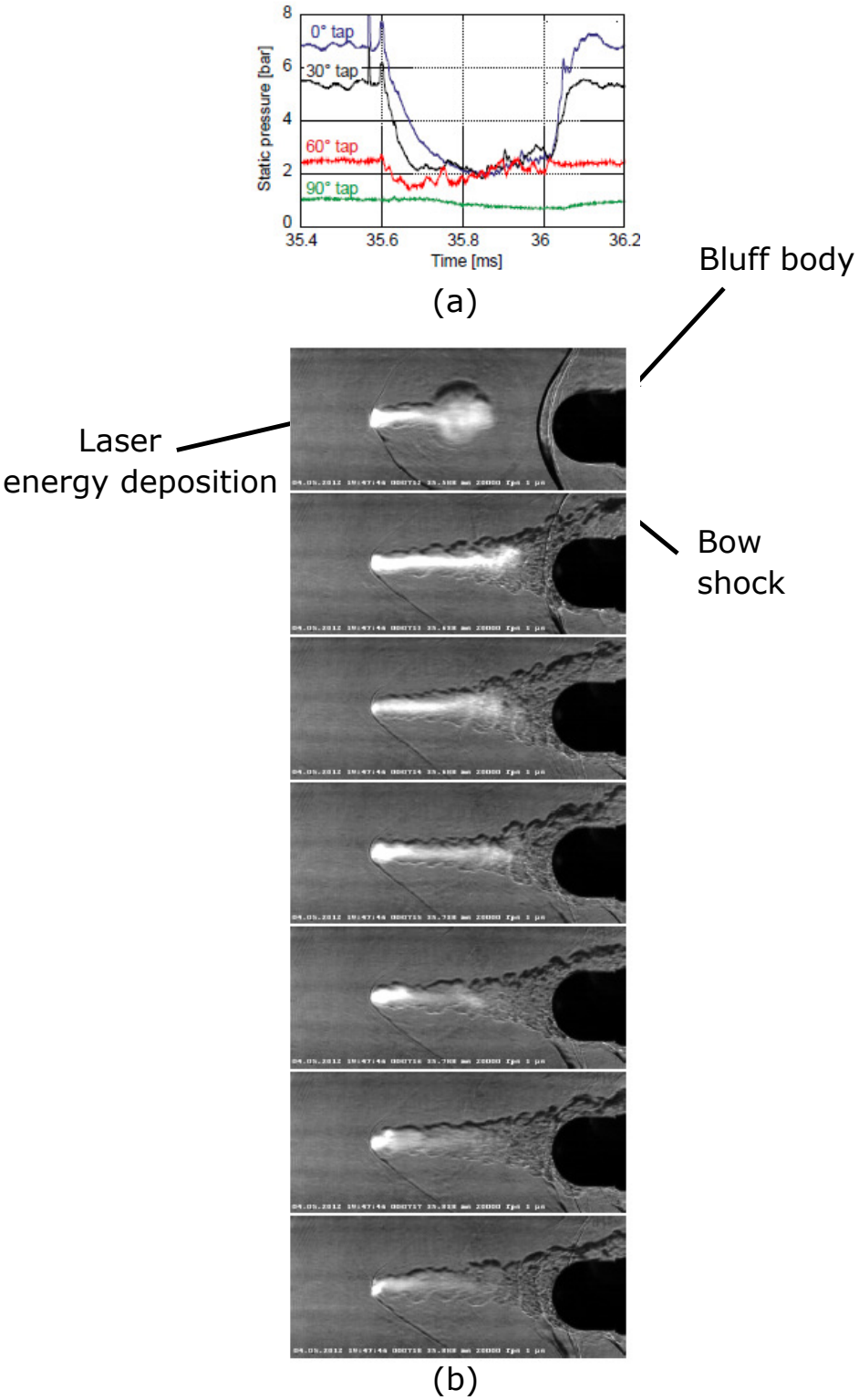

FIG. 34: Results from experiment using continuous laser energy deposition for active flow control: a) Pressure measurements at various angular positions around the half cylinder b) Schlieren image of flow[153]

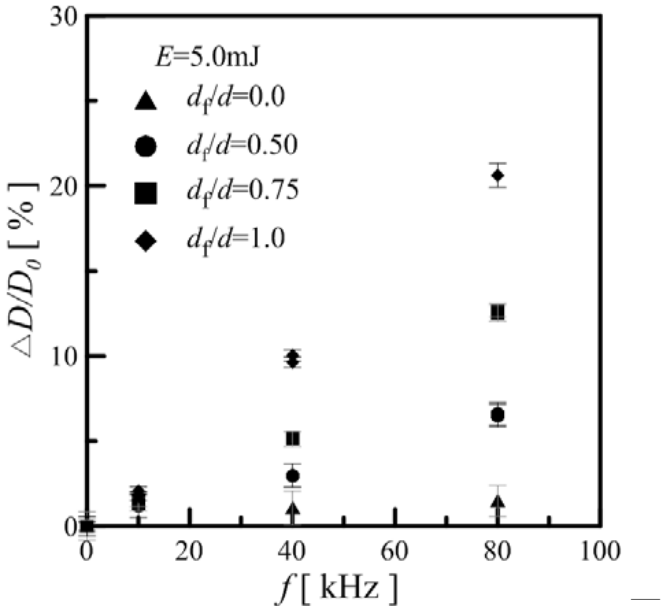

FIG. 35: Graph of percentage drag reduction against laser pulse frequency for a range of geometries where d_f/d is the nose-to-base diameter ratio of the model, ΔD is the reduction in drag and D_0 is the baseline drag[111]

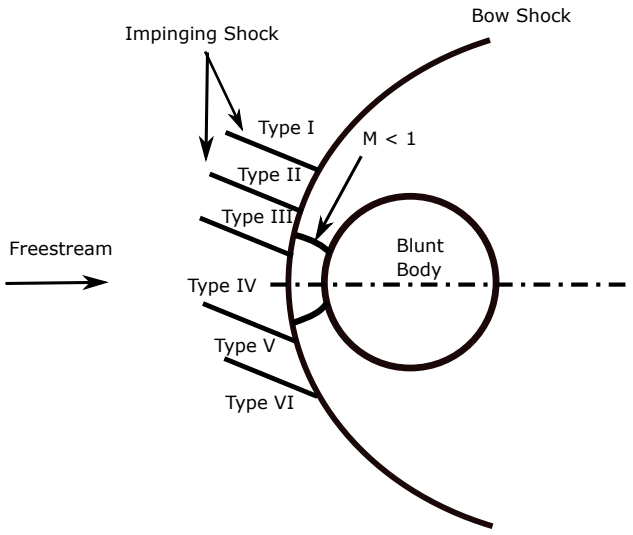

FIG. 36: Classification of different Edney type shock-shock interactions

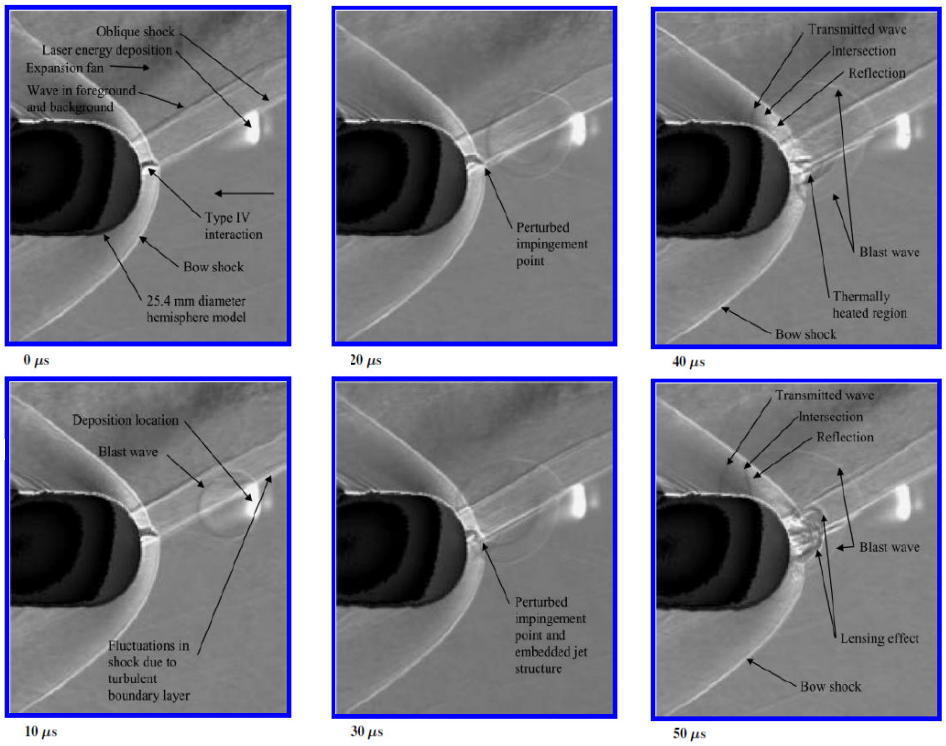

FIG. 37: Schlieren images of the interaction between a laser generated blast wave and a Edney IV shock-shock interaction[113]

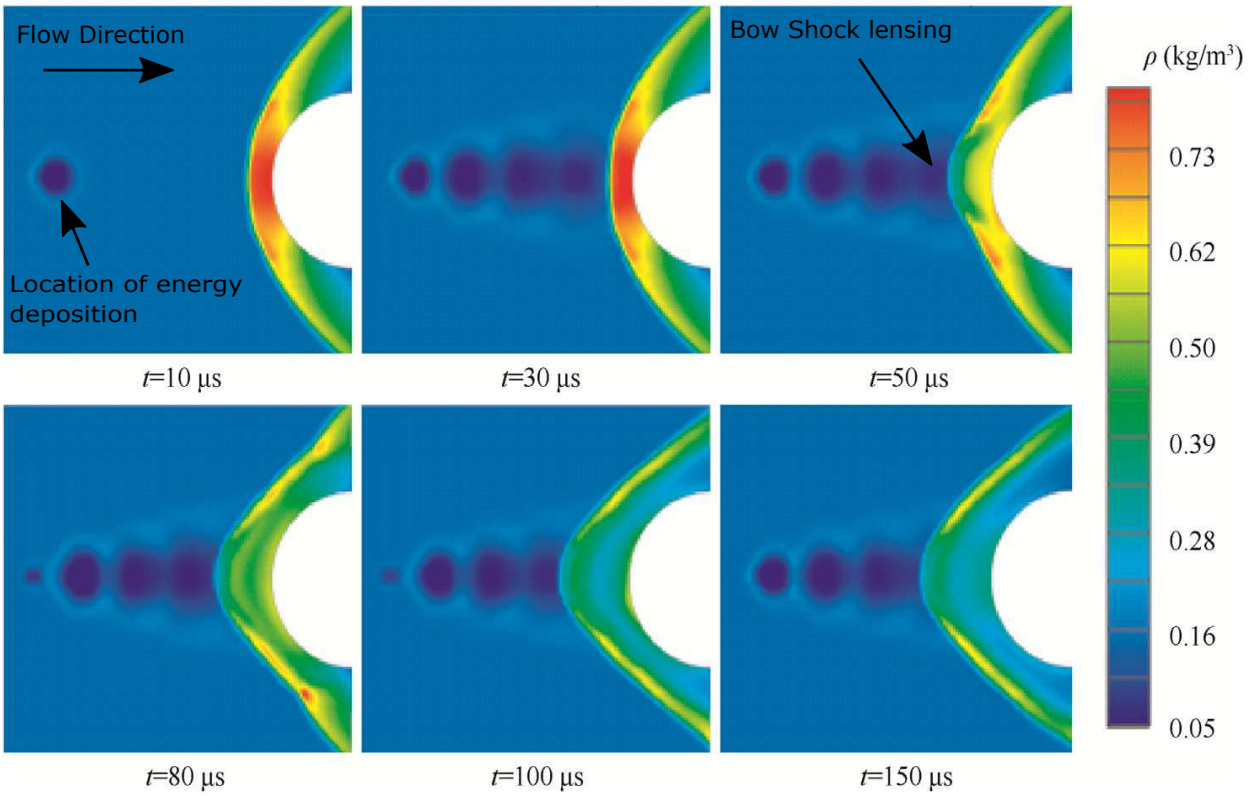

FIG. 38: Plot of density showing the effect of pulsed laser energy deposition on bow shocks at Mach 5[115]

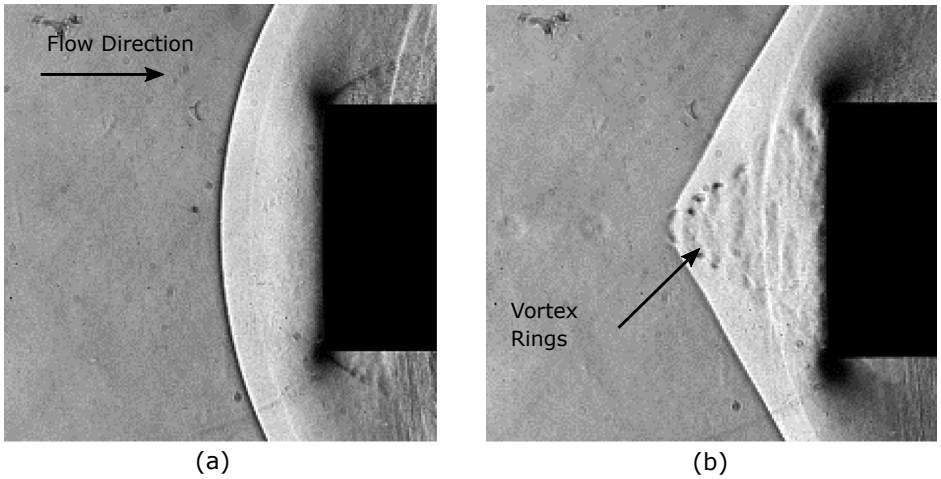

FIG. 39: Schlieren images for baseline flow (a) and flow with pulsed repetitive laser energy deposition (b) at Mach 1.94[116]

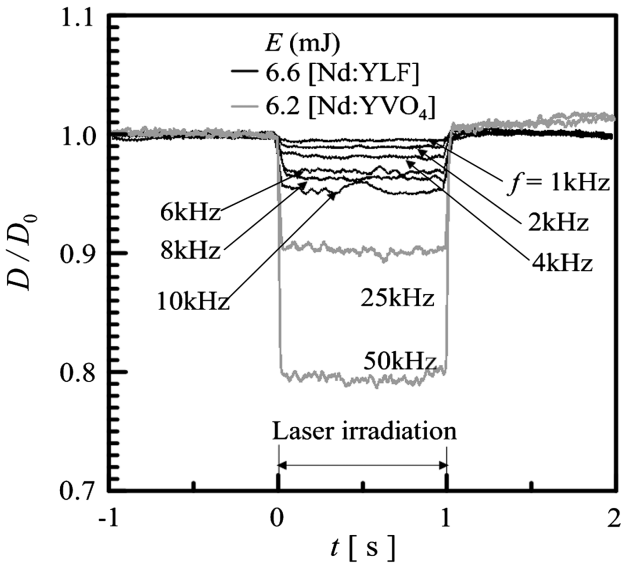

FIG. 40: Plot showing the improvements in drag reduction achieved with increasing laser pulse frequency[116]

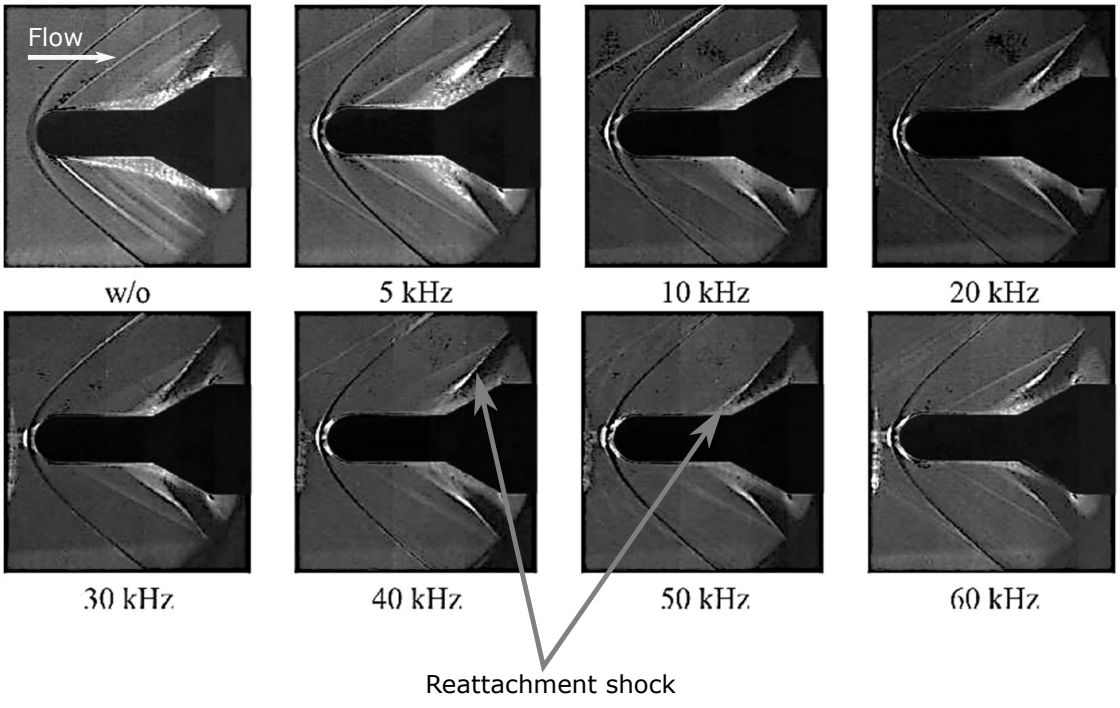

FIG. 41: RMS schlieren images of flow over a cylinder-flare combination at Mach 1.92 with different laser energy frequencies[118]

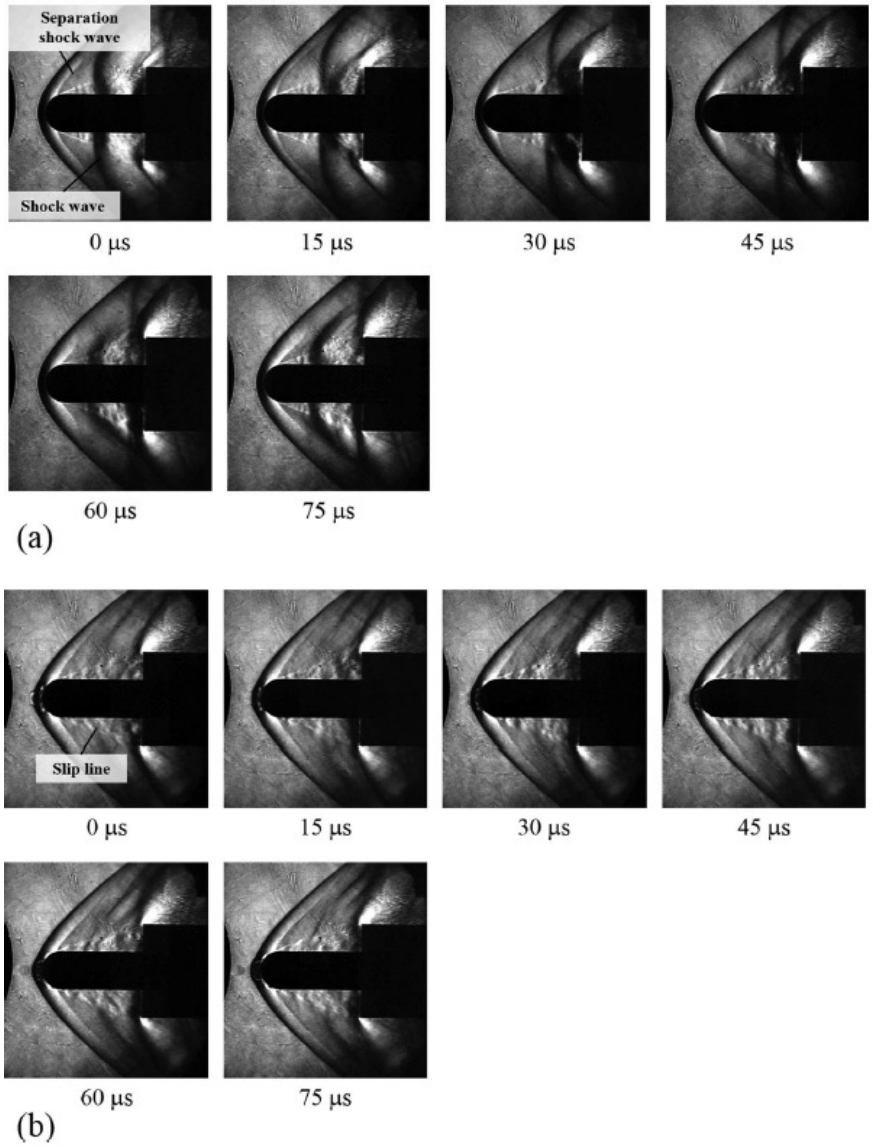

FIG. 42: Series of schlieren images showing the effect on shock wave oscillation of pulsed laser energy deposition[118]

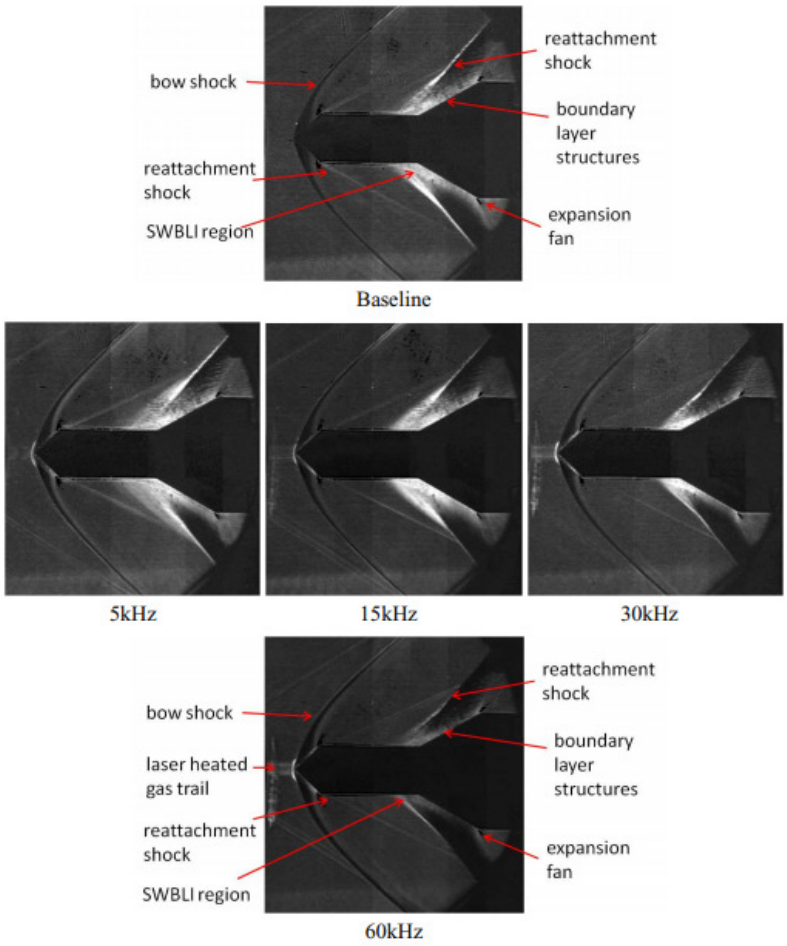

FIG. 43: RMS schlieren images of flow over a cylinder-flare combination at Mach 1.92 showing the impact on the SBLI region of different laser pulse frequencies[119]

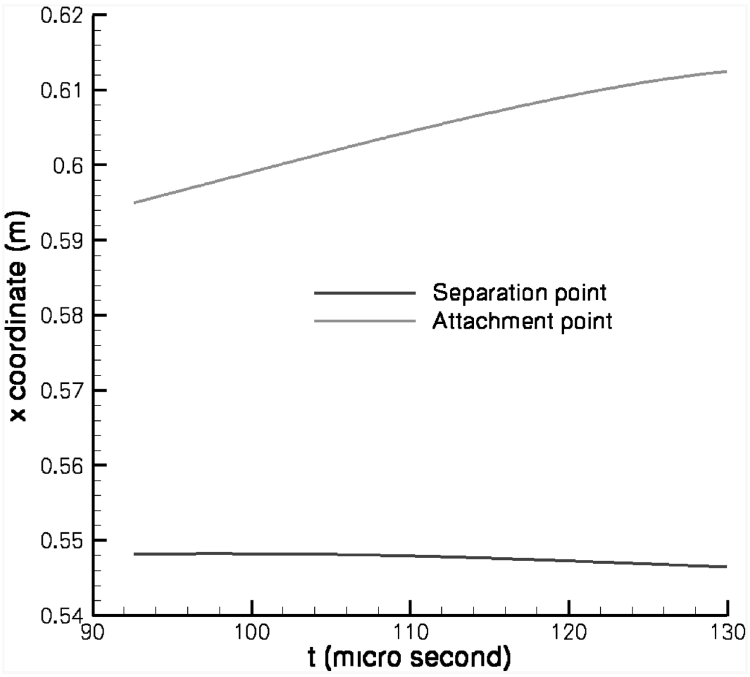

FIG. 44: Plot of separation and re-attachment locations downstream of a normal shock and their response after a pulse of laser energy deposition[120]

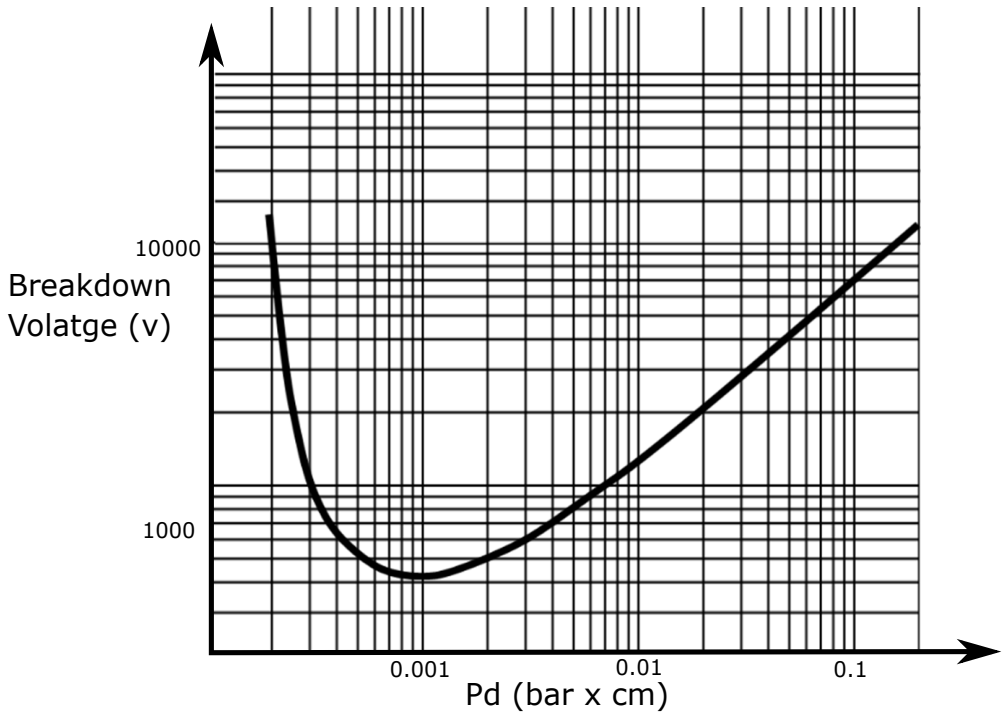

FIG. 45: Example Paschen curve (axes values are approximate to give indication of scale)

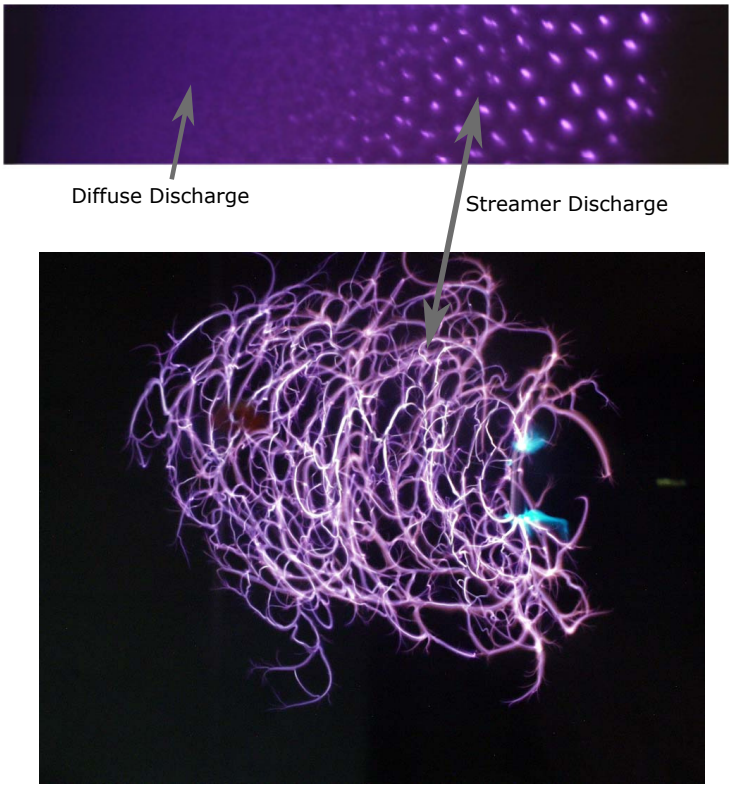

FIG. 46: Examples of different types of plasma discharges[124,154]

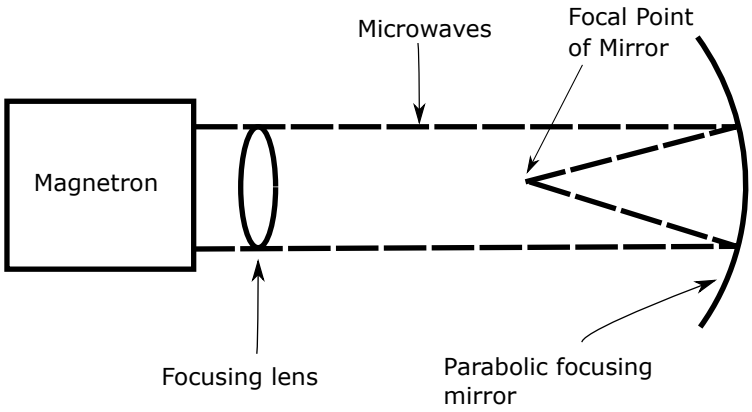

FIG. 47: Basic schematic of mirror focusing scheme for microwave radiation

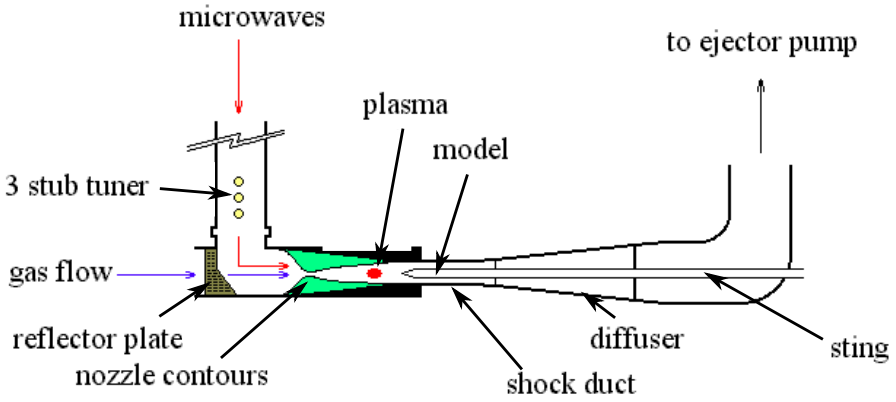

FIG. 48: Wind tunnel layout for overcritical microwave discharge[129]

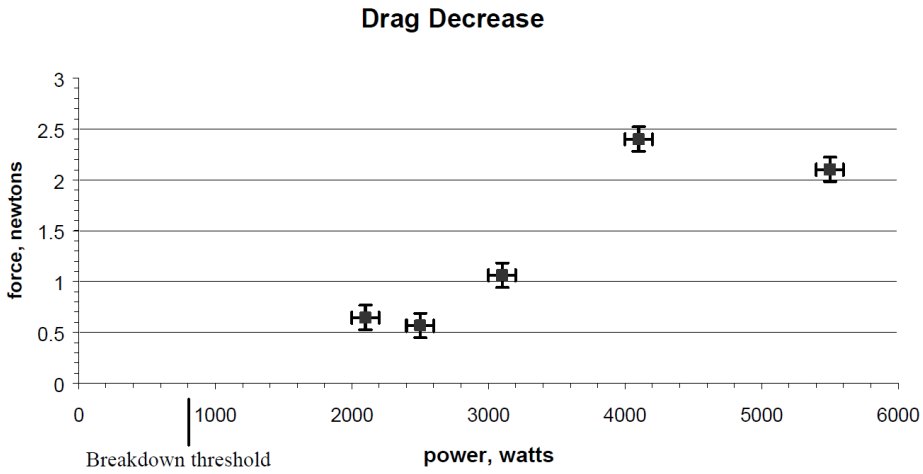

FIG. 49: Effects on drag of microwave generated plasma[129]

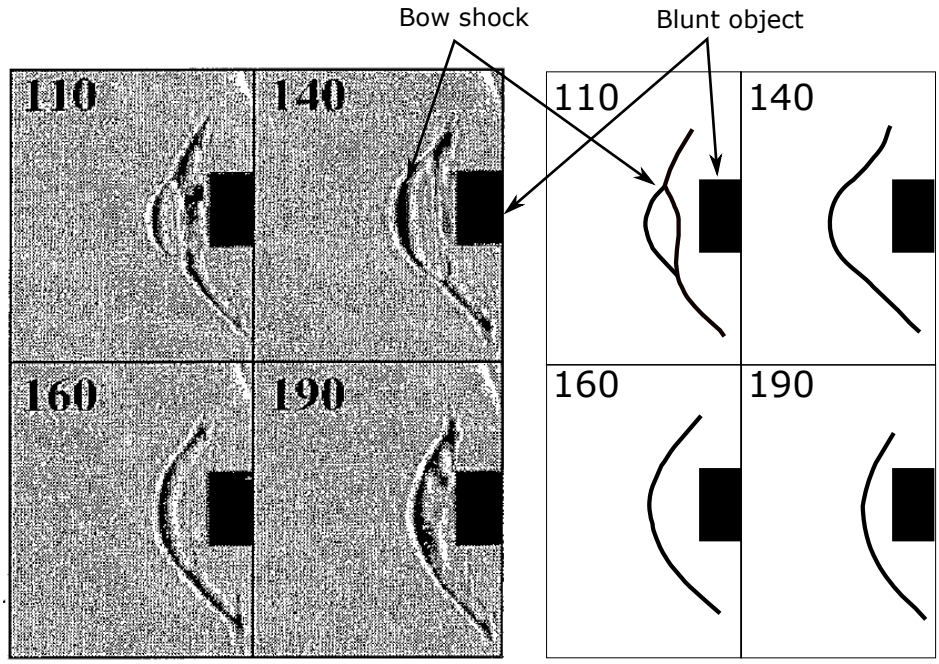

FIG. 50: Schlieren images (left) and schematic (right) of bow shock at different points in time after microwave generated plasma discharge[130]

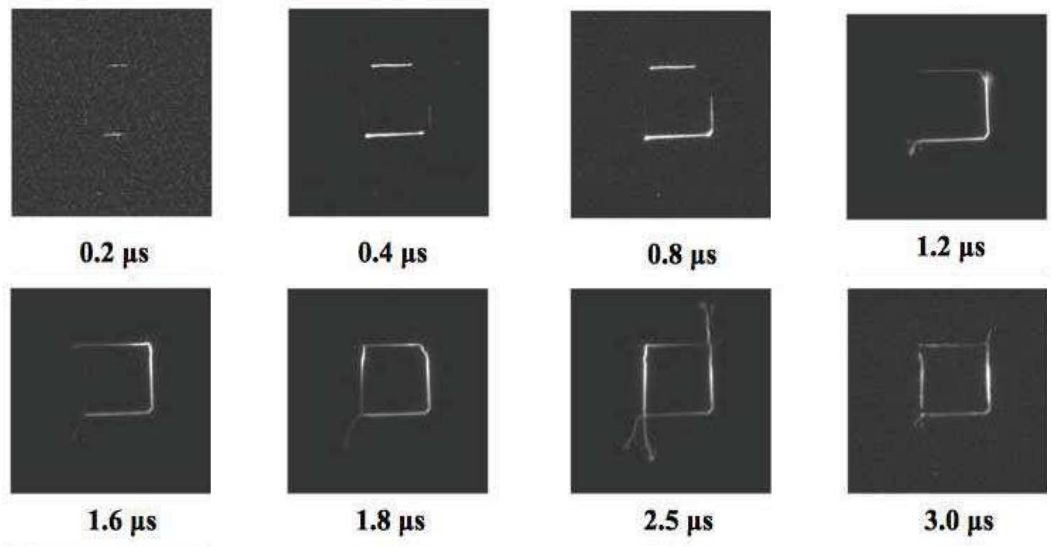

FIG. 51: Schlieren image of plasma discharge growth after pre-ionisation by femtosecond laser pulse split and directed to form a rectangular focal volume (times are irregular as only images of interest are presented)[133]

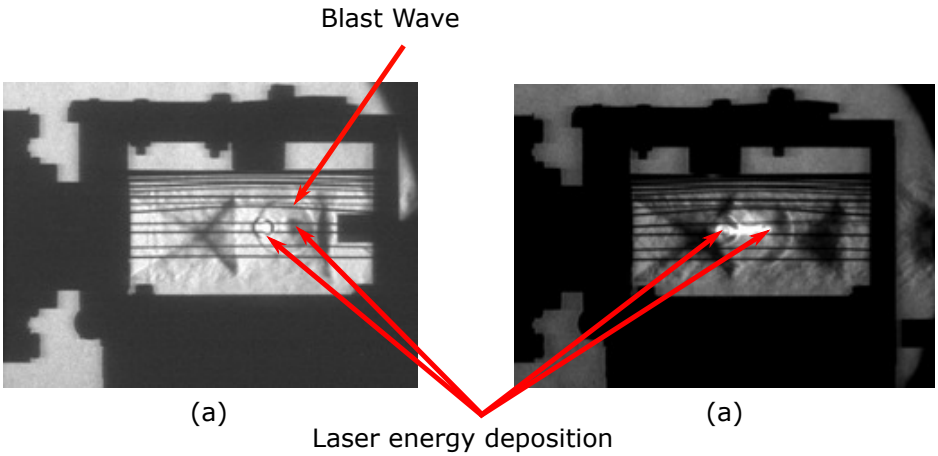

FIG. 52: Schlieren images of a) shock wave structure from double laser spark discharge and b) shock wave structure from double laser sparked microwave discharge[135]

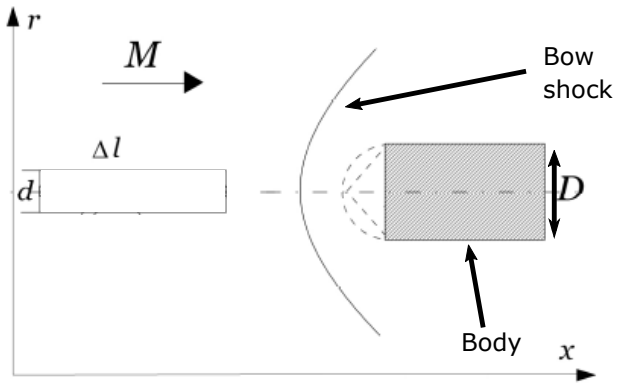

FIG. 53: Representation of computational domain used for numerical modelling of microwave energy deposition (Δl is the length of the microwave filament, d is the diameter of the microwave filament and D is the diameter of the body)[139]

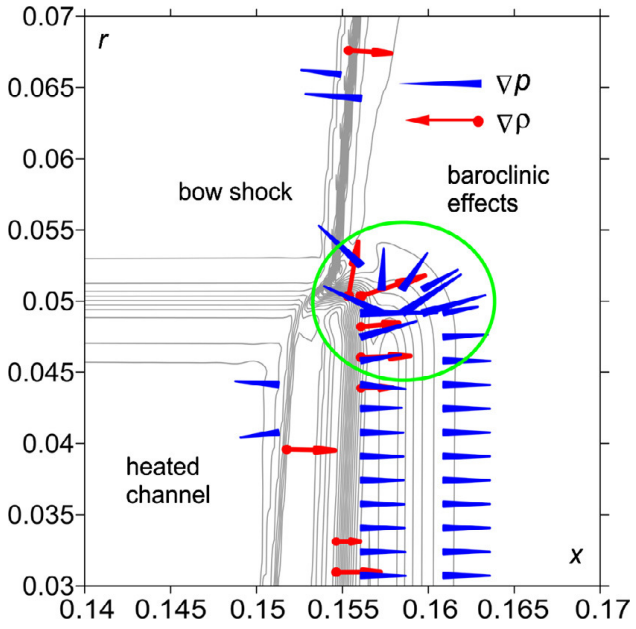

FIG. 54: Illustration of misalignment in density and pressure gradients in microwave energy deposition numerical model[140]

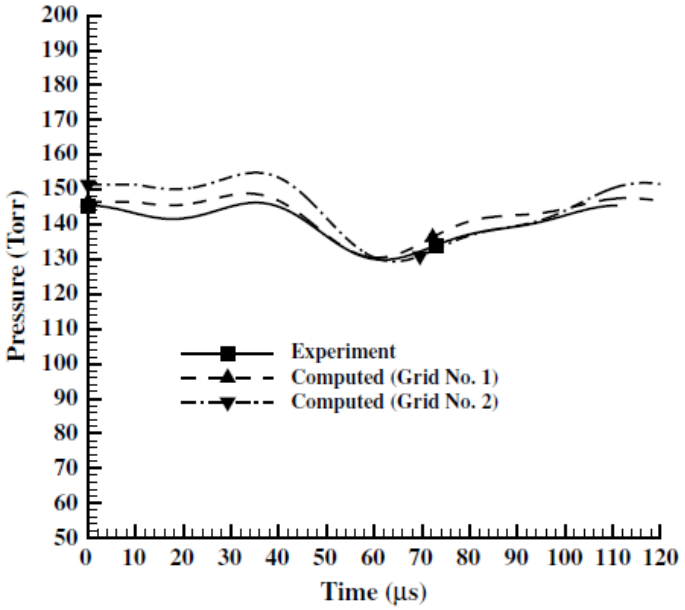

FIG. 55: Comparison of numerical data from thermochemistry model with experimental data[143]

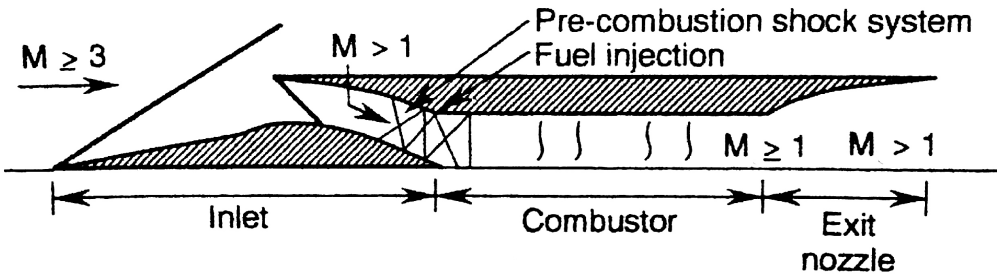

FIG. 56: Schematic of Dual-mode ram-scramjet engine[155]

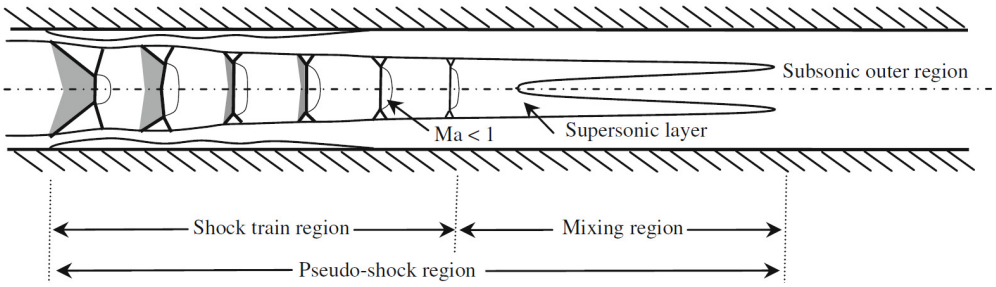

FIG. 57: Sketch of a pseudo-shock system[156]